PROTECTION OF STEEL FRAMES BUCKLING AND YIELDING UNDER EARTHQUAKE LOAD

Mohammad ALFATEH ALSALOUM

T.C.
BURSA ULUDAĞ UNIVERSITY
GRADUATE SCHOOL OF NATURAL AND APPLIED SCIENCES

PROTECTION OF STEEL FRAMES BUCKLING AND YIELDING UNDER EARTHQUAKE LOAD

Mohammad ALFATEH ALSALOUM
000-501-826-010

Prof. Dr. Babür DELİKTAŞ
(Supervisor)

MSc THESIS
DEPARTMENT OF CIVIL ENGINEERING

BURSA – 2023

THESIS APPROVAL

This thesis titled "PROTECTION OF STEEL FRAMES UNDER EARTHQUAKE LOADS" and prepared by MOHAMMAD ALFATEH ALSALOUM has been accepted as a **MSc THESIS** in Bursa Uludağ University Graduate School of Natural and Applied Sciences, Department of Civil Engineering following a unanimous vote of the jury below.

Supervisor : Prof. Dr. Babür DELİKTAŞ

Head : Prof. Dr. Babür DELİKTAŞ
0000-0002-4035-4642
Bursa Uludag University,
Faculty of Engineering
Department of Civil Engineering

Signature

Member: Prof. Dr. Mustafa Özgür YAYLI
0000-0003-2333-3062
Bursa Uludag University,
Faculty of Engineering
Department of Civil Engineering

Signature

Member: Assist. Prof. Dr. Sedef KOCAKAPLAN SEZGIN
0000-0003-2091-5155
Bursa Technical University,
Faculty of Engineering and Natural Sciences
Department of Civil Engineering

Signature

I approve the above result

Prof. Dr. Ali KARA
Institute Director
../../….

I declare that this thesis has been written in accordance with the following thesis writing rules of the U.U Graduate School of Natural and Applied Sciences;

- All the information and documents in the thesis are based on academic rules,
- audio, visual and written information and results are in accordance with scientific code of ethics,
- in the case that the works of others are used, I have provided attribution in accordance with the scientific norms,
- I have included all attributed sources as references,
- I have not tampered with the data used,
- and that I do not present any part of this thesis as another thesis work at this university or any other university.

20/06/2023

Mohammad ALFATEH ALSALOUM

TEZ YAYINLANMA
FİKRİ MÜLKİYET HAKLARI BEYANI

Enstitü tarafından onaylanan lisansüstü tezin/raporun tamamını veya herhangi bir kısmını, basılı (kâğıt) ve elektronik formatta arşivleme ve aşağıda verilen koşullarla kullanıma açma izni Bursa Uludağ Üniversitesi'ne aittir. Bu izinle Üniversiteye verilen kullanım hakları dışındaki tüm fikri mülkiyet hakları ile tezin tamamının ya da bir bölümünün gelecekteki çalışmalarda (makale, kitap, lisans ve patent vb.) kullanım hakları tarafımıza ait olacaktır. Tezde yer alan telif hakkı bulunan ve sahiplerinden yazılı izin alınarak kullanılması zorunlu metinlerin yazılı izin alınarak kullandığını ve istenildiğinde suretlerini Üniversiteye teslim etmeyi taahhüt ederiz.

Yükseköğretim Kurulu tarafından yayınlanan "**Lisansüstü Tezlerin Elektronik Ortamda Toplanması, Düzenlenmesi ve Erişime Açılmasına İlişkin Yönerge**" kapsamında, yönerge tarafından belirtilen kısıtlamalar olmadığı takdirde tezin YÖK Ulusal Tez Merkezi / B.U.Ü. Kütüphanesi Açık Erişim Sistemi ve üye olunan diğer veri tabanlarının (Proquest veri tabanı gibi) erişimine açılması uygundur.

Danışman Adı-Soyadı Tarih	Öğrencinin Adı-Soyadı Tarih
İmza Bu bölüme kişinin kendi el yazısı ile okudum anladım yazmalı ve imzalanmalıdır.	İmza Bu bölüme kişinin kendi el yazısı ile okudum anladım yazmalı ve imzalanmalıdır.

ÖZET

Yüksek Lisans Tezi

ÇELİK ÇERÇEVELERİN DEPREM YÜKLERİ ALTINDA BURKULMA VE AKMA KORUNMASI

Mohammad ALFATEH ALSALOUM

Bursa Uludağ Üniversitesi
Fen Bilimleri Enstitüsü
İnşaat Mühendisliği Anabilim Dalı

Danışman: Prof. Dr. Babür DELİKTAŞ

Depremler, can kaybına, binaların yıkımına ve büyük ekonomik etkilere yol açan doğal olaylardır. Ulusal Deprem Bilgi Merkezinin raporıuna göre yılda ortalama 20,000 deprem olmakta ve bunlardan 16'sı büyük felaketlere sonuçlanmıştır. 6 Şubat tarihinde, 7.8 büyüklüğünde Suriye'nin kuzey sınırına yakın, Türkiye'nin güneyindeki bir bölgeyi vuran depremde tahminen 14 milyon kişinin etkilendiği ve 59,259'a yakın kişin öldüğü belirtilmiştir. Bu durum binaların depreme dayanıklı tasarımı önemli kılmaktadır.

Son yıllarda depreme dayanıklı bina tasarımları ve malzemeler konusunda önemli ilerlemeler kaydedilmişdir. Depremlere karşı koymak için binalar deprem kuvvetlerine karşı güçlendirilmesi gerekmektedir. Çeşitli yöntemler arasında, deprem izolasyonu etkili yöntemlerden biridir. Bu nedenle, bu tezde, bir binanın deprem direncini artırmayı amaçlayan esnek bir temel oluşturma olarak bilinen deprem izolasyon tekniğinin performansının araştırılması amaçlandı. Sismik izolasyonun etkinliğini değerlendirmek için altı farklı senaryoyu içeren kapsamlı bir araştırma yapıldı. Her senaryo, aynı dört katlı çelik moment çerçeve sistemi oluşturuldu. Ayrıca, kauçuk yatağa ilişkin tasarım özelliklerini çıkarmak amacıyla izolasyon sistemleri için Abaqus modeli oluşturuldu.

Yapılan birçok Doğrusal Olmayan Modal Zaman-Aralığı Analizleri sonuncunda, deprem izolasyonunun sabit tabanlı çerçeveye kıyasla toplam yer değiştirme ve periyot değerlerini artırdığını gösterildi. Ayrıca, kat arası kaymalar, ivme ve taban kesme kuvvetleri belirgin şekilde azaldığı, bu da deprem izolasyonunun binanın performansı üzerinde olumlu bir etkisi olduğunu göstermektedir. Özetlemek gerekirse, bu tez çalışması sonuncunda daha düşük sertlikteki izolasyon sisteminin, çelik çerçevenin deprem yüklerine karşı korunmasında daha etkili olduğu görülmektedir.
.

Anahtar Kelimeler: Çerçeve, sap2000, yapı, sismik, izolasyon, ivme, çelik

2023, xiii + 93 sayfa.

ABSTRACT

MSc Thesis

PROTECTION OF STEEL FRAMES UNDER EARTHQUAKE LOADS

Mohammad ALFATEH ALSALOUM

Bursa Uludağ University
Graduate School of Natural and Applied Sciences
Department of Civil Engineering

Supervisor: Prof. Dr. Babür DELİKTAŞ

Earthquakes are natural phenomena with devastating consequences, leading to loss of lives, destruction of buildings, and massive economic impacts. The National Earthquake Information Center reports an average of 20,000 earthquakes each year, with 16 of them causing major disasters. One such event occurred on Feb. 6, 2023, when a magnitude 7.8 earthquake struck southern Turkey near the northern border of Syria, affecting an estimated 14 million people. The confirmed death toll stood at 59,259, emphasizing the urgent need for earthquake-resistant buildings. Therefore, Building resilient structures that can withstand seismic forces is crucial to minimize the consequences of such events.

Methods for Earthquake-Proof Buildings Engineers have made significant advancements in earthquake-resistant building designs and materials over the past few decades. To withstand earthquakes, buildings are reinforced to counteract seismic forces. Among the various methods used seismic isolation stands out as an effective strategy. Therefore, in this thesis it is aimed to investigate the performance of the seismic isolation technique known as creating a flexible foundation, which aims to enhance a building's earthquake resistance. To assess the effectiveness of seismic isolation, an extensive investigation was conducted, comprising six distinct scenarios. Each scenario revolved around an identical four-story steel moment frame. Additionally, an Abaqus model was established for the isolation units with the aim of deducing the design properties associated with the rubber bearing. we conducted frame analyses on a four-story building.

A number of analyses based on nonlinear modal time history analyses highlighted that seismic isolation led to increased total displacement and period values compared to the fixed base frame. Additionally, inter-story drifts, acceleration, and base shear forces notably decreased, signifying the favorable influence of seismic isolation on the building's performance. In summary, a lower stiffness isolation system was found to be more effective in safeguarding the steel frame against earthquake loads.

Key words: Frame, sap2000, structure, isolation, seismic, acceleration, steel

2023, xiii + 93 pages.

PREFACE AND ACKNOWLEDGEMENT

I am writing to sincerely thank, deeply appreciate and express my gratitude to Prof. Dr. Babür DELİKTAŞ, for being my mentor, my guide, my coach, my confidant, my advisor and my professor. for giving me all the resources, I needed for the research and for his never-ending support. His direction was essential to the success of this master's thesis. May Allah, my beloved supervisor, fully reward you for everything you have done for me and for others. I would also like to take this chance to thank every one of the department educators for their assistance and encouragement. Prof.Dr. Hakan T. TÜRKER, Prof.Dr.Serdar KORKMAZ, Dr.Öğr.Üye. Yeşim S. ÜNSEVER, Prof.Dr.Adem AKPINAR, Prof.Dr.Ramazan LİVAOĞLU, Doç. Dr. Ali MARDANİ, Prof.Dr.Murat KANKAL Prof.Dr.Mustafa Özgür YAYLI, and Dr.Öğr.Üye. Serkan SAĞIROĞLU, I have greatly benefited from their wealth of information and experience, knowledge, and wisdom.

It's my great pleasure to thank Uludag University and its honest and competent leadership for changing my life for the better and shaping my future. I shall always be proud of you, my university, and truly become an ambassador of yours wherever I am in the globe.

Our warm and heartfelt greeting and best regards generosity thankfulness, and salutations continue towards the best nation as a whole and country, Turkey, and its people. especially the upright, moral, honest, and ethical people of Bursa.

I am so grateful and incredibly thankful to my family for their never-ending love, encouragement, and care throughout my life, my father, my mother, my wife, my daughters, my brothers and sisters, and my wife's family many thanks to every person especially.

Thank you to all of my friends and classmates at the university.

Last but not least, I would want to express my gratitude to everyone who has helped with this thesis in any way, whether directly or indirectly.

Mohammad ALFATEH ALSALOUM
21/06/2023

Contents

SYMBOLS and ABBREVIATIONS

Symbols	Definition
KN	Kilo Newton
m	Meter
s	Second
F_y	Steel yield stress
F_{ye}	Steel expected yield stress
F_u	Steel tensile stress
F_{ue}	Steel expected tensile stress
E	Modulus of elasticity
U	Poisson
G	Shear modulus
A	Coefficient of thermal expansion
D_M	Maximum lateral displacement
h_i	Floor height
W_i	Floor Weight

Abbreviation	Definition
ASCE	American Society of Civil Engineers
ISE	Institution of Structural Engineers
LL	Live Load
DD	Died load
FF	Fixed Special Moment Resisting Frame
IF	Isolated Special Moment Resisting Frame
ELF	EQUIVALENT LATERAL FORCE PROCEDURE

FIGURES

TABLES

Pages

1. INTRODUCTION

1.1. Historical development to protect structures from earthquakes:

In ancient times, buildings were built of stone with limited heights. Despite their limited heights, most of these buildings collapsed completely or partially due to earthquakes, because stone buildings have a high mass, high stiffness, and low flexibility, see Figure1.1. Stiff buildings can cause very high floor accelerations. Therefore, there was a need to find less stiff and more flexible buildings to resist earthquakes.

Figure 1.1. Harbour Street at the ancient city of Ephesus in Turkey

Reinforced concrete structures appeared as an alternative to stone buildings, as they have less rigidity and more flexibility compared to stone buildings, but the concrete high mass problem remained as an obstacle to the construction of highly earthquake-resistant buildings (Figure1.2.). So composite and steel structures have appeared as a flexible and lightweight alternative, but also the flexible structures can cause large inter-story drifts leading to problems with providing safety and protection of the building's elements and contents.

Figure 1.2. Makkah Clock Royal Tower, 601 m height mainly constructed from concrete.

Stiff buildings can lead to extremely very high floor accelerations, and flexible structures will cause large inter-story drifts. So, the following question has been discussed: How if simply isolate the structure from the ground in a way that significantly decreases or totally prevents the transmission of seismic vibrations up through the superstructure?

This simple question needed a lot of effort and research in materials science and seismic and vibrational motions with modern computerized analysis to find isolation and damping systems to prevent seismic motions from moving into the building and dampening the resulting vibrations. Also, it still needs a lot of effort in order to obtain better results to protect the buildings seismically.

1.2. Protecting the steel structures from earthquakes:

In the last century, steel structures started to be the best choice for seismic-resistant construction as it was high resistance and ductile material. Different types of steel frames were developed to resist the vertical and horizontal loads. All steel-framed buildings resist the vertical force by frames made up of steel columns that are vertical and steel beams that are horizontal - the ends of the beams are welded to the columns in order to establish strong solid rigid connections, or we can use the bolted or riveted connections so that the buildings can resist the horizontal forces. These types of frames are called steel moment-frames and it was very popular in 1960s and 1970s. In the Northridge earthquake of 1994 and Kobe earthquake of 1995 these types of frames had several common types of damage. The most common cracks initiate in the weld itself or just next to the weld. In some cases Figure 1.3, the cracks run across the entire column, practically dividing it into two unconnected pieces.

a. Column Flange "Divot" Fracture b. Fracture at Fused Zone

Figure 1.3. Fractures of Beam to Column Joints(FEMA 2000a)

Even though steel moment-frames did not fall or collapse during the Northridge earthquake of 1994, designers, engineers and specialists became worried by the poor performance and unexpected brittle failures of beam-to-column connection which have seen a lot after these two earthquakes. A lot of research and studies were undertaken specifically to solve poor performance and the discovered problems with welded steel moment frame connections after the Northridge earthquake of 1994. Significant changes were made to seismic provisions, new moment-resisting connections were become offered and available (FEMA 2000a, AISC 2010a), and the seismic design of moment frames was subjected to stricter design and governed by more demanding detailing standards. It was found that the following factors were the main causes of the unexpected brittle failure modes seen in the steel moment-frames:

1. The significant variation in steel's real material characteristics and properties
2. Due to the connection details, there are severe stress concentrations.

3. The practice welding on-site before these earthquakes.

The research and studies also recommended the following prequalified connections for steel moment frames as shown in Table 1.1.

Table 1.1. Prequalified connections for steel moment frames. (ANSI/AISC 358-20)

<table>
<tr><th colspan="2">Prequalified Moment Connections</th></tr>
<tr><td>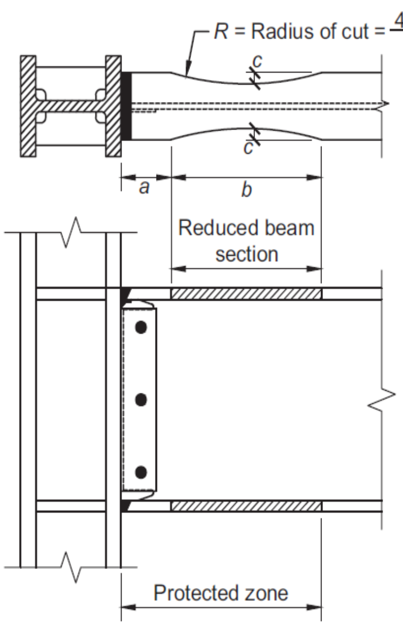
</td><td>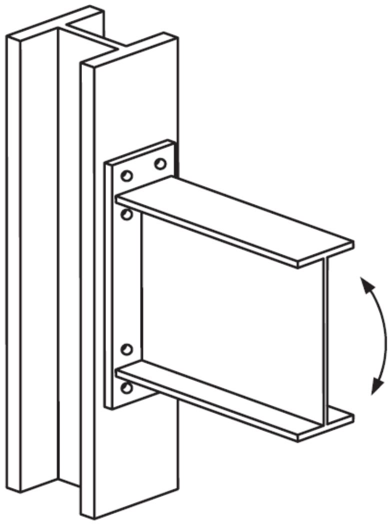</td></tr>
<tr><td>1- Beam column connection with Reduced beam section (RBS)</td><td>2- Beam column connection with Bolted unstiffened extended end plate (BUEEP)</td></tr>
<tr><td colspan="2">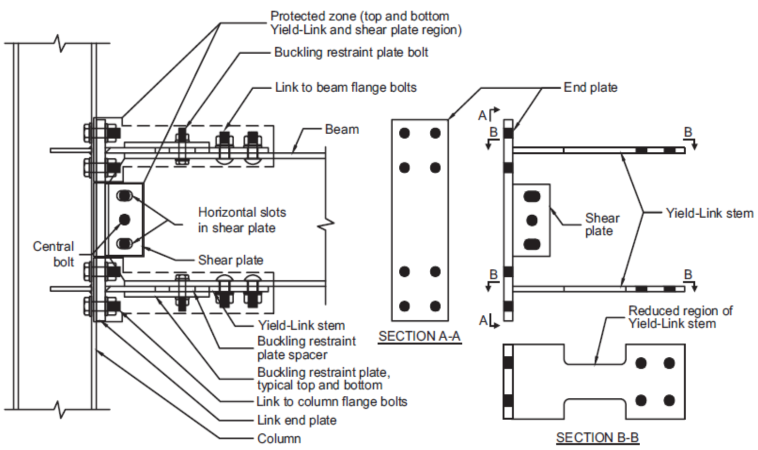
</td></tr>
<tr><td colspan="2">3- Beam column connection with Simpson Strong-Tie Strong Frame moment connection</td></tr>
</table>

Table 1.1 Complement. (ANSI/AISC 358-20)

<table>
<tr>
<td>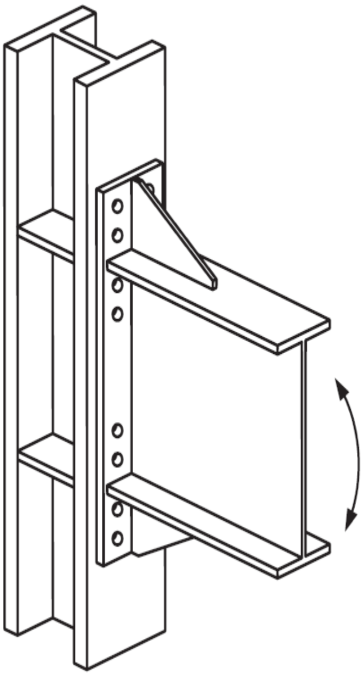</td>
<td>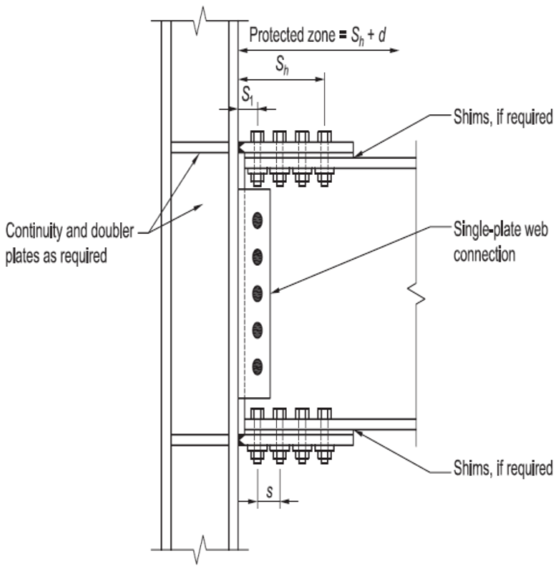
</td>
</tr>
<tr>
<td>4- Beam column connection with Bolted stiffened extended end plate (BSEEP)</td>
<td>5- Beam column connection with Bolted flange plate (BFP)</td>
</tr>
<tr>
<td>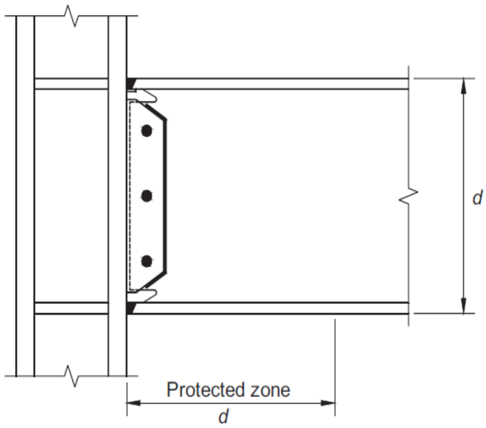
</td>
<td>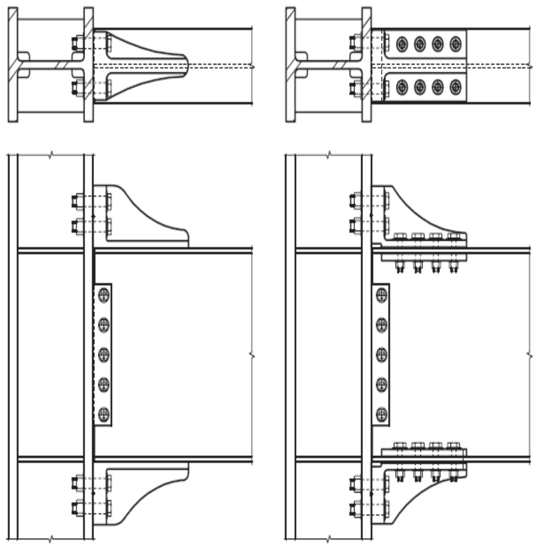</td>
</tr>
<tr>
<td>6- Beam column connection with Welded unreinforced flange-welded web (WUFW)</td>
<td>7- Beam column connection with Kaiser bolted bracket (KBB)</td>
</tr>
</table>

Table 1.1. Complement. (ANSI/AISC 358-20)

<table>
<tr><td>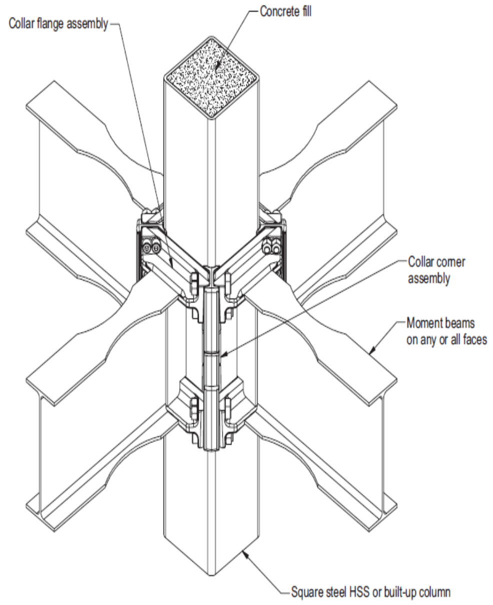
</td><td>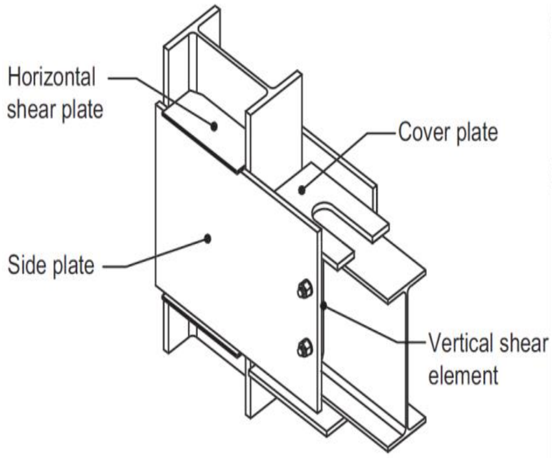
</td></tr>
<tr><td>8- Beam column connection with ConXtech ConXL moment connection</td><td>9- Beam column connection with Side Plate moment connection (Side Plate)</td></tr>
<tr><td>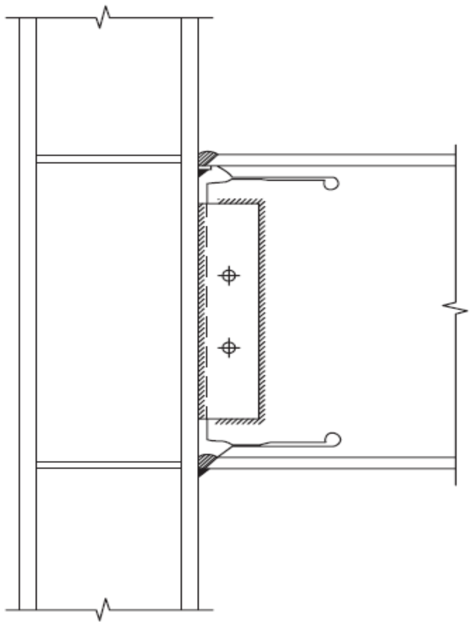</td><td>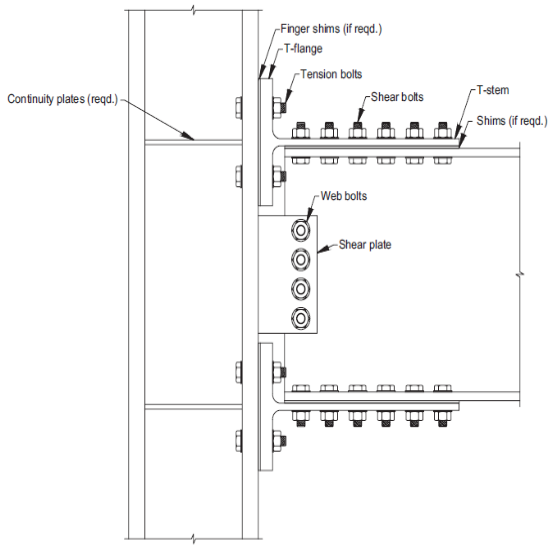
</td></tr>
<tr><td>10- Beam column connection with Slotted Web moment connection</td><td>11- Beam column connection with Double-tee moment connection</td></tr>
</table>

In general, buildings are not earthquake-proof; they will sustain damage during significant quakes, but structural engineers design these structures to avoid collapsing,

allowing occupants to leave the building safely after an earthquake. This is similar to being involved in a car accident; even though your car may sustain significant damage, you are safe and able to leave; the same is true of buildings.
Non-engineered buildings have extremely weak joints, so structural engineers use the moment frame connections to strengthen these joints, which are essential joints that are heavily welded or heavily bolted by stiffening the joints so that we can design the building to resist earthquakes. Moment frame systems have some disadvantages, including the fact that they aren't the most cost-effective option. However, architects appreciate them because they allow for more open floor plans without using walls or braces. In addition, steel building bracing systems are stiff, strong, and inexpensive when it comes to resisting earthquakes.

They are effective during earthquakes, stiffer and less likely to deform than those with moment frames, and these braces are frequently designed as the fuse of the building during earthquake events earthquake forces attack the weakest link in the building, and these braces are, but they do get in the way of the architecture. They are designed to take a beating and are very ductile. Similar to how difficult it would be to mangle or fracture apart a paper clip, they can distort and get mangled without tearing due to the earthquake forces. Because they avoid the beams, floor systems, and columns, which are the most crucial components of the structure, they concentrate all of their force on the building's weakest link, the brace.

Systems for shear walls is when we install shear walls, these are basically the strongest and stiffest of the structural systems, so it's quite commonly used in mid-rises and high-rise projects. They're also the most cost-effective option to resist earthquake forces, but they're not the architect's first choice. They basically act as walls that take the earthquake forces and prevent the building from shearing off the foundation.

Braced frames have become more common in seismically active areas as a result of the lessons learnt during the 1994 Northridge earthquake. In truth, the braced frames are one of the earliest types of resisting structure’s systems and are being used for long time in a variety of configurations. However, due to recently created strict and hard standards

for structural elements and their high labor-costly connections in moment resisting frames, practical engineers tend to prefer braced frames in seismically prone regions.
It is important to highlight that the financial factors of the system which resisting the lateral forces had a major impact on the structural system selections. Furthermore, Design engineers have found it difficult for a long time with controlling the lateral deflections in moment frames. Because moment frames are flexible, the design of a moment frame is typically dictated by the stiffness requirements (drift requirements) more than the requirements of strength, resulting in column and beam sections that are significantly have more deep and heavier than those necessary to meet the strength requirements. Due to their ease of production, relatively cheap labor costs, and substantial initial lateral stiffness that controls and limits lateral deflections, braced frames are also beneficial to and recommended for use in the steel building sector in general.

But nevertheless, the seismic performance of conventional or traditional braced frames is still so far from the best or ideals. Many engineers and researchers have experienced difficulties with unsymmetrically hysteretic performance which generated premature fracture due to the local buckling of bracing elements.

Conventional buckling braces, particularly cold-formed tubular bracings, frequently exhibit an asymmetrical hysteretic response in addition to being more likely to suffer an early fracture.

Previous research has shown that the localized strain requirements eventually cause conventional braces to fracture prematurely after the braces experience substantial local buckling at the 1st and/or 2nd reversed tension cycle. The beam-column connections would experience major damage as a result of framing action once the braces are fractured (Uriz & Mahin 2008), which could causing the vertical supports (columns) fracture or maybe the failure/collapse of the system which resists the seismic forces as shown in Figure 1.4.

Figure 1.4. Brace fracture in CBFs (Engineering Mechanics, 2020, 37(10))

Furthermore, cold-formed square or round steel tubular bracing fracture initiation is likely to happen at an equivalent story drift ratio of ratio around 2.0% shortly later local buckling, according to new researches examining large-scale hollow structural shapes (HSS) under reversed cyclic loading. This significant gap between the structural system's demands due to seismic drift and the fracture life of conventional bracings clearly resembles the assumptions made about steel moment-frames before the earthquakes of 1994and 1995.

Because it was presumed that the typical pre-Northridge connection utilized in steel moment-frame construction might sustain serious plastic rotations without materially weakening (FEMA 2000c). Since there are many high-rises braced frames in the market for steel buildings, such as office buildings and hospitals, it is important to develop a procedure that is both practical and affordable to improve the seismic performance of braced frames that are both new and existing in seismically active areas.

The dampened and seismically isolated structures appeared as a new and advanced earthquake resistant system.

1.3. Protecting seismically isolated and dampened structures from earthquakes:

Recent years have seen large investments in the development of structural vibration control technologies for the reduction of seismic hazards in both new and existing structures. By preventing both global and local buckling of the braces by applying dampers similar to modern methods to improving the seismic performance of braced frames, it is able to successfully solve the common problems relating to the seismic performance of braced frames (Figure 1.5).

Figure 1.5. Braced frames with dampers. (Damptech company site)

Advanced sustainable technology uses seismic dampers to reduce earthquake damage. Seismic dampers come in a variety of shapes and sizes, but they always work by converting seismic energy into thermal energy through friction, either between solids (friction dampers) or inside fluids (viscous dampers).

There are several different damper systems, including liquid-filled dampers, which minimize the building or structure's shaking during earthquakes. Viscous dampers or mass tuned dampers.

To reduce the response of structures subject to dynamic forces and protect the structures, base isolation systems and energy dissipation devices are well-known alternatives today (Figure 1.6).

Base isolation system means that you can't get hit by an earthquake if you're not touching the ground, so this technique is probably the closest thing to earthquake-proofing a building. In practice, this means installing base isolators, which are typically in the form of ball bearings, rubber bearings, or friction bearings, under the structure.

Figure 1.6. Aydın Şehir Hastanesi - AYDIN HOSPITAL isolation system

1.4. Purpose of this study:

In this study, we undertook a comprehensive analysis of a four-story building using frame analysis techniques. The investigation was carried out in two main phases: initially, we examined the building as it was constructed on a fixed base. Subsequently, we introduced a frame seismic isolation system to the building and conducted a reanalysis. This reanalysis involved performing analyses both with and without the isolation system in place. The purpose of this reanalysis was to facilitate a comparative evaluation of the outcomes, as depicted in Figure 1.7. By following this structured approach, we aimed to better understand the impact of the frame seismic isolation system on the building's structural behavior and seismic performance.

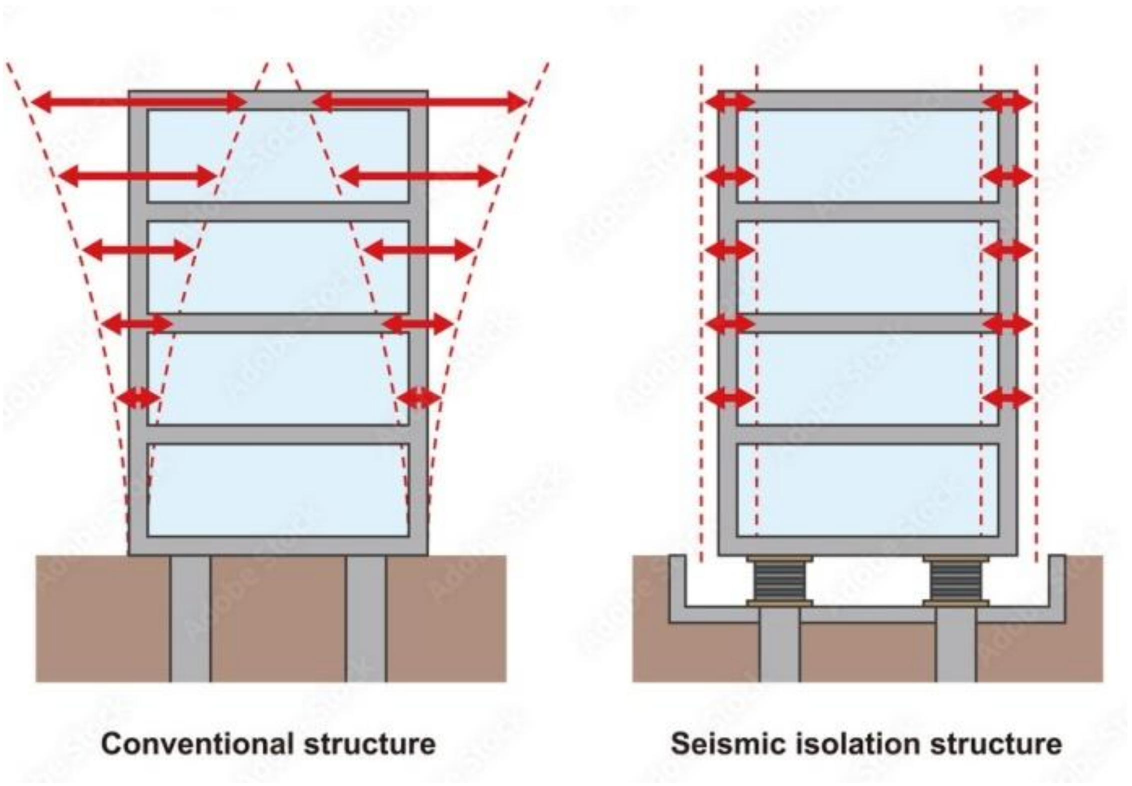

Figure 1.7. Frame with and without isolation system

2. THEORETICAL BASICS and LITERATURE REVIEW

This chapter provides an overview for recent developments and research as well as theoretical information on isolation systems.

2.1. Definition of Isolation system:

According to the ASCE 7-22 guidelines, the seismic isolation system encompasses a collection of structural elements. These elements comprise individual single isolation units, components responsible for transmitting forces between various parts of the isolation system, and structural elements that establish connections to other components within the system (Figure 2.1). This inclusive definition encompasses the entirety of the seismic isolation system and highlights its interconnected nature.

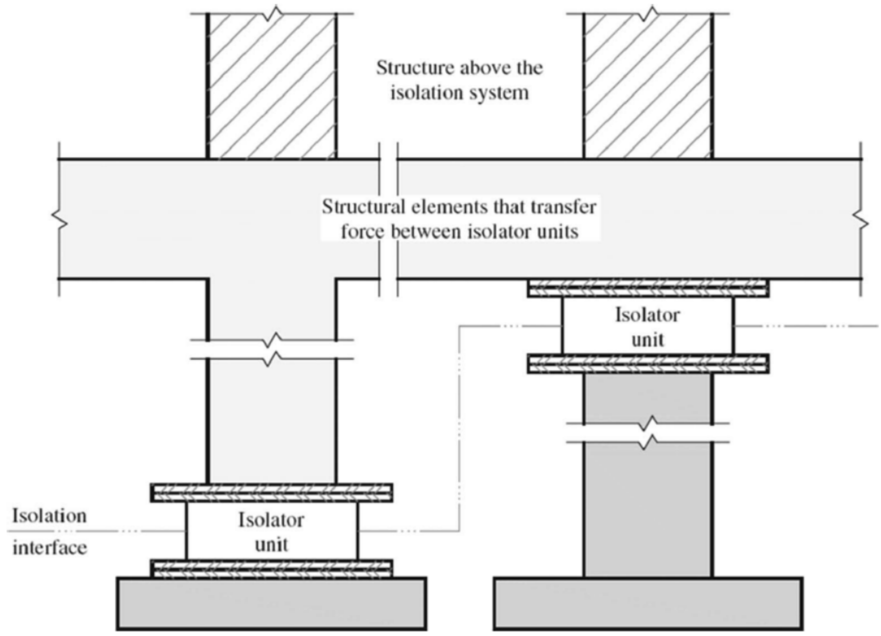

Figure2.1. The terminology of the isolation system.(ASCE 7-22)

Furthermore, the isolation system encompasses additional elements such as energy-dissipation devices, a wind-restraint system, and/or a displacement restraint system. These components are considered integral to the isolation system if they meet the design requirements stipulated for the system. This expanded definition recognizes the potential incorporation of these devices and systems into the overall seismic isolation strategy, provided they fulfill the necessary criteria.

Indeed, notable revisions have been introduced in recent code updates to streamline the process of designing and implementing seismic isolation strategies. Isolation systems that are considered acceptable generally exhibit the following key characteristics:

Stability Across Directions: These systems ensure stability not only in the horizontal plane but also in the vertical direction when subjected to design displacements. This comprehensive stability feature enhances their performance during seismic events.

Inherent Restoring Force: Acceptable isolation systems are equipped with a built-in restoring force mechanism. This inherent force intensifies as the displacement of the system increases, enhancing its resistance against seismic forces. This attribute contributes significantly to its earthquake-mitigating capability.

Resistance to Cyclic Loading: These systems demonstrate minimal degradation under repeated cyclic loading. This characteristic ensures their durability and longevity when subjected to multiple seismic events over time.

Measurable Engineering Properties: They possess quantifiable engineering attributes, such as damping and force-deflection parameters. These measurable properties facilitate accurate analysis, design, and assessment of the isolation system's performance.

By embodying these attributes, acceptable seismic isolation systems demonstrate their effectiveness in enhancing structural resilience and mitigating the impact of seismic forces on buildings and infrastructure.

Isolation systems can be categorized into four distinct groups based on their lateral force-displacement behavior, as depicted in Figure 2.2. Notably, each of these idealized curves shares a common displacement value, referred to as "DD." This systematic classification provides a clear framework for understanding the varying behaviors and characteristics of different isolation systems.

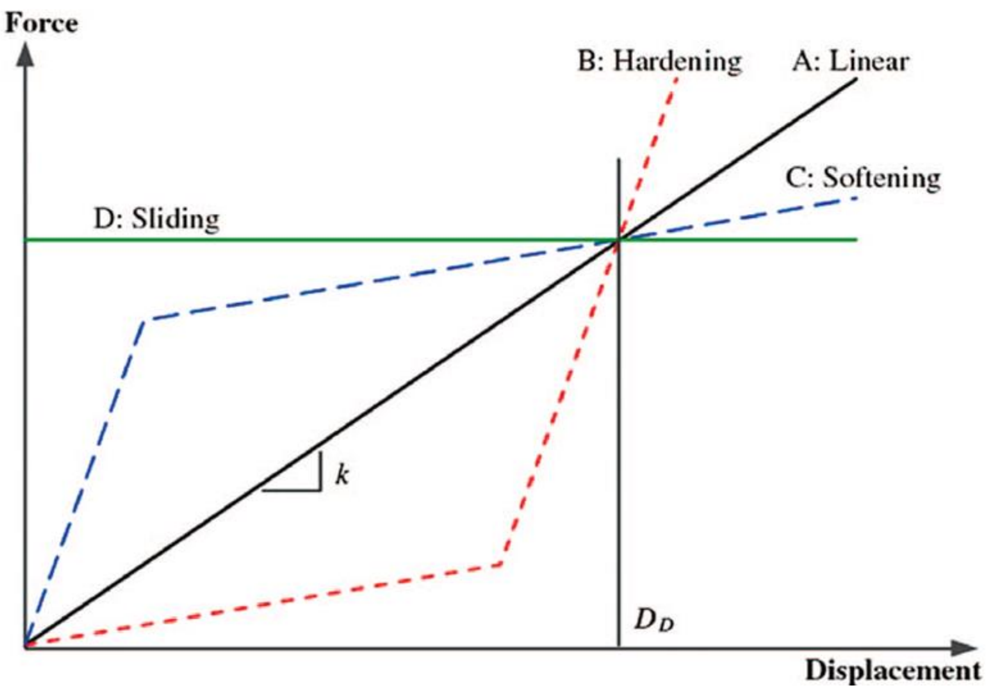

Figure 2.2. Idealized Force-Deflection Relationships For Isolation Systems,(ASCE 7-22) (For clarity, we are not displaying the stiffness effects of sacrificial wind-restraining systems).

Curve A: The force produced in the superstructure is directly linked to the displacement of a linear isolation system, which has an effective period that is constant and independent of the displacement demand.

Curve B: A hardening isolation system has a low initial lateral stiffness at low displacement demands, which is followed by a comparatively high second stiffness at larger displacement demands, which has a shorter effective period.

Curve C: The first stiffness of a softening isolation system is comparatively high (short effective period), and the second stiffness is relatively low (longer effective period) with increasing displacements.

Curve D: a sliding isolation system's response without the ability to apply lateral restoring force.

This thesis focuses on the investigation of base isolation systems. The term itself carries a self-explanatory meaning: the objective is to isolate the base, referring to a structure situated on the ground that experiences vibrations due to external ground motions. These motions can lead to significant structural displacements. Consequently, the primary sequence of examination entails establishing the safety of the equipment, followed by an evaluation of its comfort aspects.

Our exploration involves the identification of distinct approaches, namely active control methods and passive control methods. Within these categories, techniques like tuned mass dampers and tuned liquid dampers are recognized. While other methods exist, a particularly renowned one is the utilization of base isolation techniques. These techniques play a crucial role in mitigating the entry of vibrational energy into a building, effectively preventing its transmission.

To enhance the building's connection with the earth, a strategic isolation approach was adopted. This involved introducing a material layer between the structure and the ground, which effectively filters out frequencies associated with the structure's vibrations. The fundamental concept underlying the base isolation approach is to allow other frequencies to penetrate, which, even if present, would not compromise the structural integrity. This approach thus ensures that potentially harmful frequencies are isolated and that the overall stability of the building remains intact.

We will delve into the topic of the base isolation method, which serves as a pivotal aspect of our discussion. Base isolation involves a strategic technique aimed at mitigating risks associated with structures situated or founded directly on the ground. These structures are vulnerable to potential collapse when exposed to ground vibrations. The fundamental premise here is that if the ground undergoes significant vibrational forces, the structures erected upon it are at risk of succumbing to these vibrations, leading to potential structural failure. The base isolation method addresses this concern by introducing measures to enhance the structures' resilience and stability, ultimately safeguarding them against the adverse effects of ground-induced vibrations.

The core principle of fundamental isolation revolves around strategically placing buildings on the ground while incorporating isolation measures in between. This technique involves utilizing components like rubber bearings or similar types of bearings to support the isolated structure. When the Earth experiences vibrations, these isolation elements serve as a barrier, effectively preventing the transmission of frequencies to the building. By doing so, the vibrations are impeded from exerting a detrimental impact on the structure, thereby safeguarding its stability and integrity. In essence, the fundamental concept of isolation creates a protective buffer that shields the building from the potentially destructive effects of ground-induced vibrations.

Prior to designing the isolation bearings, a crucial step involves comprehending the inherent frequencies and potential vulnerabilities of the building. This understanding is essential for tailoring the bearing design to effectively counteract and exclude these specific frequencies from the incoming ground motion. This technique is aptly termed "base isolation." By employing this approach, the design of the isolation bearings is precisely calibrated to counteract the building's natural frequencies, thereby mitigating the resonance between the structure and ground vibrations. This meticulous alignment ensures that the building remains resilient and unharmed, even in the presence of ground-induced motions.

Isolator units, typically referred to as bearings, play a pivotal role in the base isolation approach. These bearings are engineered to facilitate controlled movement and rotation, all while maintaining the essential function of transferring loads between the superstructure and its supporting elements. Consequently, the classification of bearings is organized into three distinct categories within each range. This systematic categorization ensures that the functionality and purpose of bearings are well-defined and efficiently serve their role in enabling structural resilience and mitigating the impact of ground vibrations.

A. Free Bearings: these kinds of bearings transfer the vertical loads and permits full structure translational horizontally and rotational movements in all directions as shown in Figure 2.3.

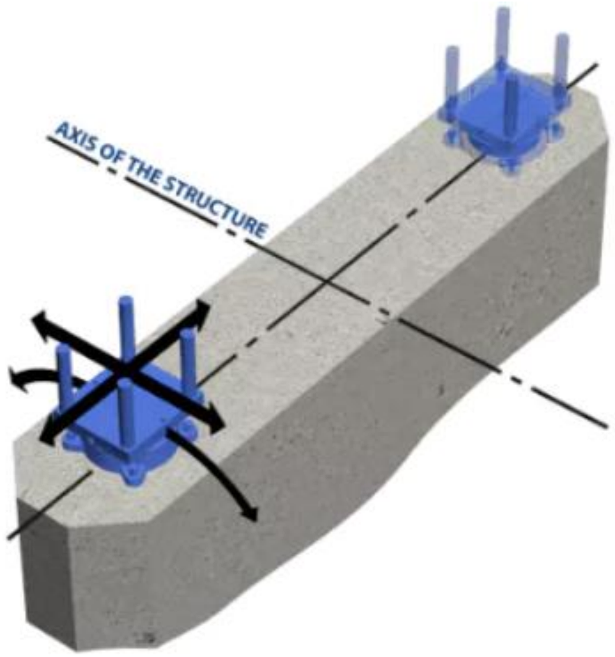

Figure 2.3. Free Bearings (CV4 Freyssinet Mechanical Bearings)

B. Guided Bearings: these kinds of bearings transfer the vertical and horizontal loads in a single direction. Both translation in the perpendicular direction and rotation in all directions are allowed as shown in Figure 2.4.

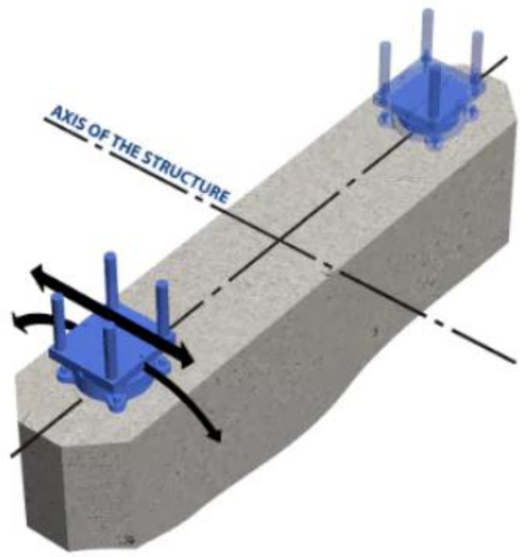

Figure 2.4. Guided Bearings (CV4 Freyssinet Mechanical Bearings).

C. Fixed Bearings: these kinds of bearings transfer all vertical and horizontal loads in all directions while allowing rotation of the superstructure in all directions as shown in Figure 2.5.

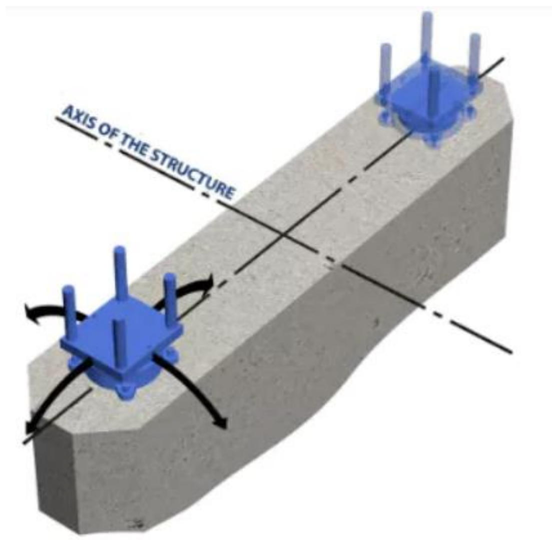

Figure 2.5. Fixed Bearings (CV4 Freyssinet Mechanical Bearings)

Also according to specific criteria, such as the principal of work, capacity and material the bearings are divided into four primary groups, as following:

- Elastomeric bearings
- Pot bearings
- Spherical bearings
- Special bearings

Figure 2.6 shows the relationship between the acceptable rotation and vertical load for each bearing type which clearly shows the spherical bearings are the largest capacity.

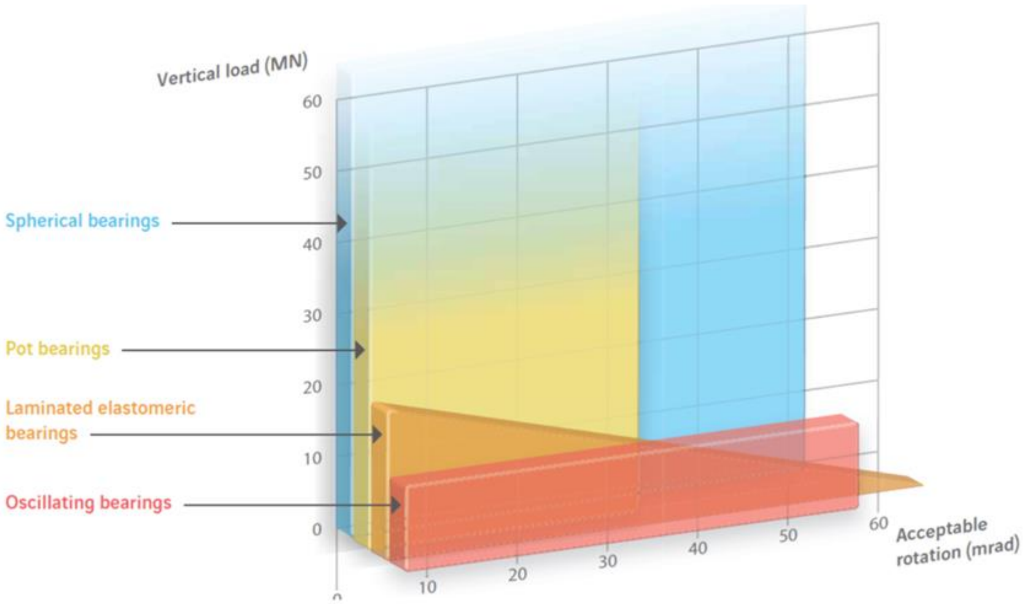

Figure 2.6. The relationship between the acceptable rotation and vertical load. (CV4 Freyssinet Mechanical Bearings)

In the following, we will get to know each of these bearing types in more detail.

- **Elastomeric Bearing or Rubber:**

There are three rubber bearing types:

1- low-damping rubber bearings,

2- high-damping rubber bearings,

3- Lead rubber bearings.

Low-damping rubber bearings, and high-damping rubber bearings consists of alternative layers of rubber and steel.

High-damping rubbers and low-damping rubbers are differentiated by the incorporation of specific additives into the rubber compound. One of these additives, known as carbon black, plays a crucial role. Its inclusion in the compound enhances the damping capacity of the rubber.

Low-damping rubber bearings are not commonly used independently; rather, they are often combined with supplementary dampers. This is because isolators offer two distinct effects: primary elongation due to heating and additional damping. Low-damping rubber alone cannot provide sufficient additional damping, necessitating the use of high-damping rubber bearings or complementary dampers in conjunction with low-damping rubber bearings.

In summary, the addition of carbon black to rubber compounds increases the damping capability of high-damping rubbers, while low-damping rubbers are typically paired with supplementary dampers due to their inability to provide adequate additional damping.

Apart from using carbon black for increased damping, another method involves lead rubber bearings. These bearings consist of low-damping rubber with an inserted lead core. The lead provides the necessary damping effect.

When the rubber is pulled, it stretches due to its elasticity. Similarly, when the building displaces during an event, the stretched rubber pulls the building back to its original position when released.

In creating laminated elastomeric bearings, steel plates separate the layers of natural rubber. These layers are then enclosed by a rubber cover (see Figure 2-7) and vulcanized to form a compact, maintenance-free bearing.

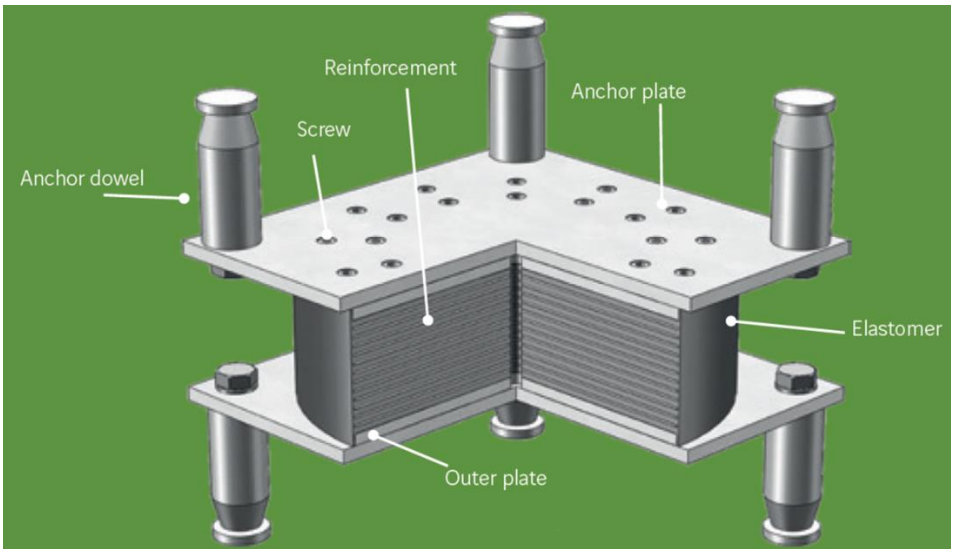

Figure 2.7. Elastomeric Bearing. (CV4 Freyssinet Mechanical Bearings)

When uniform rotation capacity is needed in all directions (both transversely and longitudinally), cylindrical bearings are preferable. However, rectangular bearings (as shown in Figure 2-8) are commonly used in practice.

Rectangular bearings are more prevalent due to the usually greater longitudinal rotation compared to transverse rotation. Cylindrical bearings are best suited when uniform rotation capacity is required in all directions (transverse and longitudinal) within a laminated elastomeric bearing.

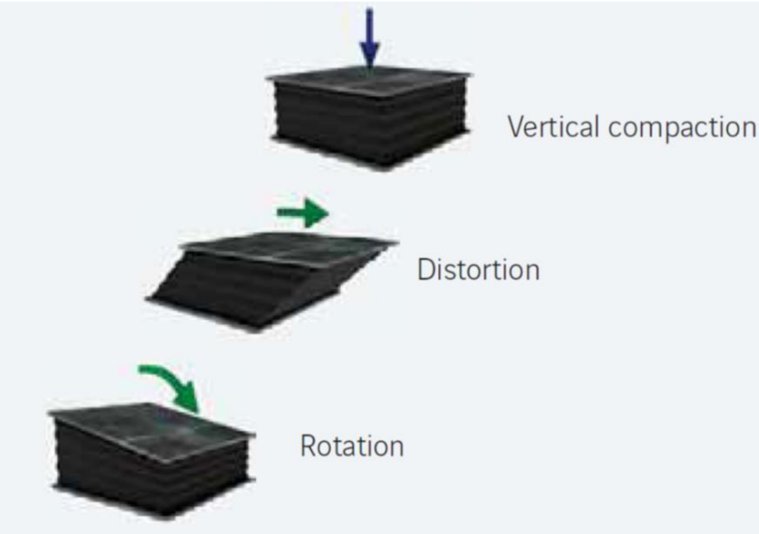

Figure 2.8. Rectangular Bearing. (CV4 Freyssinet Mechanical Bearings)

Lead rubber bearings (LRBs), similar to high-damping rubber bearings, belong to the seismic isolation category. They consist of vulcanized steel plates, encasing a central lead core, and multiple thin elastomeric layers (see Figure 2-9). These bearings commonly employ natural rubber with a shore hardness ranging from 45 to 55, providing greater flexibility than elastomeric bearing pads. The utilization of ductile lead contributes to the construction of LRBs. Under vertical impact pressure, lead undergoes plastic bending and is secured by steel plates and natural rubber.

Consequently, the hysteresis curve of the bearing is modified, endowing it with favorable damping characteristics. Bearings featuring a central lead core can endure substantial deformations, effectively absorbing and dissipating energy to safeguard against harm during intense compression events.

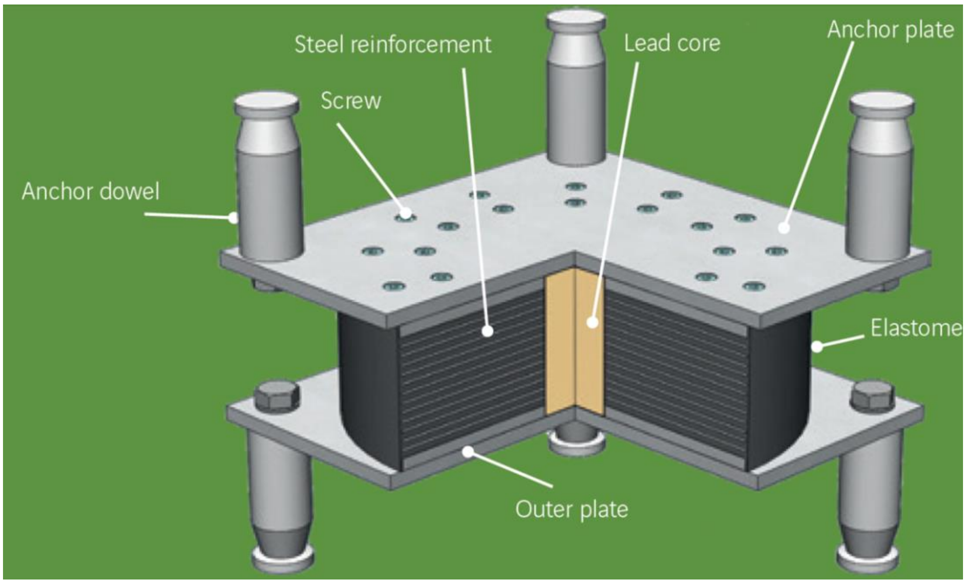

Figure 2.9. Lead rubber bearing (LRB). (CV4 Freyssinet Mechanical Bearings)

➢ **POT BEARING:** Comprising an unarmored elastomer disc within a metal cylinder, supported by a metal piston. It enables omnidirectional rotation horizontally and provides vertical load support and transfer (see Figure 2-10).

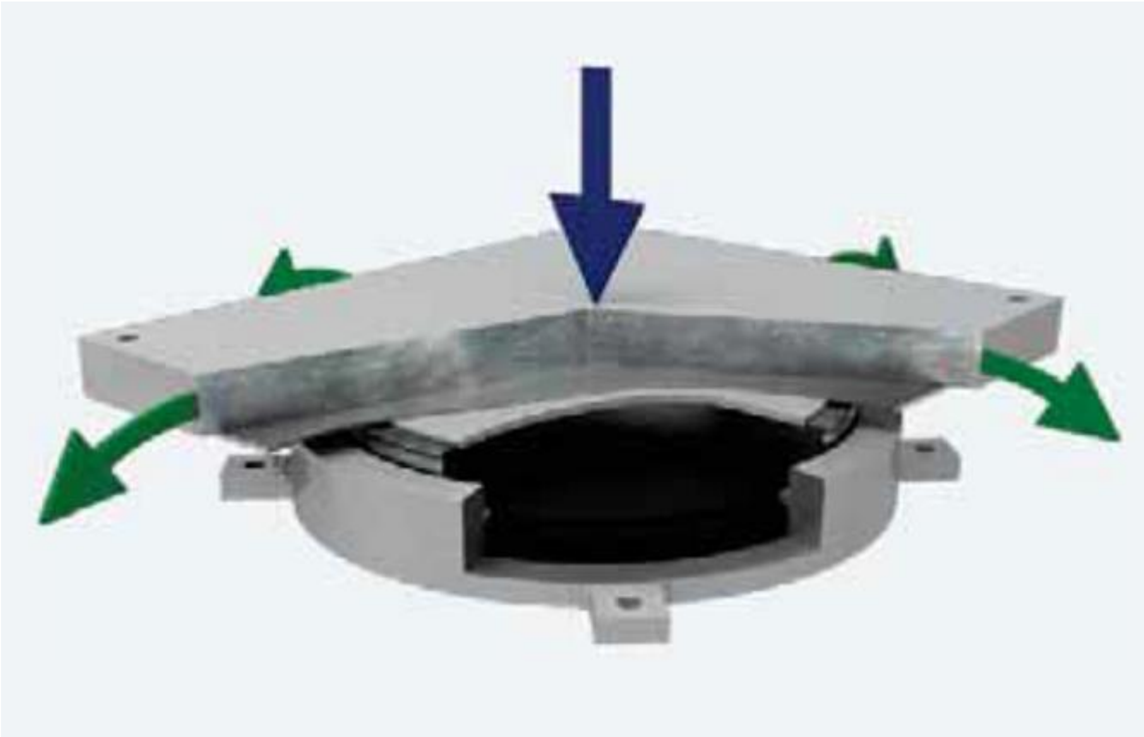

Figure 2.10. Pot bearing. (CV4 Freyssinet Mechanical Bearings).

A sliding arrangement, composed of a stainless-steel polished plate affixed to a metal back plate, operates within the recess on the piston within pot bearings. This setup can be guided along a specific direction to bear and transmit horizontal force. These bearings are termed "sliding or guided pot bearings." Different types of pot bearings can be employed, categorized based on the desired freedom level:

A. Fixed Pot Bearings: Enable rotation around any axis while preventing movement in all directions, as the elastomeric bearing pad functions akin to an incompressible confined fluid (see Figure 2.11).

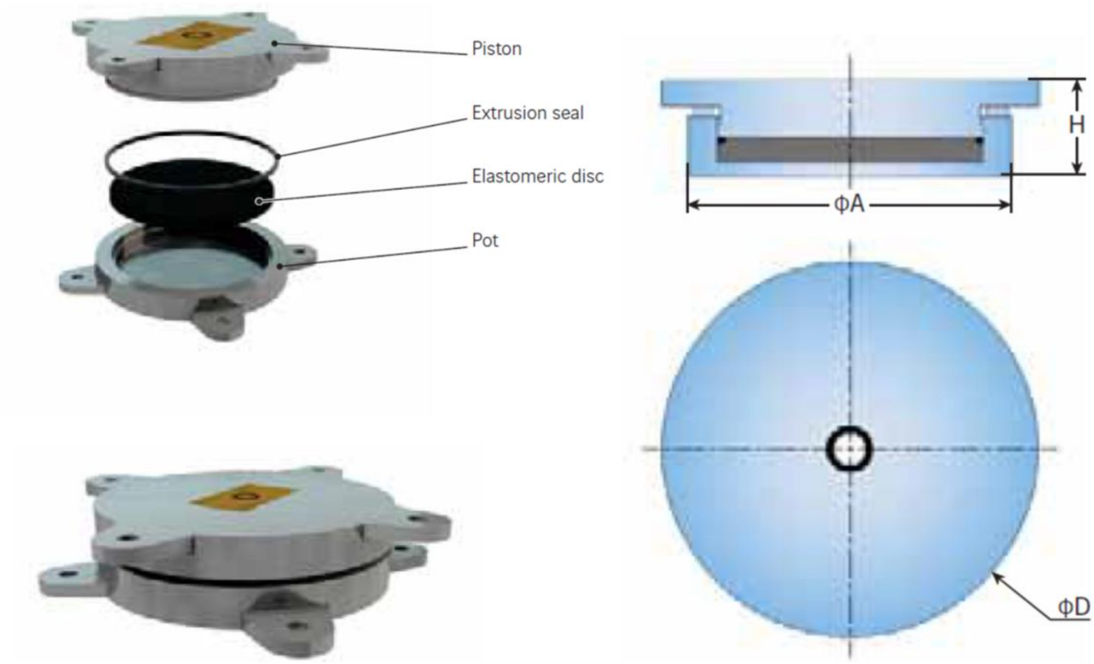

Figure 2.11. Fixed pot bearing (CV4 Freyssinet Mechanical Bearings).

B. Guided Pot Bearing: Equipped with a steel guide edge, movement is confined to a single direction (see Figure 2.12).

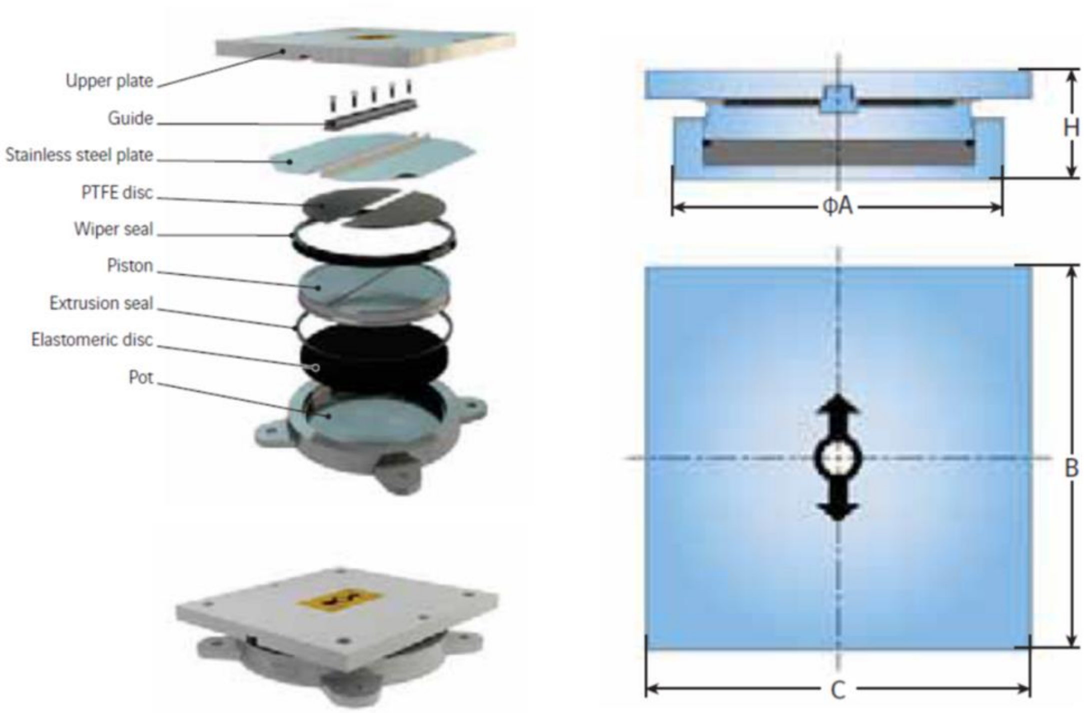

Figure 2.12. Guided pot bearing. (CV4 Freyssinet Mechanical Bearings).

C. Free Pot Bearing: Achieves rotation and unrestricted movement in all directions. Incorporating an extra PTFE and stainless steel sliding surface between the piston and sole plate creates a bearing configuration allowing horizontal movement in all directions (refer to Figure 2.13).

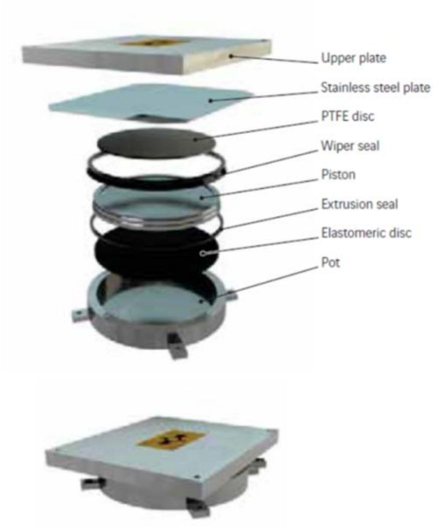

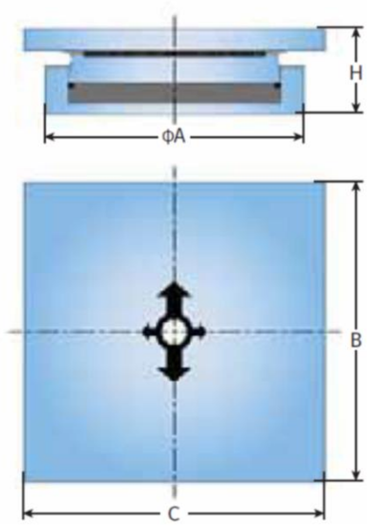

Figure 2.13. Free pot bearing. (CV4 Freyssinet Mechanical Bearings).

SPHERICAL BEARINGS: Comprising concave and convex steel backing plates with a low-friction sliding surface between them, spherical bearings facilitate rotation through inward sliding (see Figure 2.14).

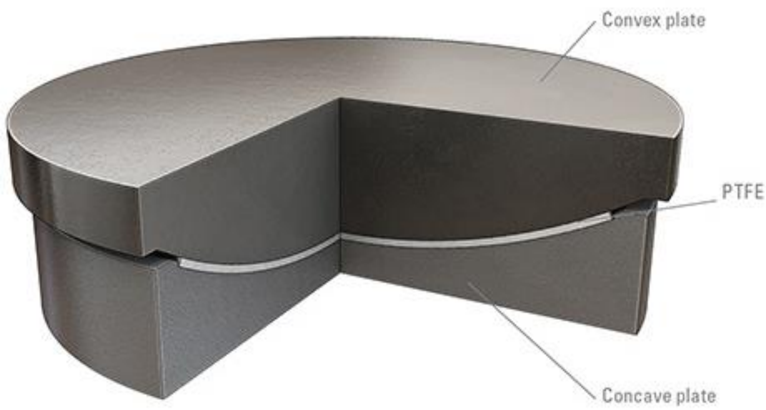

Figure 2.14. Simplified spherical bearing principle. (CV4 Freyssinet Mechanical Bearings).

Also, there are three types of spherical bearings depending on the desired level of freedom:

A. Fixed spherical bearings: Permit rotations around any axis while inhibiting movement in all directions (refer to Figure 2.15).

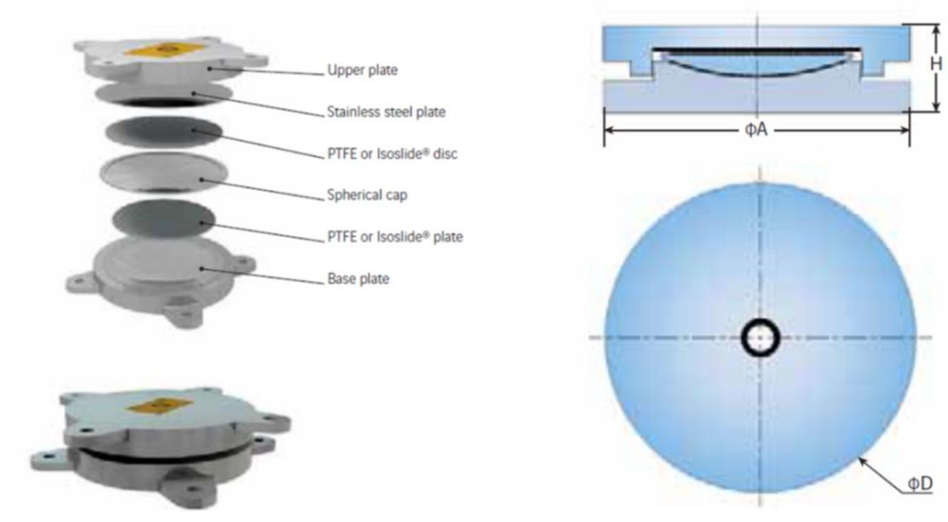

Figure 2.15. Fixed spherical bearings. (CV4 Freyssinet Mechanical Bearings).

B. Guided spherical bearings: Movement constrained to a single direction (see Figure 2.16).

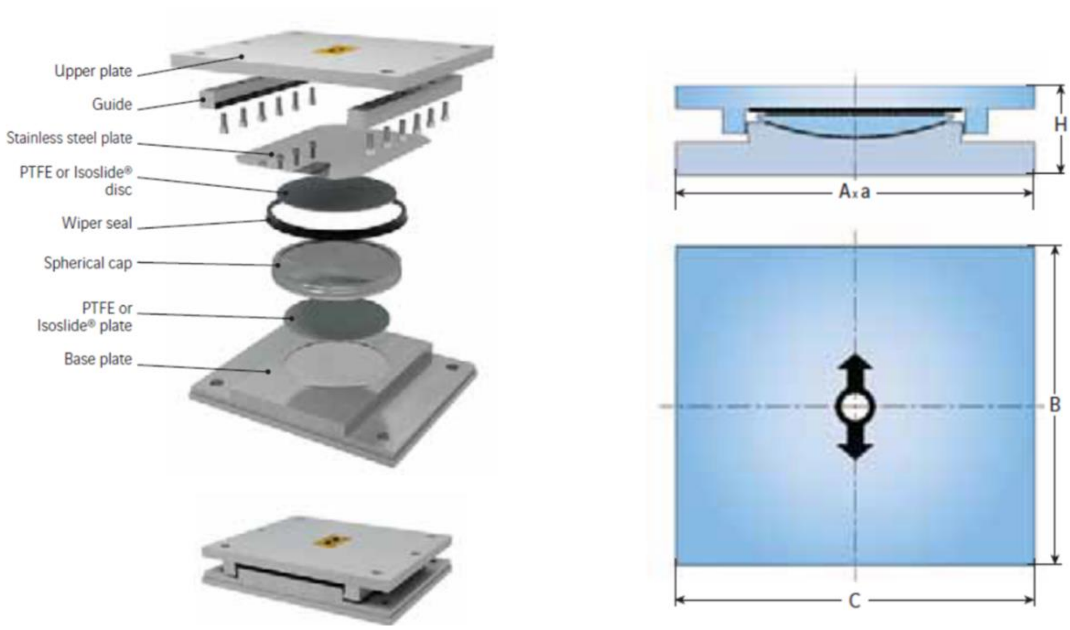

Figure 2.16. Guided spherical bearing. (CV4 Freyssinet Mechanical Bearings).

C. **Free spherical bearings:** Enable rotations and unrestricted horizontal movement in all directions (refer to Figure 2.17).

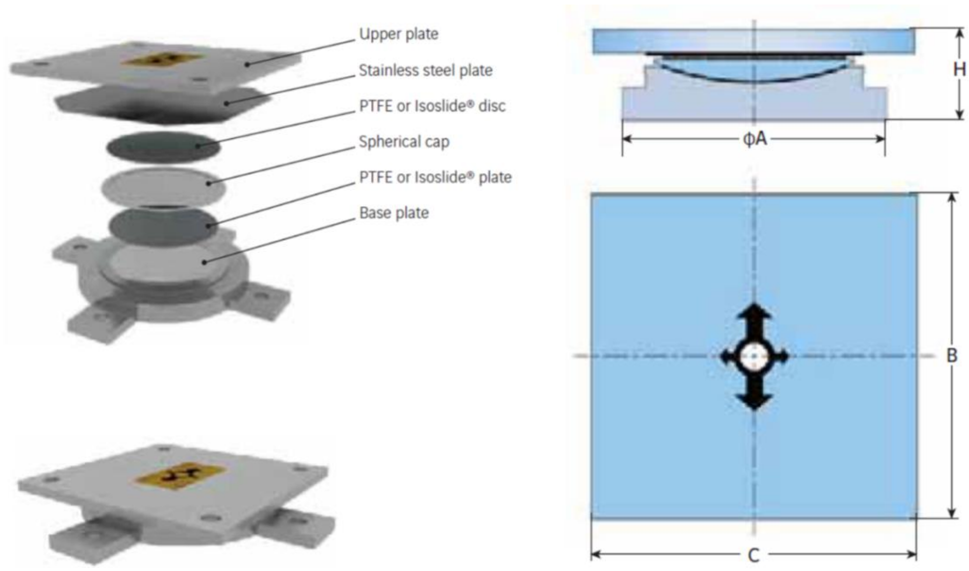

Figure 2.17. Free spherical bearing. (RCV4 Freyssinet Mechanical Bearings).

Spherical bearings stand out as superior installations due to their remarkable ability to bear vertical loads and their flexibility, enabling extensive rotation and horizontal movement (see Figure 2.18).

Figure 2.18. Spherical Bearings before Installation.

PTFE (polytetrafluoroethylene), a prominent polymer of note, boasts a repertoire of distinctive attributes. Its coefficient of friction, capable of descending to an astonishingly low value of 0.01 when subjected to sliding against a meticulously polished surface, draws a compelling parallel to the friction encountered between sheets of ice. Moreover, a noteworthy facet of PTFE is its propensity to manifest the least coefficient of friction when confronting the most elevated specific pressures, rendering it an exceedingly judicious selection for applications involving structural bearings (as illustrated in Figure 2.19). This unique amalgamation of qualities underscores the aptitude of PTFE as an optimal material choice, firmly establishing its efficacy within the realm of structural engineering, particularly in the realm of bearing systems.

Figure 2.19. PTFE at Sliding Bearing.

2.2. Isolation System Design Properties:

In the Introduction, we will elucidate the modeling process of rubber bearings. Figure 3.20 presents a straightforward depiction of a bilinear representation of rubber bearings, predominantly leather bearings. However, how do these bearings actually behave?

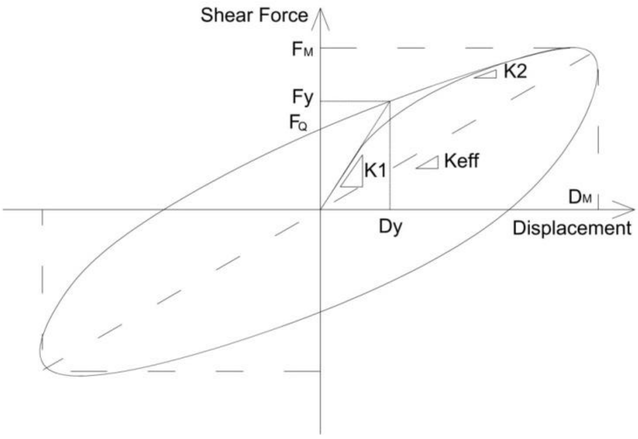

Figure 2.20. Bilinear representation of rubber bearing.

The initial branch portrays the elastic stiffness or initial stiffness, noticeable only during the initial loading phase. Subsequently, the isolator transitions into the secondary slope or secondary sequence branch, characterized by a force-displacement relationship.

The effective stiffness K_{eff} is calculated by Equation (2.1):

$$Keff = \frac{|F\Delta+| + |F-|}{|\Delta+| + |\Delta-|} \qquad (2.1)$$

Where: F^+ and F^- are the maximum and minimum forces at the maximum positive displacements Δ^+ and minimum negative displacements Δ^- respectively.

Characteristic Strength for the rubber isolation unit (FQ): calculated by the yielding of the rubber using the Equation (2.2)

$$FQ = Ap * \tau yp \qquad (2.2)$$

τ yp = Nominal Shear Stress for the rubber.

Ap = Cross-sectional Area for the rubber.

Yielding Force of the rubber isolation unit (Fy): calculated by Equation (2.3)

$$\text{Fy} = \frac{\text{FQ} * \text{K1}}{\text{K1} - \text{K2}} \tag{2. 3}$$

Where

FQ = Characteristic Strength for the rubber isolation unite.

K1 = the elastic stiffness of the rubber isolation unite.

K2 = the post yielding stiffness of the rubber isolation unite.

Yielding Displacement of the rubber isolation unite (Dy): fined by Equation (2.4)

$$\text{Dy} = \frac{\text{Fy}}{\text{K1}} \tag{2. 4}$$

Where

Fy = the yield force of the rubber isolation unite.

K1 = the elastic stiffness of the rubber isolation unite.

During the design of rubber bearings using software like SAP2000 (or any similar program), we typically employ the bilinear representation, encompassing the initial and secondary stiffness. Understanding all components of this representation facilitates straightforward modeling of lead or rubber bearings.

The first branch, k1, signifies the initial stiffness, which relies on the secondary stiffness and the lead plaque's properties. The secondary stiffness, in turn, is contingent solely on the rubber compound. This implies that altering the isolator's size or the rubber compound's shear modulus can modify the secondary stiffness. Calculating the initial stiffness is achievable by multiplying the secondary stiffness by a factor of 10. Additionally, k1 can be determined from the yield force and displacement. If the lead plug's area is known and multiplied by its shear strength, the characteristic strength can be calculated. Using similarity equations, Fy yield force can be deduced. With knowledge of Fy and the initial stiffness, yield displacement can be computed, thereby establishing the bilinear representation. Incorporating this process into software, such as SAP2000 in this thesis, enables seismic isolator analysis.

In the design process, we begin with an equivalent linear analysis, followed by a non-linear time history analysis. Since rubber behavior is highly non-linear, non-linear time history analysis is essential. We consistently compare results from non-linear time analysis with those from equivalent linear analysis. For equivalent linear analysis, determining the equivalent damping of the isolation system is crucial. This damping relies on the energy dissipated within a cycle, which can be computed by calculating the area under the energy dissipation cycle. Treating this area as a trapezoid provides insight into the energy dissipated per cycle (see Figure 2.21).

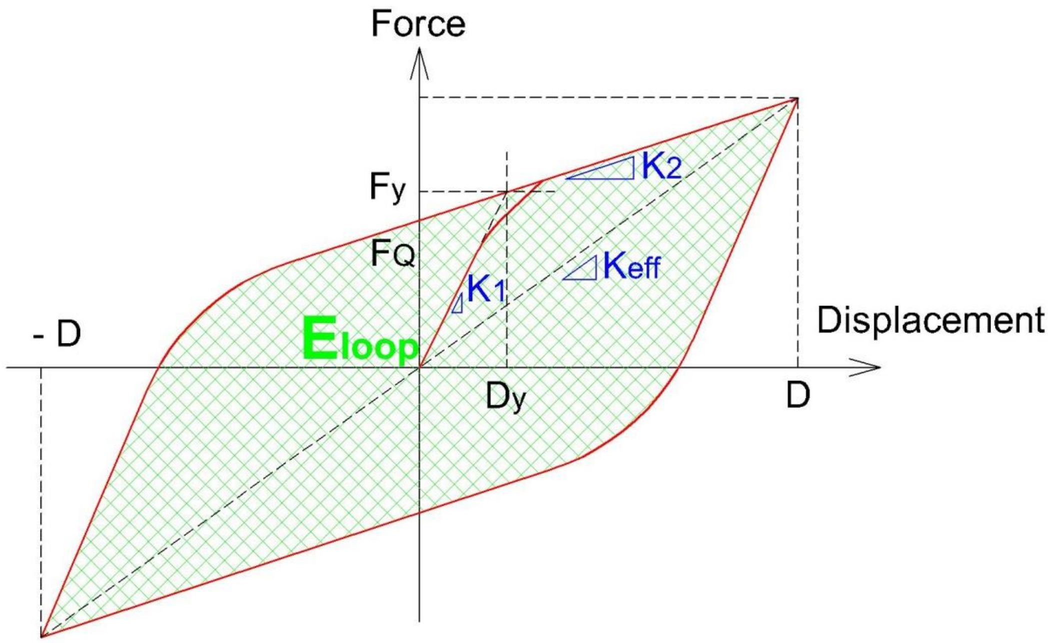

Figure 2.21. E_{loop} the energy dissipated per cycle of loading.

$$Beff = \frac{2}{\pi} \frac{Eloop}{Keff(|\Delta +| + |\Delta -|)2} \quad (2.5)$$

Where

B_{eff} = the effective damping of the isolation system at the maximum displacement.

K_{eff} = the effective stiffness is calculated by Equation (2.1).

By employing the provided formulas, we can compute the equivalent damping for our structure. Referring to the American code ASCE Table 2.1, if the damping is 20, it permits a reduction of the percent acceleration spectrum by 1.5. For instance, with a five percent damping utilized in our design, the reduction factor is one. If the damping is twenty percent, the factor becomes 1.5, while if it exceeds fifty percent, the reduction factor

Table 2.1. Damping Factor, BM. (ASCE 7-22)

Effective Damping, βM (percentage of critical)[a,b]	B_M Factor
≤2	0.8
5	1.0
10	1.2
20	1.5
30	1.7
40	1.9
≥50	2.0

[a] The damping factor shall be based on the effective damping of the isolation system.
[b] The damping factor shall be based on linear interpolation for effective damping values other than those given.

2.3. Advantages of seismic isolation:

During moderate to large earthquakes, codes and studies indicate that isolated structures are anticipated to exhibit significantly superior performance compared to fixed-base structures. Table 2.2 of ASCE-7-22 contrasts the expected behavior and performance of isolated base structures with that of fixed-base structures.

Table 2.2. Expected Performance for fixed and isolated building during Earthquakes. (ASCE 7-22)

Performance Measure	**Earthquake Ground Motion Level***		
	Minor	**Moderate**	**Major**
Life safety: Loss of life or serious injury is not expected	F,I	F,I	F,I
Structural damage: Significant structural damage is not expected	F,I	F,I	I
Nonstructural damage: Significant nonstructural or content damage is not expected	F,I	F	F

*F Indicates fixed-base, I indicates isolated.

Seismic isolation is anticipated to safeguard the building and its facilities, preserving operational functionality, and mitigating both structural and nonstructural damage.

We can summarize the advantages of seismic isolation as following:

1- Enhances seismic performance
2- Accelerates the return to service after the earthquake
3- Positive viewed by the public
4- Improves design capability and adaptability
5- Gives confidence in obtaining regulatory approval despite the uncertainty around the seismic hazard.

2.4. Disadvantages of seismic isolation:

We can summaries the disadvantages of seismic isolation as following:

1- Limited knowledge of seismically isolated structures.
2- Lack of experienced staff (designers, skilled laborers, etc.).
3- Perhaps increased costs are required in order to improve performance.
4- Delicate Strict codes requirements for the designing, testing, and execution of isolation systems.

2.5. Review of Previous Experimental Studies of Isolated Frame:

The Earthquake Engineering Research Center (EERC), now referred to as PEER, the Pacific Engineering Research Center at the University of California, Berkeley, initiated research on natural rubber bearings for earthquake isolation in 1976. Directed by Professor James M. Kelly, graduate students at EERC played a vital role in making substantial theoretical and experimental contributions to this study.

While the concept of base isolation wasn't entirely novel at that time, a few ideas involving sliders or rollers had been proposed. However, most of the structural engineering community deemed it highly impractical. The study began with a modest experiment using a three-story, single-bay, 20-ton model equipped with a set of custom-made, extremely low-modulus rubber bearings. Shaking table tests revealed that isolation bearings could lead to acceleration reductions of up to 10 times compared to conventional designs. As intended, the isolation system would undergo all deformation, causing the model to behave as a rigid body.

In 1978, a more impactful demonstration of the isolation concept was achieved. A 5-story, 3-bay model, closer to real-world conditions and weighing 40 tons, was utilized. This model incorporated damping-enhanced bearings produced through industrial techniques. Extensive investigations of the 5-story frame indicated that the utilization of rubber bearings for isolation could significantly diminish the accelerations experienced by internal equipment, surpassing the reductions observed in the structure itself.

Nonetheless, identical tests exposed that incorporating supplementary elements to enhance the damping ratio and increase damping—such as frictional systems, introducing lead plugs into the bearings, or utilizing steel energy-absorbing devices—did not result in reduced equipment acceleration. These additions triggered responses in higher modes of the structure, impacting the equipment. It became evident that enhancing damping within the rubber itself was the most effective approach.

In 2011, Benzoni et al. reported on the effects of the 2011 Tohoku-Pacific Earthquake on seismic isolation methods. The earthquake, measuring 9.0 on the Richter scale, struck on March 11, 2011. The Shimizu Corporation's Institute of Technology in Tokyo featured three distinct buildings, each utilizing different types of seismic isolation techniques. These structures employed a variety of methods for seismic isolation.

1- The column-top seismic isolation (CTSI) system is used in the Main Building.
2- Core suspended isolation (CSI) technology is being used in the Safety and Security Center.
3- Using a partly floating seismic isolation (PFSI) technique for the Wind Tunnel Testing Laboratory tests wind tunnels.

Tohoku University, in collaboration with Shimizu Corporation, erected a seismic isolation test building on the Sendai campus in Miyagi prefecture. This location was in close proximity to the epicenter of the 2011 Tohoku–Pacific Earthquake.

The earthquake responses of the four seismically isolated buildings affected by the 2011 Tohoku-Pacific Earthquake provided validation for the efficacy of the seismic isolation techniques employed. Recorded floor accelerations in each of the three institute buildings utilizing seismic isolation were reduced by approximately fifty percent compared to conventionally grounded floors. Comparatively, the roof accelerations in Tohoku University's test seismic isolated building were diminished by roughly one-third.

The observed vertical responses in seismically isolated buildings highlight that seismic isolation techniques may not effectively mitigate vertical movements. This consideration becomes crucial in the design of long-span and suspended structures, where vertical response amplification in a building must be taken into account.

In an article titled "Rubber Bearing Isolation for Structures Prone to Earthquake - A Cost Effectiveness Analysis" Islam(date of publıcation)), published in Earthquakes and Structures in October 2020, the cost implications of isolation systems were explored. The study concluded that the base isolation technique effectively reduces structural responses, significantly mitigating the impact of lateral loads on multi-story buildings. Although seismic isolators raise building costs and installation expenses, the higher expense can be partially offset by the reduced steel reinforcement costs on upper floors. Consequently, the diminished need for reinforcement leads to overall cost savings. However, these savings depend on building height, and the rate of cost reduction diminishes with an increasing number of stories.

Isolators are advantageous for achieving reduced member sections, allowing for potential downsizing of structural components or steel reinforcement while still meeting safety and serviceability criteria of local design codes. This reduction in construction materials also mitigates the environmental impact of resource extraction, such as rock blasting and iron ore mining. Architecturally, smaller structural members can enhance the aesthetic appeal of multi-story buildings, while also increasing their usable clear

To validate the optimization, additional isolation systems could be introduced. Further research might involve static pushover analysis to examine multi-story building responses to seismic activity, supplementing existing studies. The chosen buildings were strategically placed on soft to medium site soil, aligned with site-specific bilateral earthquake data for free field ground shaking. However, caution is crucial to avert resonance effects in structures on soft soils during prolonged seismic excitations, especially those with long periods.

In a conference paper titled "Seismic Isolation Systems in Structures - The State of Art Review" by Tafheem et al. (2015), the study explored isolation systems in structural buildings. It characterized isolation as a practical, logical, and effective approach to safeguarding against earthquake-induced accelerations. The paper's conclusion yielded the following insights:

1- Compared to a fixed-base structure, the structure's fundamental period increases when we use a proper base isolation system.

2- As the earthquake intensity becomes greater, the effectiveness of the base isolation system improves and increases.

3-A base-isolated system's efficacy is influenced by the nature/specification of the input excitations and the parameters of the isolation devices and superstructure. Therefore, it is imperative to conduct a thorough initial investigation to determine the effectiveness of a specific base-isolation system for a structure in relation to the local seismic map and the features of the expected earthquakes.

3. MATERIALS and METHODS:

3.1. Materials:

Steel Grade 50 will be used according to ASTM A992, the steel specifications clarified at the table 3.1.

Table 3.1. Steel specifications.

F_y (Mpa)	F_u (Mpa)	E (Mpa)	F_{ye} (Mpa)	F_{ue} (Mpa)
345.0	450.0	200,000.0	379.5	495.0

And defined at SAP2000 as following:

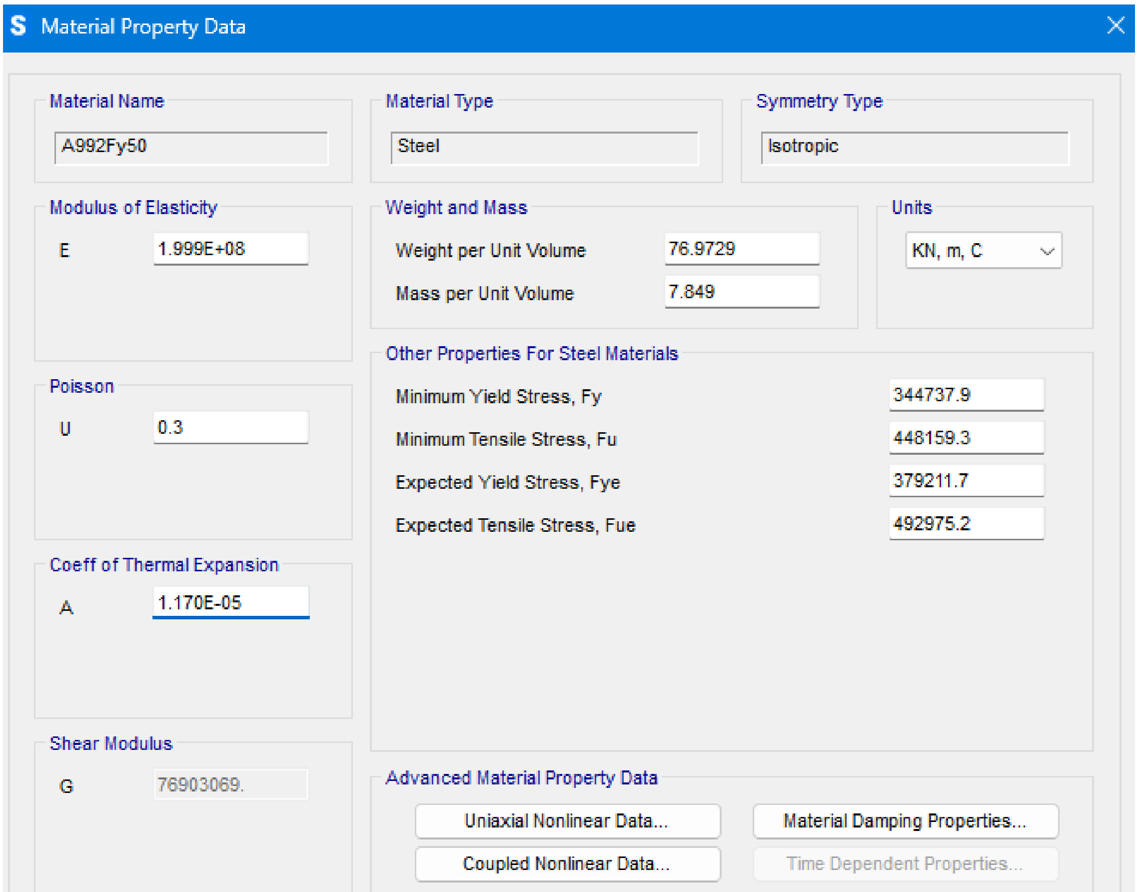

Figure 3.1. Steel specifications at SAP2000.

3.2. General Models Descriptions:

To comprehend the distinctions in earthquake load protection techniques for structural frames, we will utilize the SAP2000 program to model the frame twice. The first model will represent the conventional fixed base, while the second will depict the frame isolated using a base isolation system.

1- Conventional or Fixed Special Moment Resisting Frame (FF)
2- Isolated Special Moment Resisting Frame (IF)

3.2.1. Frame Type and Geometric Properties:

Extensive examination of the Conventional building was previously documented (Arat et al., 2022). The design details for the Conventional buildings are restated below for reference.

Table 3.2. Conventional building.

Building floors	Floor Hight (m)	Floor Area (m2)
4	4	1944(54x36)

The seismic-resistant system employs high ductility moment-resisting frames (süneklik düzeyi yüksek moment aktaran çerçeveler).

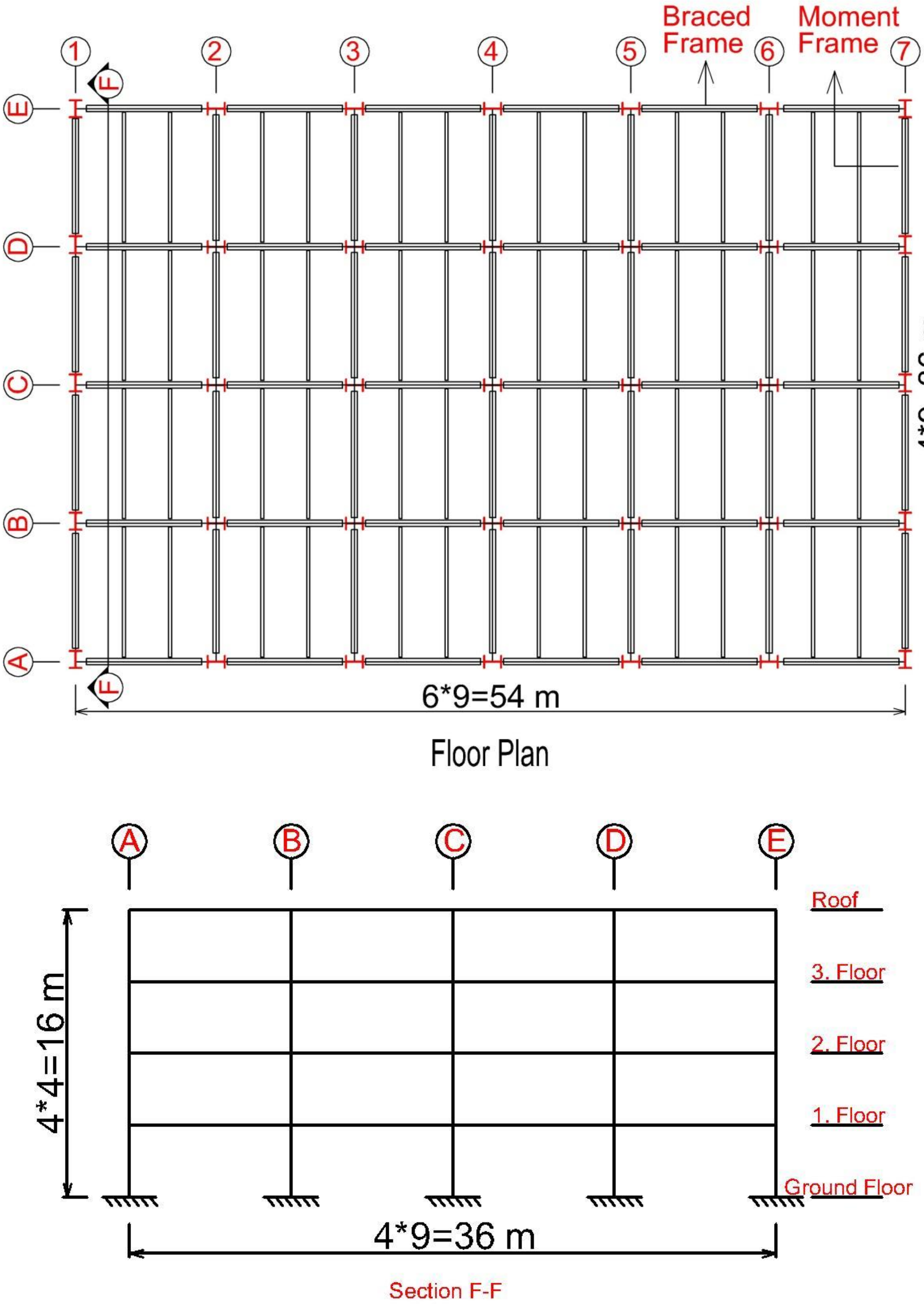

Figure 3.2. Frame type and geometric properties.

3.2.2. Loads:

The loads are calculated according to the Table 3.3. and Figure 3.3. as following:

Table 3.3. Conventional Building Loads.

Level	Type	Loads (KN/m^2)	Area(m^2)	Weight (KN)	Floor W_t (KN)
Roof	Steel construction	0.3	1944(54x36)		10,303.2
	Total Dead load	4.3		8,359.2	
	Live Load	1		1,944	
Typical Floor	Steel construction	0.3			16,135.2
	Total Dead load	5.3		10,303.2	
	Live Load	3.0		5,832	

The beams and columns load distribution as showing in Figure 3.3:

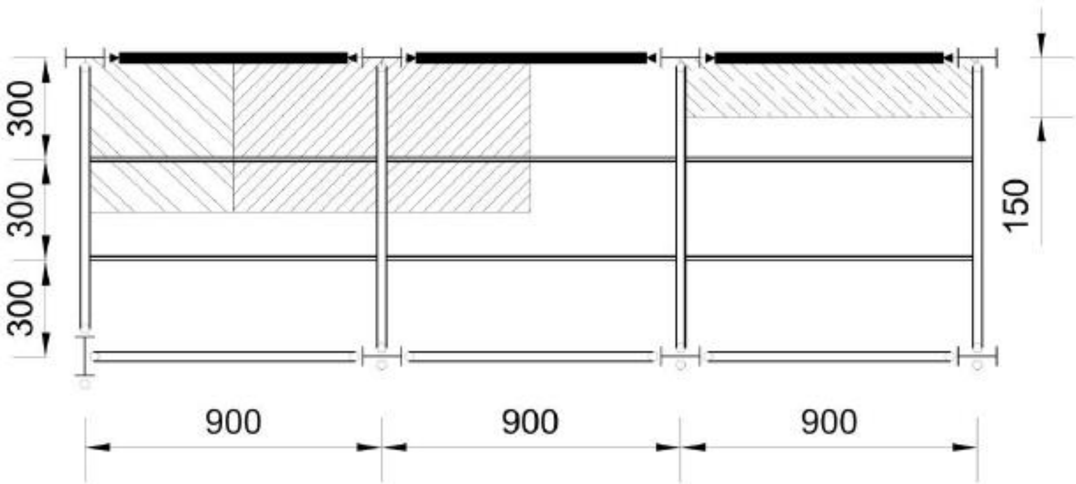

Figure 3.3. Frame's Loaded Area.

$q1_{DD}$= 4.30 KN/m2 * 1.50 m = 6.45 KN/m

$q1_{LL}$= 1.0 KN/ m2* 1.50 m = 1.5 KN/m

$q2_{DL}$= 5.30 KN/m2* 1.50 m = 7.95 Kn/m

$q2_{LL}$= 3.0 KN/ m2* 1.50 m = 4.50 KN/m

$P1_{DL}$ = 4.3 KN/m2 * ((4.50 m* 4.50 m) – (1.50 m*4.50 m)) = 58.0 KN

$P1_{LL}$ = 1.0 KN/m2 * ((4.50 m*4.50 m) – (1.50 m*4.50 m)) = 13.5 KN

$P2_{DL}$ = 2.0 x $P1_{DL}$ = 116.0 KN

$P2_{LL}$ = 2.0 x $P1_{LL}$ = 27.0 KN

$P3_{DL}$= 5.3 KN/m2 * ((4.50 m*4.50 m) –(1.50 m*4.50 m)) = 71.55 KN

$P3_{LL}$ = 3.0 KN/m2 * ((4.50 m*4.50 m) –(1.50 m*4.50 m)) = 40.5 KN

$P4_{DL}$= 2.0 x $P3_{DD}$ = 143.1 KN

$P4_{LL}$= 2.0 x $P3_{LL}$ = 81.0 KN

Table 3.4 Frame loads.

Level	Type	Point Loads (KN)	Distributed loads (KN/Lm)	Weight(KN)
Roof	Total Dead load	58*2+116*3	6.45*9*4	696.2
	Live Load	13.5*2+27*3	1.5*9*4	162
Typical Floor	Total Dead load	71.55*2+143.1*3	7.95*9*4	858.6
	Live Load	40.5*2+81*3	4.5*9*4	486
The effective seismic weight W= 696.2 + 3*858.6 = 3272 KN				

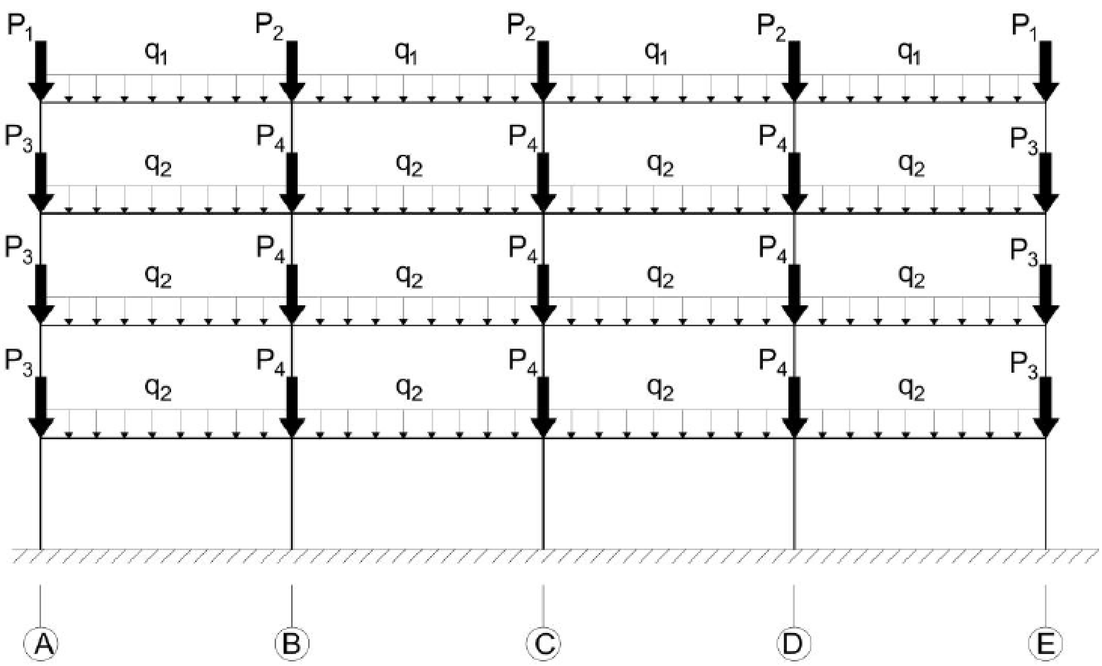

Figure 3.4 Frame elevation loads.

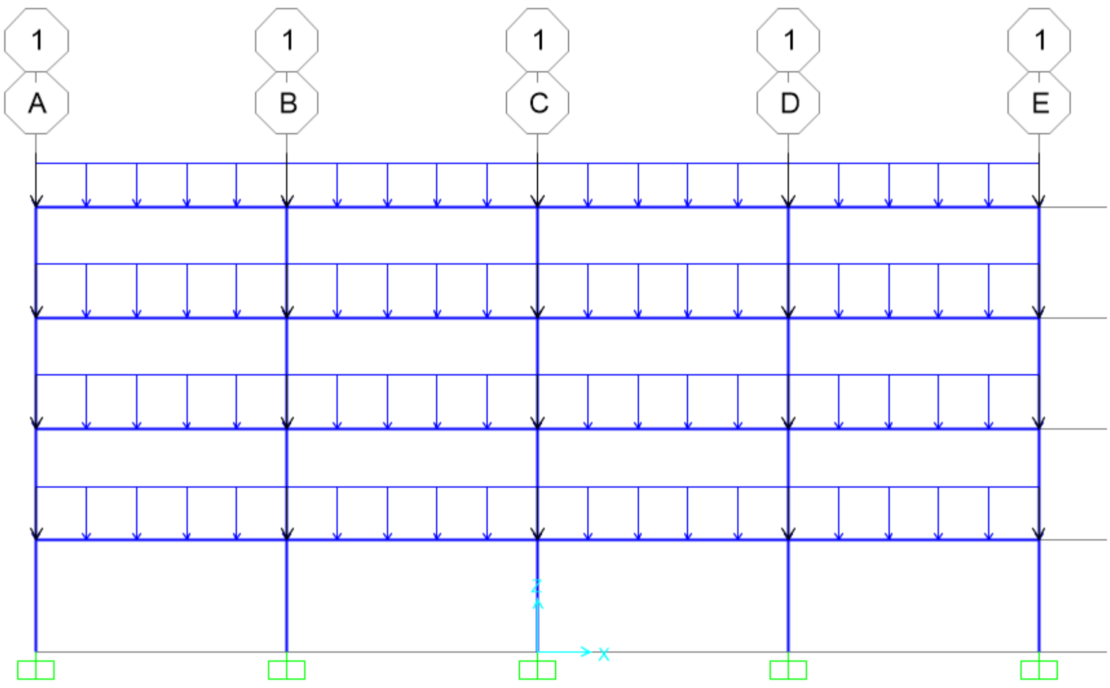

Figure 3.5. Frame elevation loads at SAP2000.

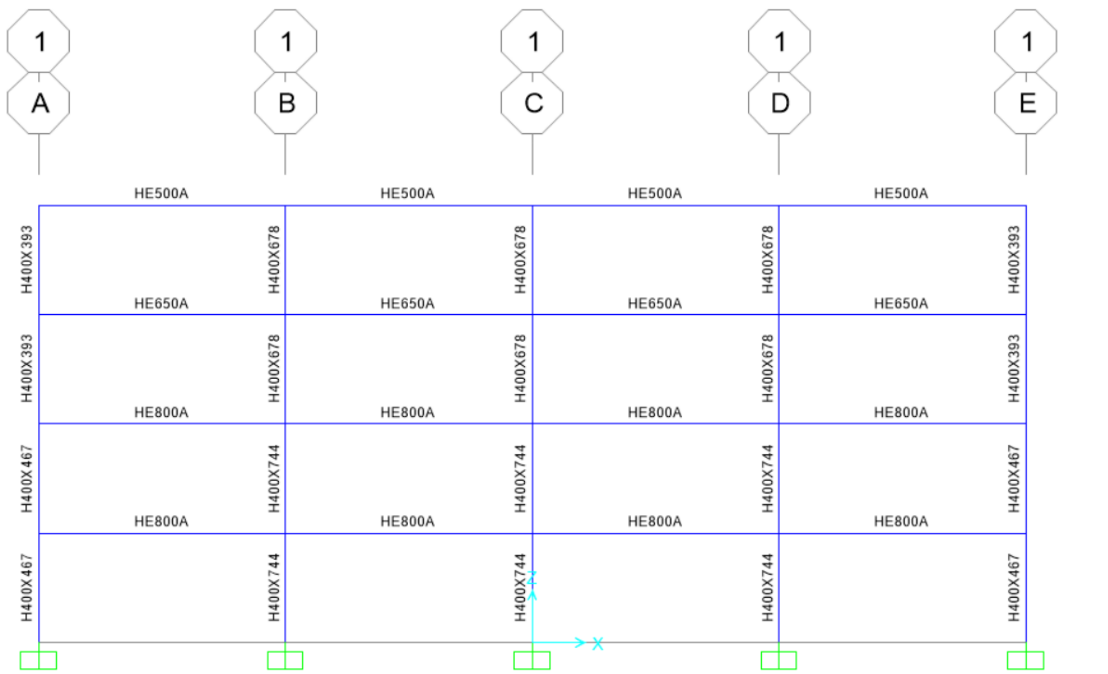

Figure 3.6. Frame elevation sections.

3.2.3. Seismic Loads and Seismic Design Criteria:

Seismic loads and seismic design criteria are determined following the guidelines outlined in the ASCE 7-22 standard. This standard provides instructions for calculating the forces exerted by seismic activity and establishes criteria for designing structures to withstand these forces.

Risk Category of Building: II (ASCE_7_22 Table 1.5 - 1)

Importance Factor (I) = 1 (Offices) (ASCE_7_22 Table 1.5 - 2)

Site Class : B Medium hard rock (ASCE_7_22 Table 20.2 - 1)

According to ASCE_7_22 we found the seismic design criteria as show Table 3.5.

Table 3.5. Building Seismic Coefficients and Factors According ASCE7-22.

Seismic Coefficients and Factors	Value
0.2 Sec Spectral Acceleration (S_S)	2.29 Unitless
1 Sec Spectral Acceleration (S_1)	0.869 Unitless
Long-Period Transition Period	8 Second
Site Class	B
Site Coefficient (F_a)	0.9 Unitless
Site Coefficient (F_v)	0.8 Unitless
Calculated Coefficient $S_{DS}=(2/3)*F_a*S_s$	1.374 Unitless
Calculated Coefficient $S_{D1}=(2/3)*F_v*S_1$	0.4635 Unitless
Response Modification Factor (R)	8 Unitless
System Overstrength Factor, Omega (Ω)	3 Unitless
Deflection Amplification Factor (C_d)	5.5 Unitless
Occupancy Importance Factor (I)	1 Unitless

3.3. The Methods:

3.3.1. Isolation System Design:

The design of isolation system components must adhere to predefined performance criteria. This encompasses the selection of suitable isolator properties (such as stiffness and damping), the sizing of bearings or pads, and the confirmation of compatibility with the structure. The integration of the isolation system into the broader building design necessitates consideration of architectural, structural, and mechanical aspects, with meticulous attention to preventing interference with other building components.

Subsequent to the integration phase, dynamic analysis is conducted to evaluate the interaction between the building and the isolation system during seismic events. This process serves to validate the alignment of the isolation system's behavior with the established performance criteria. In the dynamic analysis phase, calculated seismic loads are applied to the isolated structure to assess its response. This assessment is carried out by ensuring that the building remains within predefined limits pertaining to factors such as displacements, accelerations, and other relevant performance benchmarks.

In accordance with the outlined procedure, this thesis commenced by calculating the Characteristic Strength of the isolation system, denoted as FQ. This strength is estimated to fall within the range of approximately 10% to 20% of the effective seismic weight of the structure. In the specific frame under examination, the effective seismic weight (W) has been ascertained as 3272 KN, as documented in Table 3.4. As a result, the projected interval for the Characteristic Strength (FQ) is expected to span between 327.2 KN and 654.4 KN. Since there are five isolation units situated beneath the frame, the Characteristic Strength of each separate isolation unit can be derived by dividing the Characteristic Strength of the isolation system by five. Consequently, a spectrum of 65.44 KN to 130.88 KN is established for the Characteristic Strength of each individual isolation unit.

Next, the effective period (represented as TM) of an isolated building or structure, particularly at the displacement DM in the designated direction of concern, is computed. Based on the analysis performed utilizing SAP2000, the elastic period of the fixed-base frame is determined to be 0.4647 seconds. Hence, in the case of the isolated frame, the effective period (TM) is expected to fall within a range exceeding 3 times the value of 0.4647 seconds (equivalent to 1.394 seconds) and being less than 5 seconds. This particular criterion bears significance when contemplating the application of the Equivalent Lateral Force (ELF) methodology.

Finally to compute the effective stiffness of the isolation system Equation (3.1) is used

$$\mathrm{TM} = 2\pi \sqrt{\frac{W}{KM * g}} \tag{3.1}$$

Where, W represents the effective seismic weight of the structure positioned above the isolation interface, as computed in Table 3.4, and it amounts to 3272 KN. KM stands for the effective stiffness of the isolation system at its maximum displacement. The measurement unit for effective stiffness is (KN/mm). g refers to the acceleration resulting from gravity, and its units are in millimeters per second squared (mm/s²). The computation results in the maximum effective stiffness value for the isolation system, which is found to be KM = 6.776 KN/mm. As there are five isolation units beneath the frame, we can determine that the maximum effective stiffness value for a single isolation unit will be obtained by dividing the maximum effective stiffness value of the isolation system by five, as demonstrated below.

$$\text{KM for isolation unite} = \frac{KM\ for\ isolation\ system}{5} = \frac{6776}{5} = 1355.2\ N/mm$$

By substituting the maximum value of TM (5 seconds) into Equation (3.1), we obtain the minimum value for the effective stiffness (KM) of the isolation system, which results in KM = 0.5267 KN/mm. This calculation adheres to the condition set by the effective period TM and the characteristics of the structure. Considering the scenario with five isolation units positioned beneath the frame, the minimum effective stiffness value assigned to an individual isolation unit will be determined by dividing the minimum effective stiffness value attributed to the entire isolation system by five. This division ensures a uniform distribution of stiffness characteristics among the five isolation units, leading to an effective KM for each isolation unit equal to 105.34 N/mm, as demonstrated below.

$$\text{KM for isolation unite} = \frac{KM\ for\ isolation\ system}{5} = \frac{526.7}{5} = 105.34\ N/mm$$

Taking into account the ranges obtained for both FQ (which ranges from 130 KN to 65 KN) and KM (ranging from 1355 N/mm to 105 N/mm), it can be inferred that the displacement will likely fall within the approximate range of 95 mm to 619 mm. This inference is based on Equation (3.2).

$$\mathrm{D} = \frac{F}{K} \tag{3.2}$$

Where F represents the applied force acting on the rubber isolation unit. K signifies the elastic stiffness of the rubber isolation unit.

This encompasses the selection of suitable isolator properties (such as stiffness and damping), the sizing of bearings or pads, and the confirmation of compatibility with the structure.

3.3.2. Evaluating the performance of the isolation units:

We utilized the Abaqus software program to formulate and optimize the design of three different types of isolation units. This was done while considering three levels of stiffness for the rubber properties: low, medium, and high. Our objective is to ascertain the design properties related to the rubber bearing and to comprehend the seismic behavior of the isolation units.

During the modeling stage of the isolation units in Abaqus, we took into account the geometry of the isolation units as illustrated in Figure 3.7.

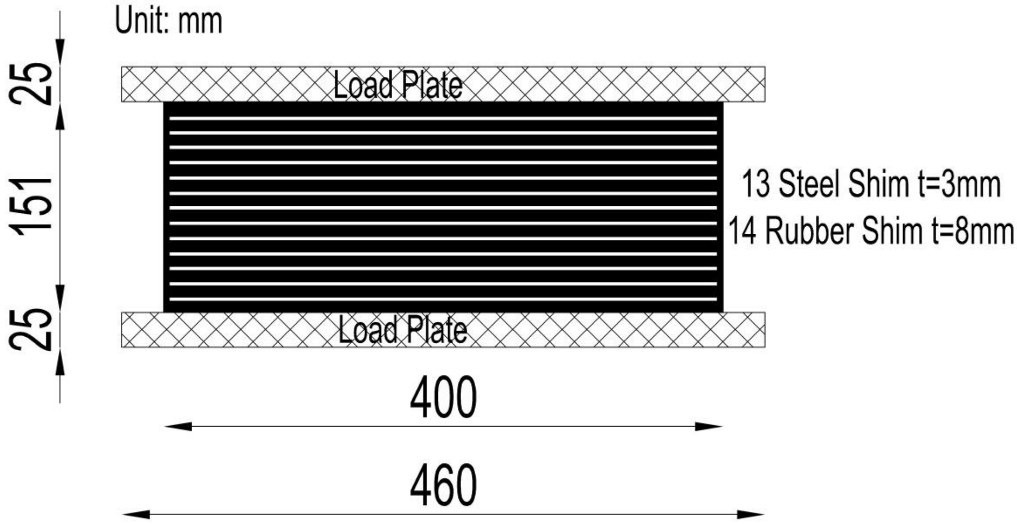

Figure 3.7. Rubber Bearing dimensions (mm).

Modeling and Material Characterization:

The inception of our modeling endeavor involves the meticulous creation of essential components, including the load plate, rubber shim, and steel shim. This preliminary stage lays the foundation for our subsequent analysis, enabling us to delve into the intricate mechanical interplay of these components under varying loading scenarios.

Defining Material Properties:

In our study, the properties of steel were defined in accordance with ASTM A36, which specifies the requirements for structural steel. ASTM A36 steel is characterized by a yield strength of 250 Mpa

Subsequently, our focus extends to the realm of rubber materials, essential constituents endowed with remarkable elasticity. We opt for a robust material model, the Mooney-Rivlin model, renowned for its prowess in encapsulating the intricate mechanical behavior of rubber-like materials. This hyperelastic model, conceived by M. Mooney and S. Rivlin, offers a mathematical avenue to portray stress-strain relationships within these materials, particularly as they traverse finite deformations.

The Mooney-Rivlin model finds its mathematical expression in terms of strain energy density (W), intricately tied to strain invariants (I1 and I2). Its formulation takes the following form:

$$W = C10 * (I1 - 3) + C01 * (I2 - 3) \tag{3.3}$$

Where:

W symbolizes the strain energy density.
C10 and C01 stand as the defining material constants.
I1 corresponds to the first strain invariant, intrinsically linked to principal stretches.
I2 embodies the second strain invariant, intricately connected to the principal stretches as well.

This model facilitates a nuanced simulation of rubber material behavior across a spectrum of strains. By fitting empirical data, engineers discern the precise values of material constants C10 and C01 tailored to specific rubber compositions. These constants, in turn, unravel the material's innate properties—its stiffness, elasticity, and resistance to deformation.

However, it is vital to acknowledge that the Mooney-Rivlin model represents a simplification of rubber's multifaceted behavior. This is especially pronounced in the realm of higher strains, where nonlinear phenomena and strain-softening effects may influence the material's response. Therefore, while the Mooney-Rivlin model is a valuable tool, its accuracy is contingent upon the specific rubber material and the range of deformation under consideration.

The shear modulus (G), a paramount parameter, can be interlinked with the Mooney-Rivlin constants. This nexus unfolds as:

$$G = 2 * (C10 + C01) \tag{3.4}$$

Given the Freyssinet company's provision of rubber materials with shear moduli spanning from 0.25 Mps to 1 Mpa, our analysis incorporates this variability. Thus, our material characterization echoes through the intricate details encapsulated in Figures 3.8 to 3.12 a meticulous portrayal of the interplay between material constants, shear moduli, and the ensuing mechanical responses.

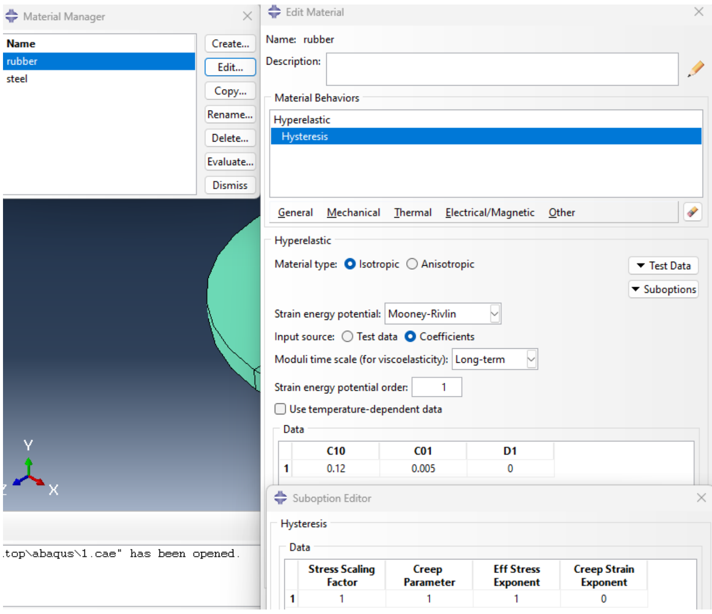

Figure 3.8. Low Stiffness Rubber properties.

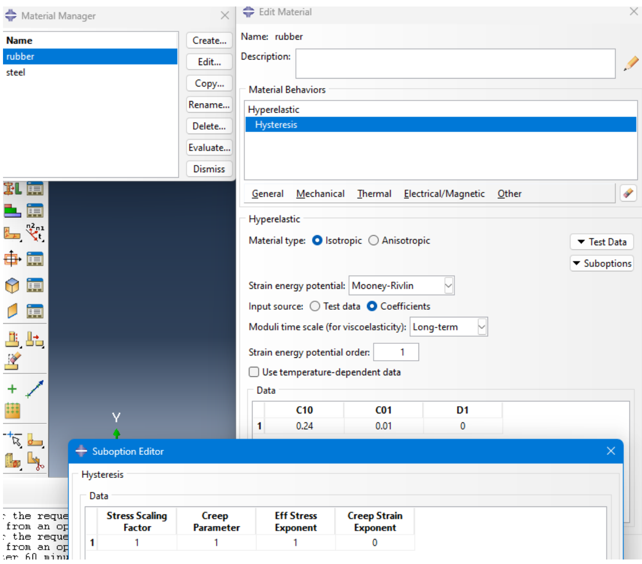

Figure 3.9. Medium Stiffness Rubber properties.

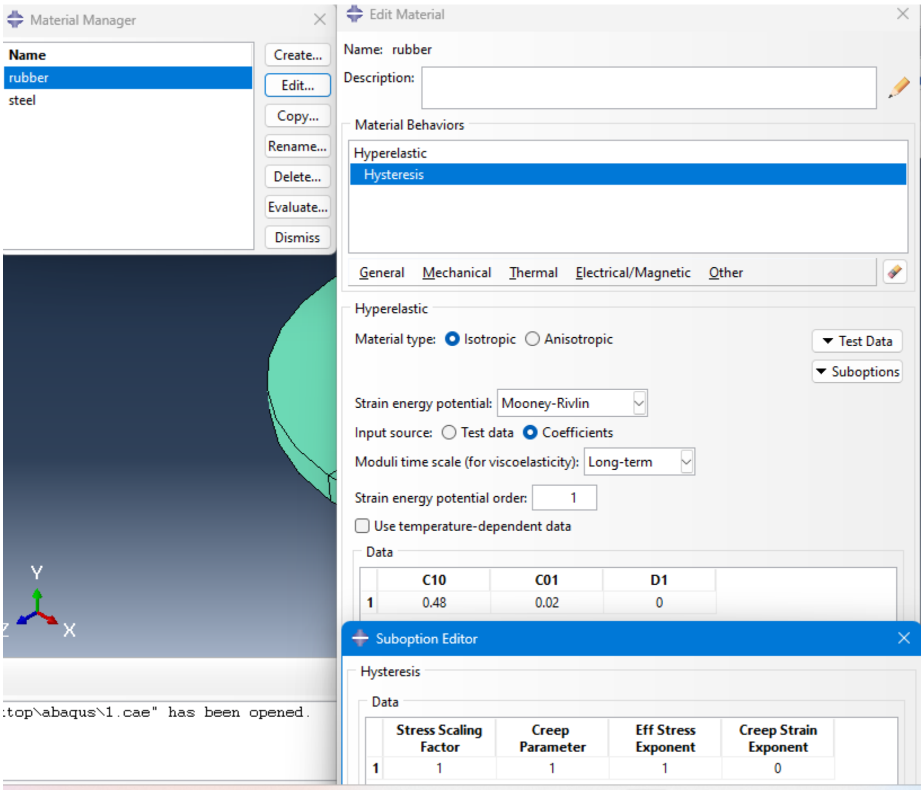

Figure 3.10. High Stiffness Rubber properties.

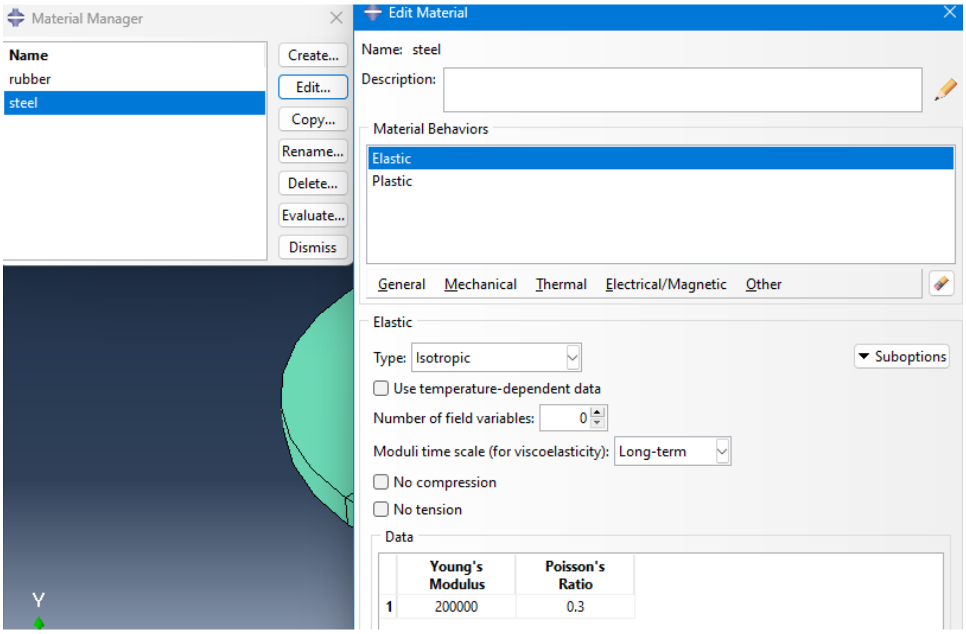

Figure 3.11. Steel elastic properties.

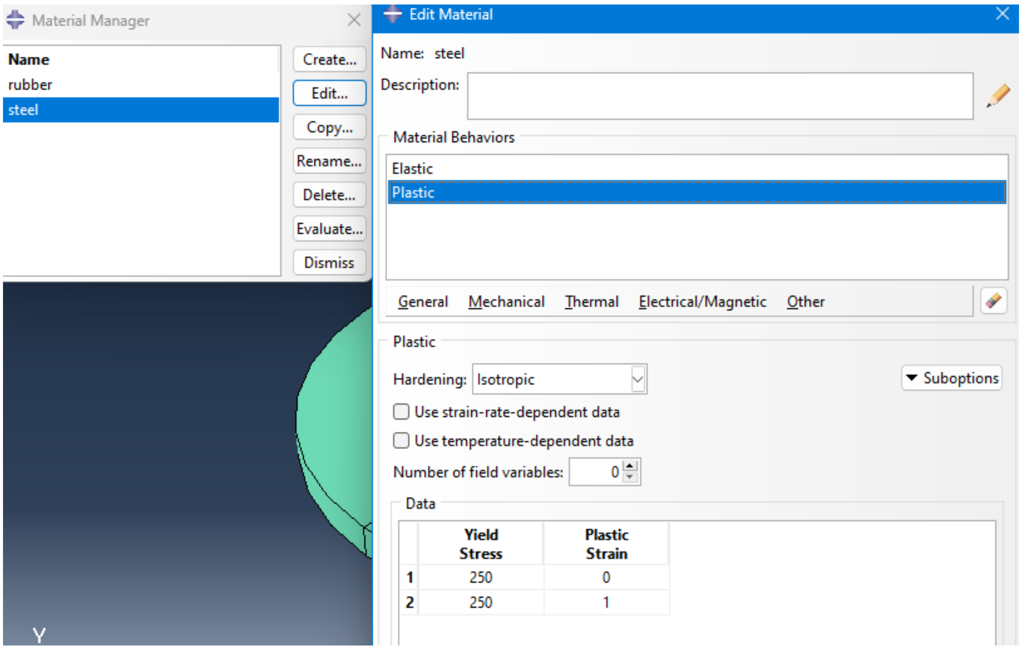

Figure 3.12. Steel plastic properties.

After assigning the properties, our next step will involve assembling the individual components. We will apply the steel properties to the load plate and steel shim, and assign the rubber properties to the rubber shim. To facilitate point selection and enhance part meshing, we suggest partitioning the components into four quadrants. This strategic division not only improves the model's geometry but also streamlines the meshing process. As a result, the model's appearance will resemble the representation shown in Figure 3.13.

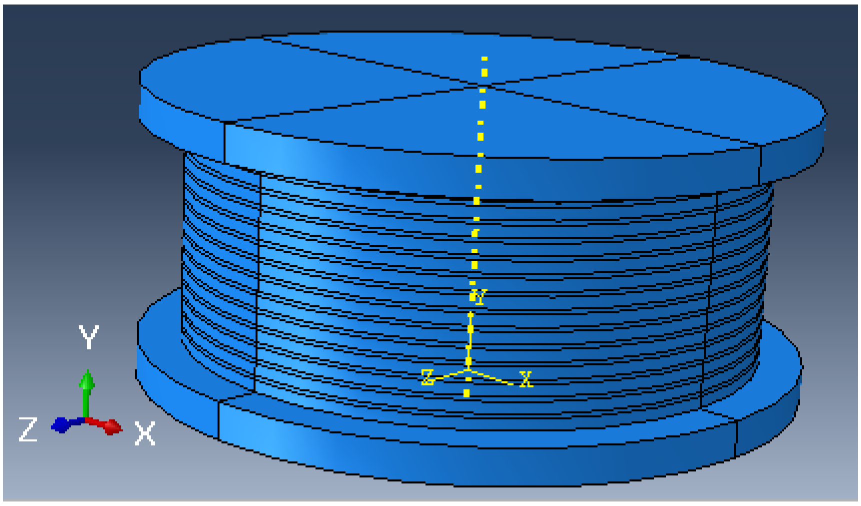

Figure 3.13. The rubber bearing model after parts assembly.

After the assembly and partitioning, our next phase involves defining two distinct analysis steps. The first step will focus on simulating the vertical load, while the subsequent step will address the cyclic load. You can refer to Figure 3.14 in the design documentation for visual clarification of these steps.

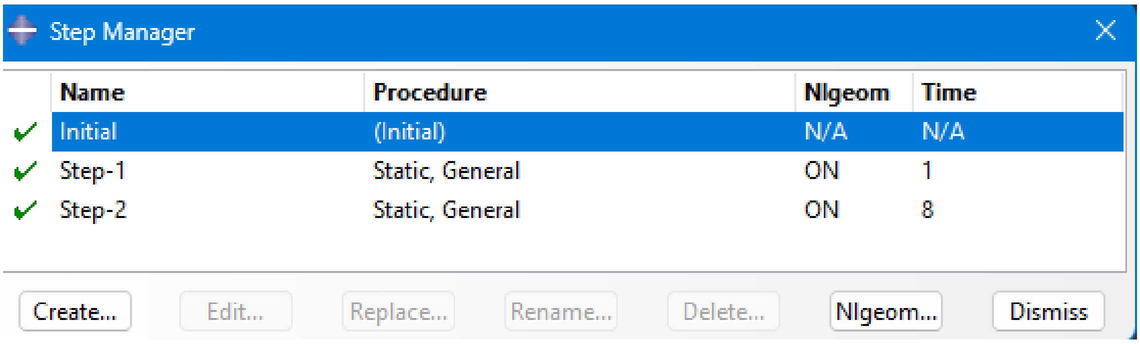

Figure 3.14. The Steps definition.

Once the load steps have been defined, the subsequent phase involves applying the loads. The vertical load magnitude, which has been determined using the SAP2000 model, is set at 900 KN. This load will be applied as a compressive force onto the load plate of the rubber bearing during Step 1. As per the preliminary design calculations, the expected displacement is projected to fall within the range of approximately 95 mm to 239 mm.

Moving forward to Step 2 of the analysis, a cyclic load will be introduced. This cyclic load will encompass both positive and negative displacements, each set at 260 mm, serving as an additional parameter.

After applying these loads, the model will undergo meshing procedures, which will be configured in alignment with the layout illustrated in Figure 3.15.

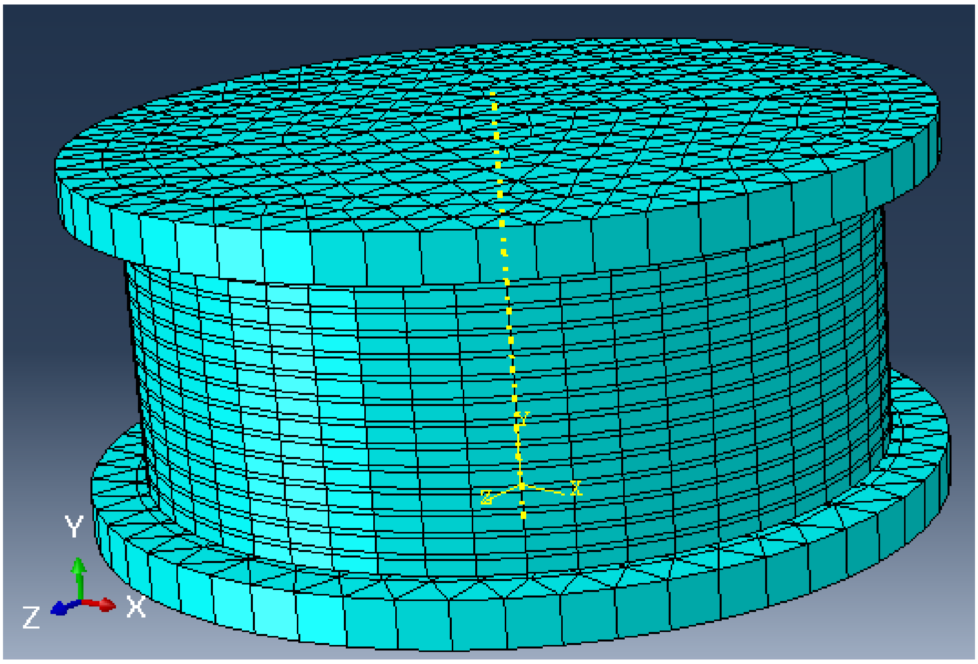

Figure 3.15. The rubber bearing model after mesh implementation.

Following these preparatory steps, the subsequent action involves the submission of the analysis job. This process aims to yield the essential results necessary for the determination of the design properties pertaining to the rubber bearing. The resulting counter plots in term of displacement are presented in Figure 3.16.

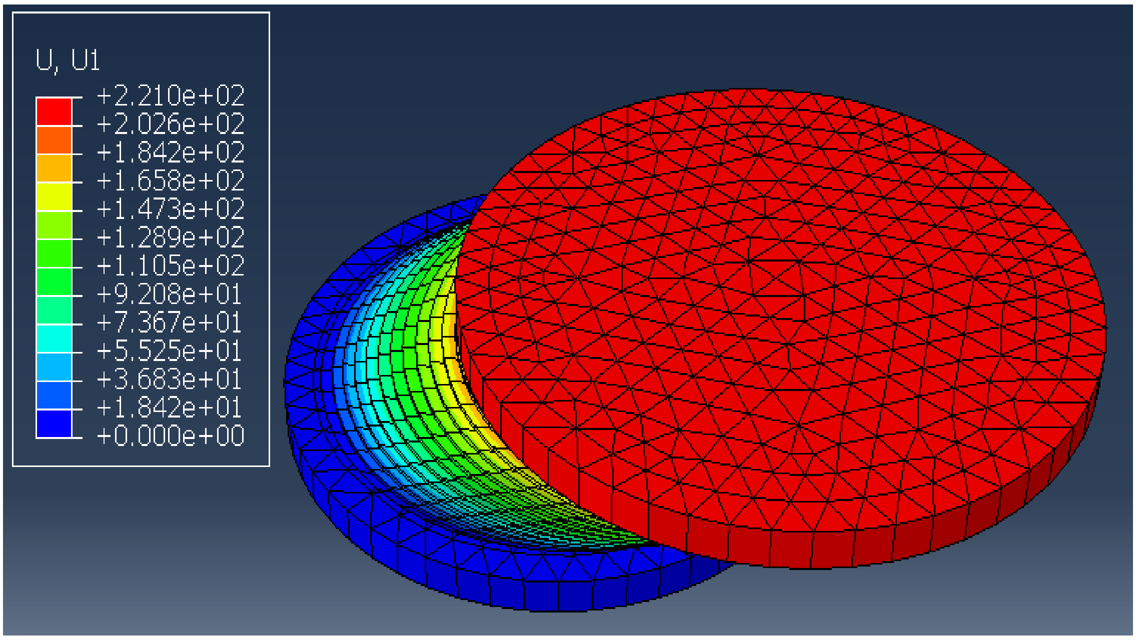

Figure 3.16. The rubber bearing model under maximum displacement.

Next, our focus shifts to generating a graphical representation that illustrates the relationship between displacement and force. This chart, depicted in Figure 3.17., provides a visual understanding of the system's behavior under the specified conditions. It aids in interpreting the analysis results and gaining insights from them.

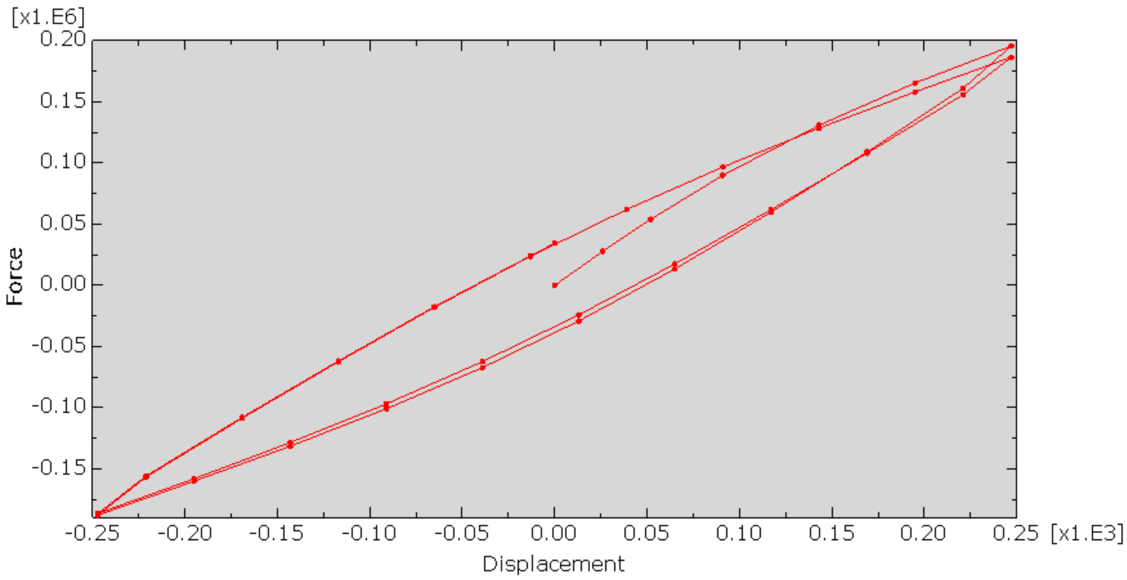

Figure 3.17. Chart Between The Displacements (mm) And the Force (N).

Moving forward, our next step involves extracting data from the generated chart, a crucial action for the subsequent calculation of the rubber bearing properties. This extracted data, from Abaqus analysis, for medium stiffness rubber bearing is meticulously organized and presented in Table 3.6. , as illustrated in Figures 3.18 and 3.20. This tabulated information serves as a fundamental foundation for determining the design attributes of the rubber bearing.

Table 3.6. Medium Stiffness Rubber bearing cyclic load, displacement (mm) and the force (KN).

First Cyclic Load			Second Cyclic Load	
Displacement (mm)	Force (KN)		Displacement (mm)	Force (KN)
0.00	0.00		0.00	34.51
26.00	27.73		39.00	62.02
52.00	54.02		91.00	96.70
91.00	89.87		143.00	128.41
143.00	130.83		195.00	158.05
195.00	165.42		247.00	186.46
247.00	195.53		221.00	155.81
221.00	161.00		169.00	107.89
169.00	108.96		117.00	61.81
117.00	59.77		65.00	17.46
65.00	13.32		13.00	-24.19
13.00	-29.21		-39.00	-62.31
-39.00	-67.15		-91.00	-96.85
-91.00	-100.88		-143.00	-128.46
-143.00	-131.47		-195.00	-158.04
-195.00	-160.10		-247.00	-186.41
-247.00	-187.72		-221.00	-155.79
-221.00	-156.68		-169.00	-107.90
-169.00	-108.62		-117.00	-61.85
-117.00	-62.47		-65.00	-17.51
-65.00	-18.03		-13.00	24.13
-13.00	23.75		0.00	34.40

Abaqus analyses are conducted to extract force-displacement data, as like in Table 3.6, for three types of rubber bearing systems. The force-displacement curves for these systems are then plotted in Figures 3.18 through 3.21.

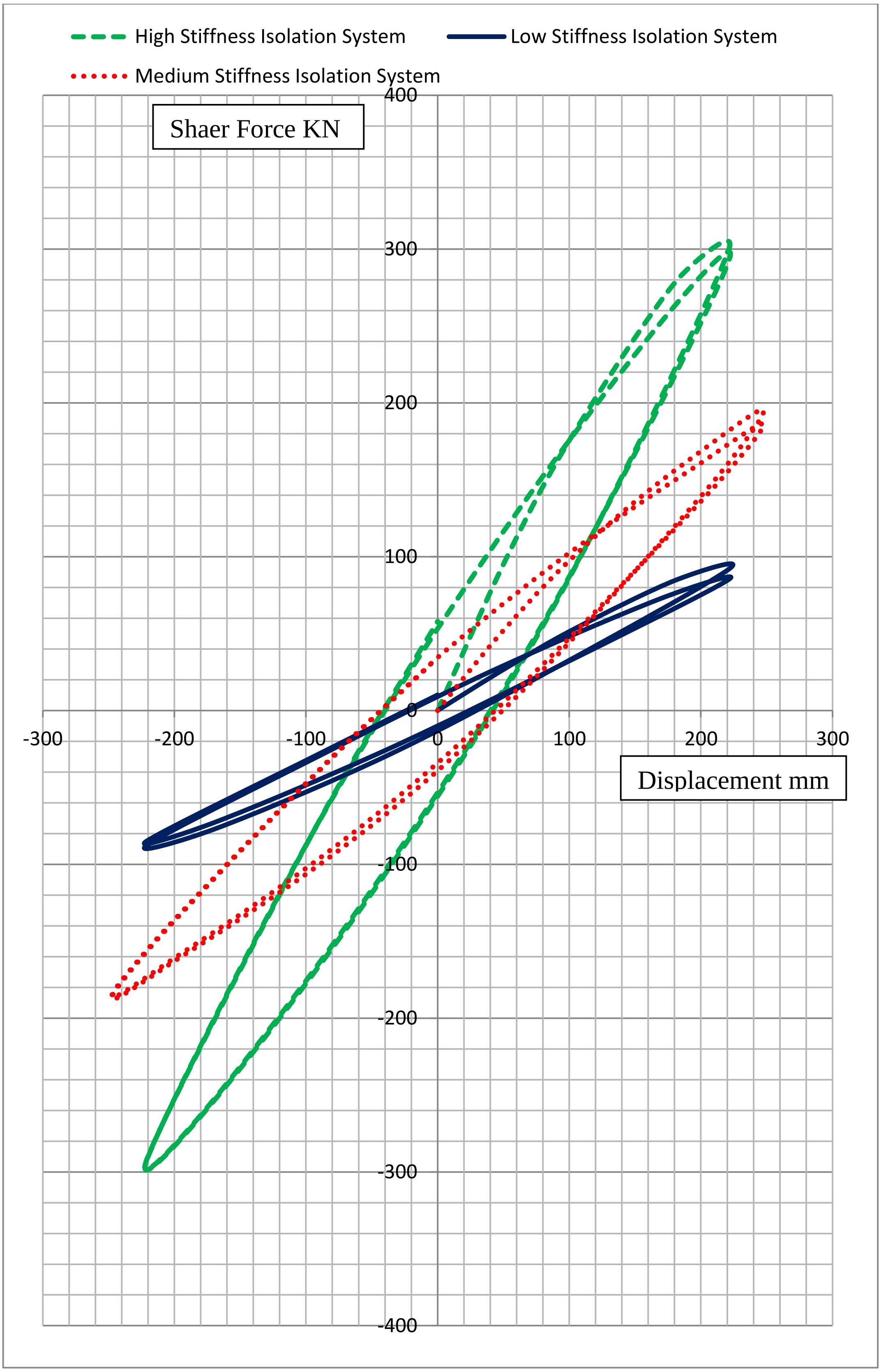

Figure 3.18. Displacement-Force Relationship for the Low, Medium, and High Stiffness Rubber.

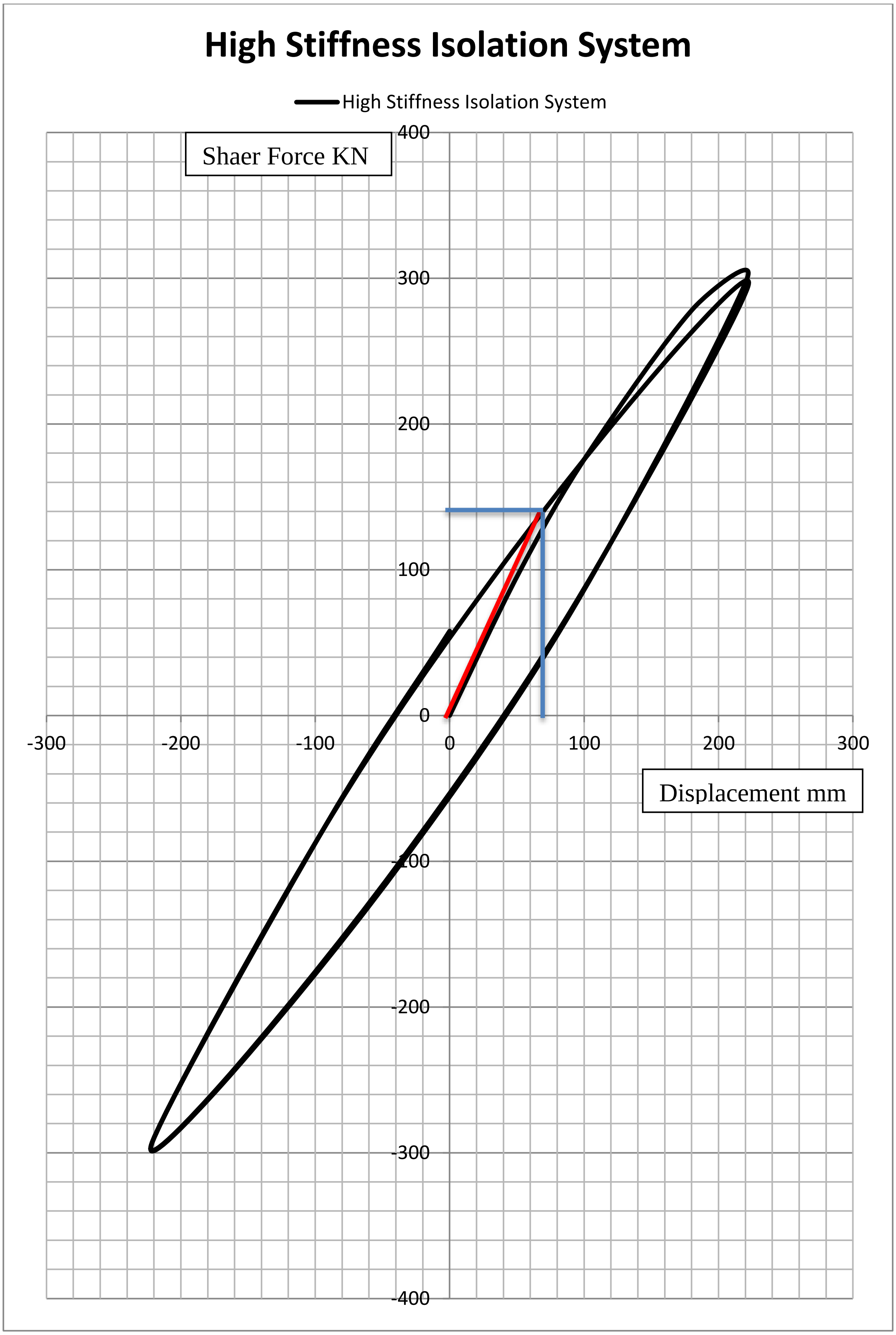

Figure 3.19-. Displacement-Force Relationship for the High Stiffness Rubber.

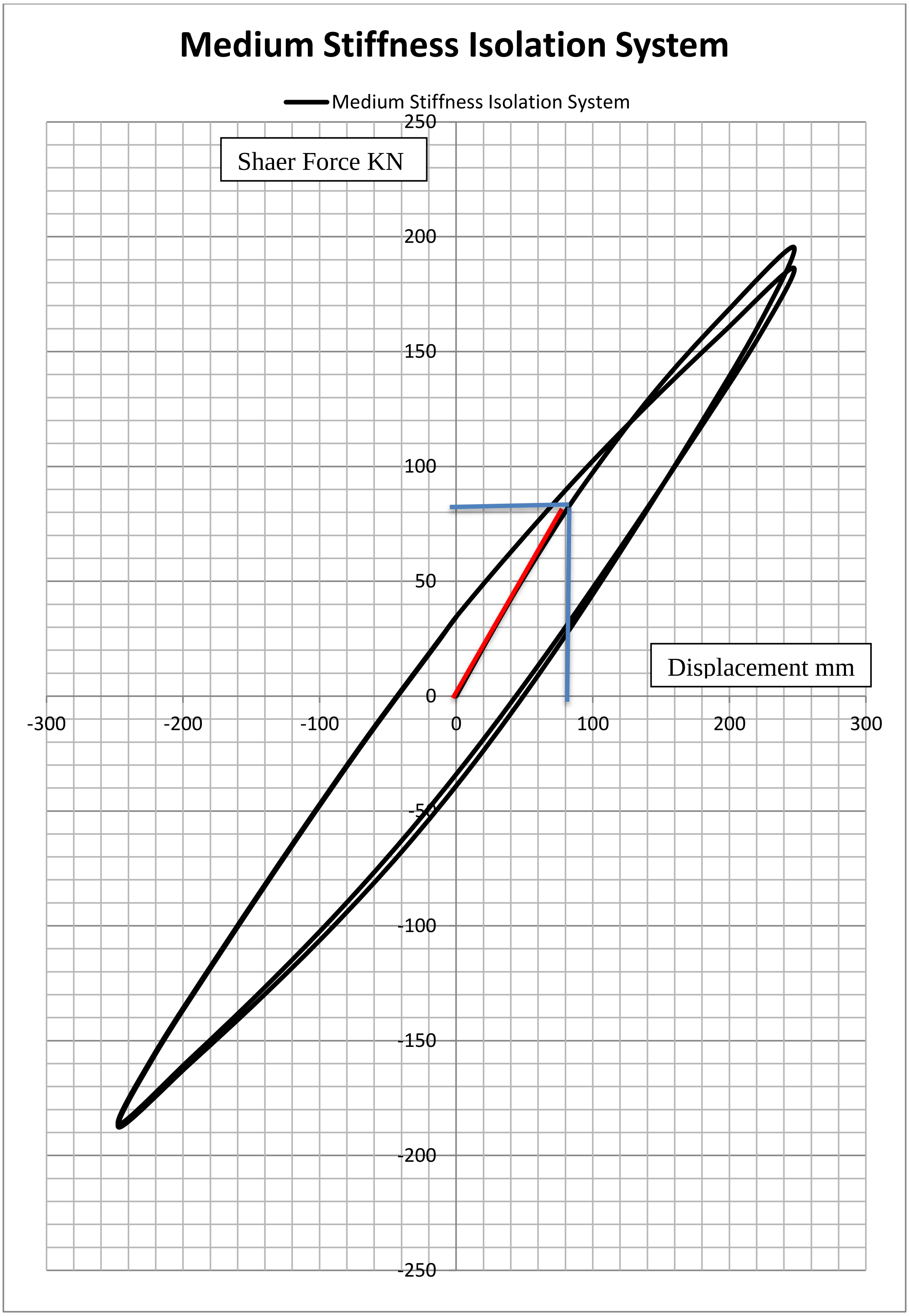

Figure 3.20. Displacement-Force Relationship for the Medium Stiffness Rubber.

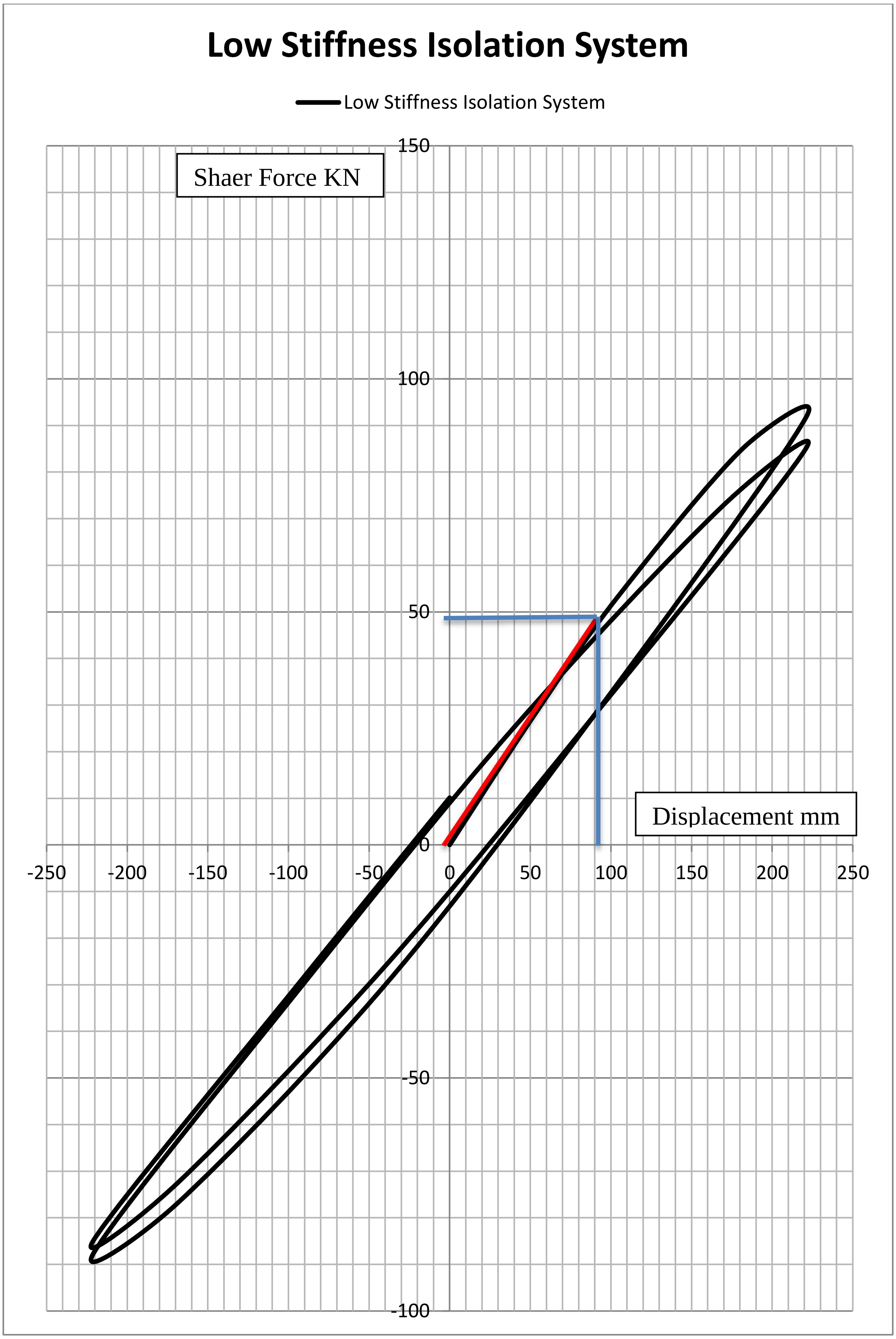

Figure 3.21. Displacement-Force Relationship. for the Low Stiffness Rubber.

The rubber bearing properties for various stiffness categories can be determined based on the values extracted from the cyclic load displacement-force chart. The calculations are presented as follows:

High Stiffness Rubber bearing:

Effective stiffness $Keff = \frac{299.2+292.3}{0.221+0.221} = 1338.22\ KN/m$

Yielding Force Fy = 140 KN

Yielding Displacement Dy = 70 KN

Elastic Stiffness K_1 = 140/70= 2 KN/mm=2000 KN/m.

Post yield stiffness K_2 = (299.2-140)/(221-70)=1.054KN/mm = 1054KN

The effective stiffness values of the high stiffness bearing obtained from the finite element analysis closely align with the values calculated according to ASCE7-22 standards. Similarly, the effective stiffness values of the medium and low stiffness bearings calculated from the finite element analyses are presented below.

Medium Stiffness Rubber bearing:

Effective stiffness $Keff = \frac{195.53+187.72}{0.247+0.247} = 775.82\ KN/m$

Yielding Force Fy = 82 KN

Yielding Displacement Dy = 83 KN

Elastic Stiffness K_1 = 82/70= 1.171 KN/mm=1171 KN/m.

Post yield stiffness K_2 = (195.53-82)/(247-70)=0.641KN/mm = 641 KN

Low Stiffness Rubber bearing:

Effective stiffness $Keff = \frac{91.73+87.68}{0.221+0.221} = 405.9\ KN/m$

Yielding Force Fy = 47 KN

Yielding Displacement Dy = 95 KN

Elastic Stiffness K_1 = 47/70= 0.671 KN/mm=671 KN/m.

Post yield stiffness K_2 = (91.72-47)/(221-70)=0.296KN/mm = 296 KN.

These calculations allow for the determination of the rubber bearing properties across various stiffness categories, aiding in the understanding of their behavior under different load conditions.

3.3.3. Equivalent Lateral Force Procedure - ELF:

We will commence the analysis of the frame through both software program SAP2000 and manual methods. Beginning with SAP2000, the initial step involves defining the earthquake load pattern. This pattern is established using the seismic coefficients and factors calculated as per ASCE7-22, as outlined in Table 3.4 of the documentation. The representation of this process is illustrated in Figure 3.22. This step is crucial in simulating the seismic forces that act upon the structure in accordance with established design codes and criteria.

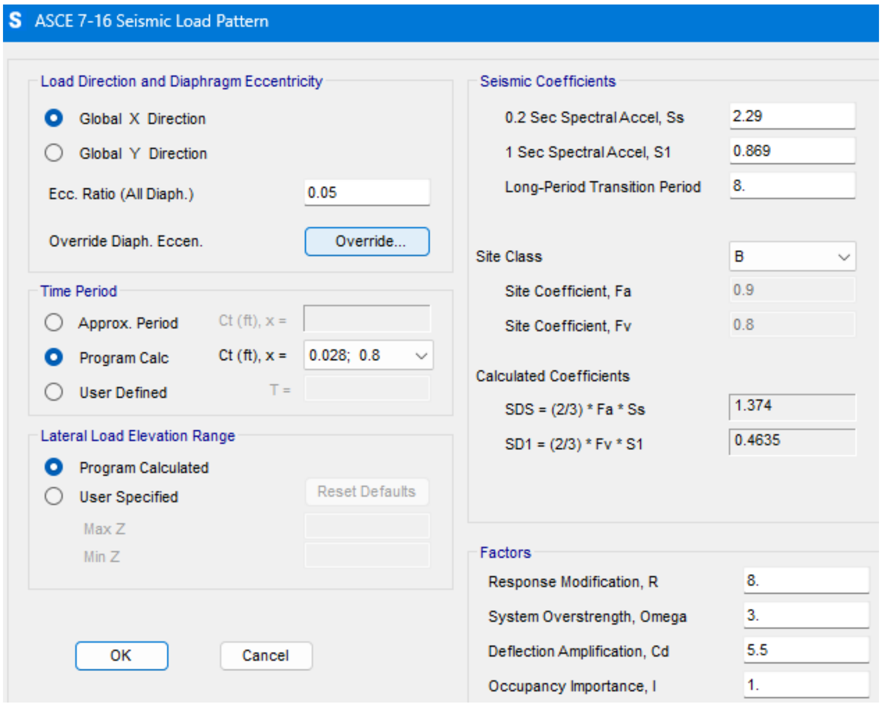

Figure 3.22. Seismic Load Pattern Definition.

Following the completion of the analysis, the observed base shear force is determined to be 407.98 KN, as visually represented in Figure 3.23. This outcome substantiates the accuracy of the analysis and underscores the response of the structure under the imposed seismic loading conditions.

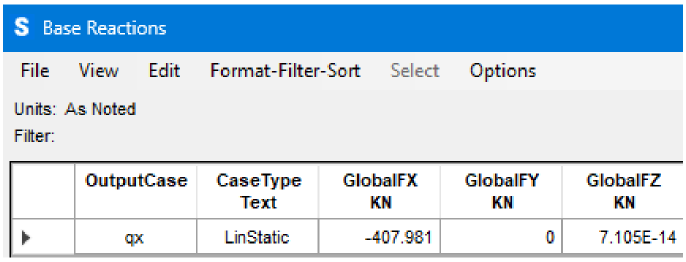

	OutputCase	CaseType Text	GlobalFX KN	GlobalFY KN	GlobalFZ KN
▸	qx	LinStatic	-407.981	0	7.105E-14

Figure 3.23. Base shear force according to ELF procedure by SAP2000.

Certainly, the process of calculating and distributing the base shear force and seismic forces vertically is outlined as follows:

Calculation of Fixed Frame Base Shear Force (V):

The total design lateral force or shear at the base (V) is computed using the seismic response coefficient (Cs) and the effective seismic weight (W) as defined by Equation (3.5):

$$\mathrm{V} = \mathrm{Cs} * \mathrm{W} \qquad (3.5)$$

Where Cs is the seismic response coefficient, calculated based on Equation (3.6). W is the effective seismic weight of the structure, which, for an office building, is considered equal to the dead load.

Calculation of Seismic Response Coefficient (Cs):

The seismic response coefficient (Cs) is initially calculated using Equation (3.6). However, the calculated value must satisfy certain constraints as outlined in Equations (3.7), (3.8), (3.9), and (3.10).

$$\mathrm{Cs} = \frac{\mathrm{SDS}}{\left(\frac{\mathrm{R}}{\mathrm{Ie}}\right)} = \frac{1.374}{\left(\frac{8}{1}\right)} = 0.17175 \qquad (3.6)$$

Where, S_{DS} = Design spectral response acceleration parameter in the short period range is calculated in Table 3.4. R = Response modification factor determined in Table 3.4. I_e = Importance Factor determined in Table 3.4.

The value of Cs computed in accordance with Equation (3.6.) need not be exceed the following conditions:

For $T \leq T_L$,

$$\mathrm{Cs} = \frac{\mathrm{SD1}}{\mathrm{T}(\frac{R}{Ie})} \tag{3.7}$$

For $T > T_L$,

$$\mathrm{Cs} = \frac{\mathrm{SD1} * \mathrm{TL}}{\mathrm{T\hat{}2}(\frac{R}{Ie})} \tag{3.8}$$

Where, T = the fundamental period of the structure = 0.4647 sec which is obtained from the SAP2000 modal. T_L, Long-Period Transition Period equals 8 second from Table 3.4. S_{D1}, Calculated Coefficient is calculated in Table 3.4.

T = 0.4647 sec which is less than T_L = 8 sec therefore, Equation (3.7) is used to calculate Cs as shown below

$$\mathrm{Cs} = \frac{\mathrm{SD1}}{\mathrm{T}(\frac{R}{Ie})} = \frac{0.4635}{0.4647(\frac{8}{1})} = 0.124677$$

The lower value for C_S shall not be less than the one calculated using Equation(3.9):

$$\mathrm{Cs} = 0.044\ \mathrm{SDS} * \mathrm{Ie} \ \geq 0.01 \tag{3.9}$$

So C_S is calculated as (0.044*1.374*1=0.06 which is not less than 0.01)

Also when the structures is in location where $S_1 \geq 0.6$, C_S Shall not be less than the following:

$$\mathrm{Cs} = 0.5\mathrm{S1}/(\frac{\mathrm{R}}{\mathrm{Ie}}) \tag{3.10}$$

The studied location $S_1 = 0.869 \geq 0.6 \Rightarrow$

$$\mathrm{Cs} = 0.5 * \frac{0.869}{\frac{8}{1}} = 0.0543$$

So the accepted value for the seismic response coefficient is Cs = 0.124677 and we use this value in Eq.3.3 to calculate the base shear force.

As the structure is an office building, we can assume that the effective seismic weight for the building is equal to the dead load alone, in accordance with ASCE-7-22. This can be calculated as W = 696.2 + 3 * 858.6 = 3272 KN (refer to Table 3.4).
Now, utilizing the calculated values for Cs (Cs = 0.124677) and W (W = 3272 KN), we will apply Equation (3.1) to determine the total design lateral force or shear at the base of the frame.

$$\mathrm{V} = \mathrm{Cs} * \mathrm{W} = 0.124677 * 3272 = 407.94\ \mathrm{KN}$$

Vertical Distribution of Seismic Forces at the Fixed Frame:

The vertical distribution of seismic forces entails two steps. First, we calculate the vertical distribution factor (Cvx) using Equation (3.12). Then, we distribute the calculated base shear force (V) using Equation (3.11).

$$\mathrm{Fx} = \mathrm{Cvx} * \mathrm{V} \tag{3.11}$$

$$\mathrm{Cvx} = \frac{\mathrm{Wx} * \mathrm{hx}^{\mathrm{k}}}{\sum_{\mathrm{n}}^{\mathrm{i}} \mathrm{Wi} * \mathrm{hi}^{\mathrm{k}}} \tag{3.12}$$

Where, Cvx is the vertical distribution factor. Wx is the portion of the total effective seismic weight located at level x. hx is the height from the base to level x. k is the exponent related to the structure's period.

These calculations lead to the distribution of seismic forces along the vertical direction, as summarized in Table 3.7. This procedure ensures an accurate representation of the structure's response to seismic loading conditions across different levels.

Table 3.7. Fixed Frame - Seismic Forces Distribution in the vertical direction.

Floor	hi (m)	Wi (KN)	Wi*hi (KN*m)	Cvx	Fx=Cvx*V
4	16	696.2	11139.2	0.351	143.14
3	12	858.6	10303.2	0.325	132. 4
2	8	858.6	6868.8	0.216	88.26
1	4	858.6	3434.4	0.108	44.13
$\sum$		3272	31745.6	1	407.94

Calculation of Isolated Frame Base Shear Force (V):

Aligns with the conditions specified in the ASCE 7-22 guidelines, allowing for the application of the equivalent lateral force procedure in the design of seismically isolated buildings or structures. Our diligent assessment has affirmed the fulfillment of the following criteria for the Isolated Frame IF3:

1- Site Classification: The structure or the building location must be a Site Class A, B, C, or D site, the studied building site class is B $\Rightarrow$ this item is fulfilled.

2- The isolated structure's effective period at its max displacement is 5.0 s or less, and the studied building's effective period is 1.64 s< 5 s $\Rightarrow$ this item is approved

3- The height of the structure or the building over the isolation interface, measured from the base level, has to be equal to or less than four stories, or 19.8 m (65 feet), This is a condition fulfilled due to the building consisting of 4 stories with height 16 m ≤19.8 m from the base level.

4- At the max displacement, the effective damping of the isolation system is lower or equal to 30%. In the studied isolation system effective damping is 5% and it is satisfied.

5- As per rational modal analysis, the isolated building's effective period (TM) must exceed three times the elastic period of the fixed-base building over the isolation system. The isolated structure's effective period is 1.64 seconds, whereas the fixed-base building's elastic period is 0.4647 seconds, satisfying the condition (1.64 > 3 * 0.4647).

6- No structural irregularity can be found in the structure constructed above the isolation system, the studied building is regular so this item is satisfied.

7- The isolation system satisfies each need listed below:

a) The effective stiffness of the isolation system at the maximum displacement is greater than one-third of the effective stiffness at 20% of the maximum displacement.

b) According to Section 17.2.4.4 of ASCE-7-22, both the upper bound and lower bound isolation system properties must be configured in a way that generates a restoring force. This force should result in a lateral force at the maximum displacement, which is at least 0.025 W greater than the lateral force at 50% of the corresponding maximum displacement.

3.3.3.1. Minimum Lateral Displacements Needed for Design:

The isolation system needs to be designed and constructed to withstand, at the very least, the maximum displacement specified as DM.

The equation to compute DM is as follows:

$$DM = \frac{g\,SM1 * TM}{4\pi^2 BM} \tag{3.13}$$

Where, g is acceleration caused by gravity (mm⁄s2) if the units of the displacement DM are in (mm). SM1 is MCER 5% damped spectral acceleration parameter at 1 sec period in units of g-sec

$$\mathrm{SM1} = 1.5 * \mathrm{SD1} \tag{3.14}$$

Then SM1 can be found using Equation (3.14) as 1.5* SD1=1.5*0.4635=0.69525 (SD1=0.4635 calculated in Table 3.4).

TM, efffective period of the seismically isolated structure (s) at the displacement DM in the direction under consideration as defined in Equation (3.1)

$$\mathrm{TM} = 2\pi\sqrt{\frac{W}{KM * g}} \tag{3.1}$$

Where, W is the effective seismic weight of the structure above the isolation interface calculated as 3272 KN in Table 3.4. K_M is the effective stiffness (KN⁄mm) of the isolation system at the maximum displacement. g is the acceleration caused by gravity (mm⁄s2) if the units of K_M are in (KN/mm). Then TM is found by using the following relation $2\pi\sqrt{}$ (W/(KM*g))= $2\pi\sqrt{}$ (3272/(0.775*9810)) as to be 4.12 sec for the Isolated Frame IF3. Using Equation (3.13) with BM , numerical coefficient as outlined in Table 2.1. DM can be calculated as (9810*0.69525*4.096)/(4*π^2*1)=711.8 mm

3.3.3.2. Minimum Lateral Forces Required for Design:

The isolation system, foundation, and all structural components located below the base level should be engineered and built to withstand a specified minimum lateral seismic force, denoted as Vb, as outlined in Equation 3.15.

$$\mathrm{Vb} = \mathrm{KM} * \mathrm{DM} \tag{3.15}$$

Using value computed for KM and DM in Equation (3.15) one can calculate the specified minimum lateral seismic force for the Isolated Frame IF3 as, Vb = 0.775*711.8 = 555.466 KN

The components of the structure above the base level must be designed and constructed in accordance with all relevant criteria for a nonisolated structure. This is necessary to account for a minimum shear force, denoted as Vs, which is calculated using Equation 3.16.

$$\mathrm{Vs} = \frac{Vb}{Ri} \tag{3.16}$$

Here, the value of Ri is associated with the Response Modification Factor (R) and should be set at three-eighths of the R value. Ri is capped at a maximum of 2.0 and a minimum of 1.0. Consequently, Vs can be calculated as 555.466 divided by 2, resulting in Vs = 277.733.

These calculations lead to the distribution of seismic forces for the isolated frame IF3 along the vertical direction, as summarized in Table 3.8.

Table 3.8. Isolated Frame IF3 -Seismic Forces Distribution in the vertical direction.

Floor	hi (m)	Wi (KN)	Wi*hi (KN*m)	Cvx	Fx=Cvx*V
4	16	696.2	11139.2	0.351	97.48
3	12	858.6	10303.2	0.325	90.26
2	8	858.6	6868.8	0.216	59.99
1	4	858.6	3434.4	0.108	29.99
∑		3272	31745.6	1	277.73

3.3.4. Time History Method:

We have planned to conduct a Nonlinear Modal Time-History Analysis (FNA) to gain a deeper understanding of how the seismic isolation system impacts the structural behavior and seismic performance of the building. In SAP2000, it's crucial to note that effective stiffness properties are not applied to nonlinear degrees of freedom when performing nonlinear time-history analysis.

Nevertheless, it's essential to emphasize that nonlinear modal time-history (FNA) analyses do utilize the vibration modes computed based on the effective stiffness. This is particularly relevant when the modal analysis itself employs stiffness derived from zero initial conditions. As the analysis progresses through time integration, these modes undergo adjustments to account for the actual stiffness and other specified nonlinear parameters. This dynamic approach guarantees that the structural response accurately captures the genuine stiffness and nonlinear characteristics of the system.

Importantly, modifying the effective stiffness has the potential to improve the convergence rate of the nonlinear iteration process. Therefore, in order to precisely capture the genuine stiffness of the isolator, we have chosen to utilize FNA for the analysis of isolated structures. This approach within SAP2000 ensures an accurate portrayal of the isolator's behavior and its consequential influence on the overall structural response.
As we proceed, we are currently in the process of defining the necessary time history input parameters within the SAP2000 software. For the execution of this analysis, we will be employing the El Centro earthquake data, as illustrated in Figures 3.24 to 3.29.

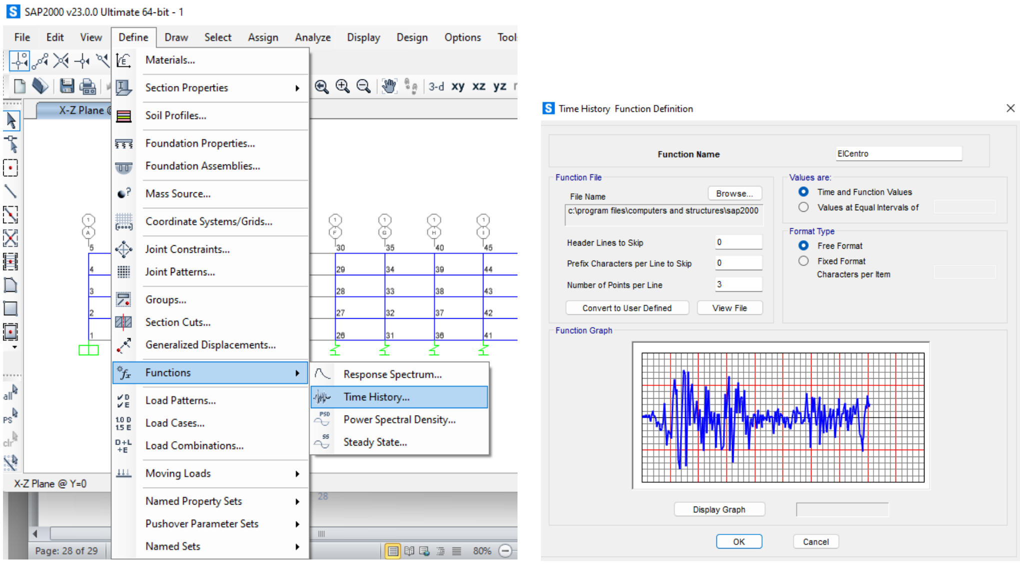

Figure 3.24. Time History Function Definition SAP2000-El Centro Earthquake.

Additionally, we will be implementing a ramp function to apply the dead and live loads. It's imperative that the isolators are subjected to the vertical load prior to commencing the earthquake analysis. Consequently, we are required to define the dead and live loads using a time history approach. In this scenario, we will employ a gradual ramp function to incrementally introduce the load. This approach will be combined with high damping to approximate a static load condition. This method ensures accuracy and stability in representing the load behavior.

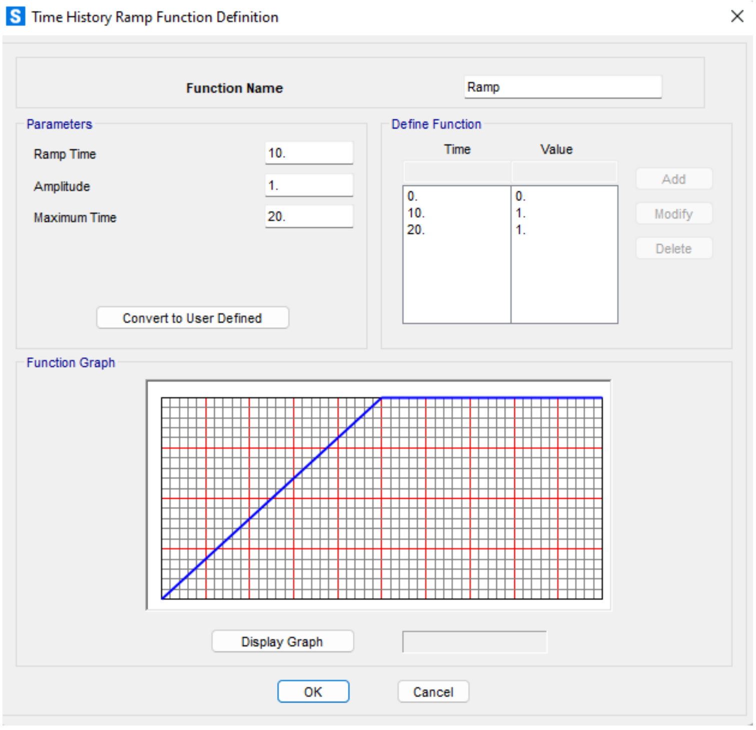

Figure 3.25. Time History Ramp Function Definition.

Subsequent to this, we will proceed to define the load cases, beginning with the Modal Case, as depicted in Figures 3.26 to 3.29.

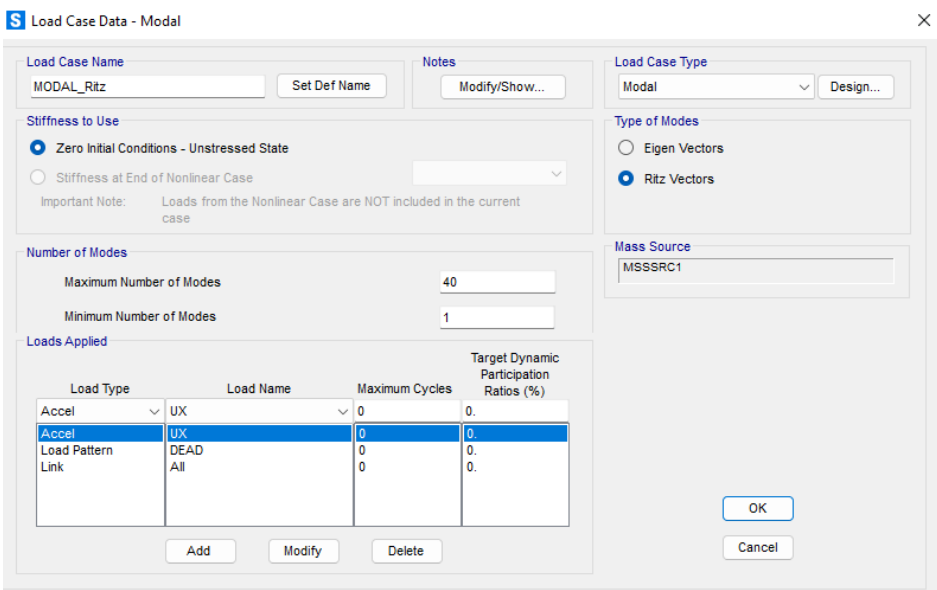

Figure 3.26. Modal_Ritz Load Case Definition.

Dead Load Case:

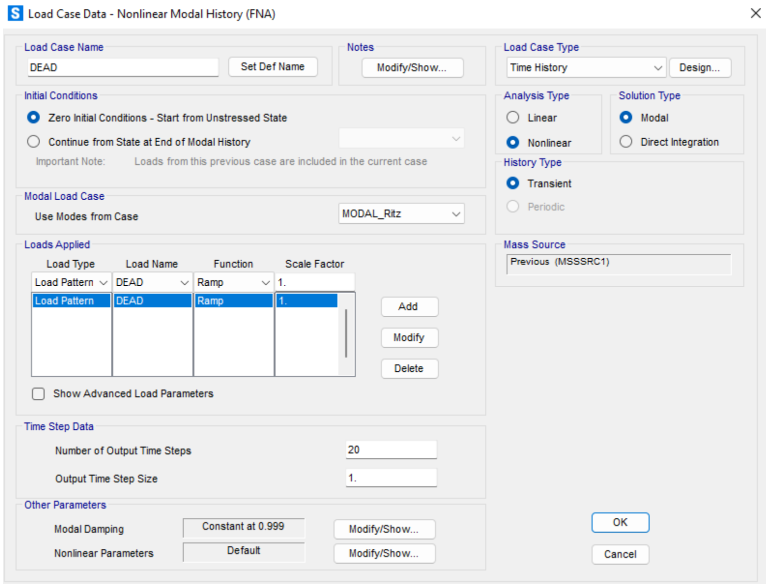

Figure 3.27. Dead Load Case Definition.

Live Load Case:

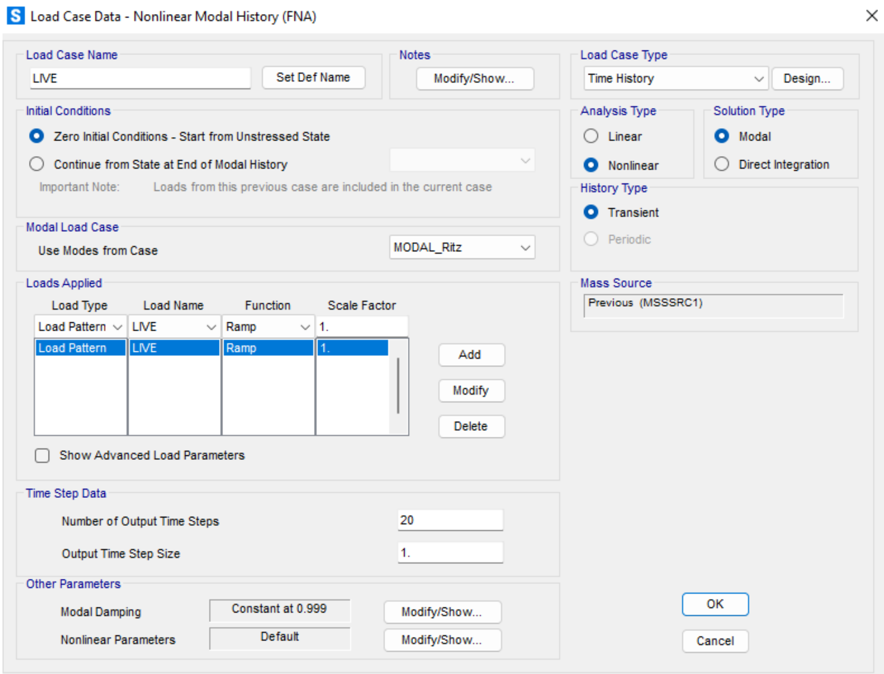

Figure 3.28. Live Load Case Definition.

Nonlinear Modal Time-History Analysis (FNA) constitutes an innovative and sophisticated computational technique situated at the forefront of the structural engineering domain. Engineered with precision, it is designed to elucidate the intricate dynamics exhibited by structures when subjected to nonlinear behaviors, particularly within the context of seismic or dynamic loading conditions. The methodology deftly amalgamates principles derived from modal analysis, time-history analysis, and nonlinear structural behavior. The resultant amalgamation culminates in an analytical framework that offers an exponentially augmented and intricately detailed representation of a structure's response, meticulously capturing the intricate nonlinearities at play.

Fundamental Components of Nonlinear Modal Time-History Analysis:

Modal Analysis: Anchoring the foundation of FNA is modal analysis—a cardinal methodology harnessed to unveil the innate properties of a structure, encompassing its natural frequencies, mode shapes, and damping ratios. These fundamental modes of vibrational resonance serve as a profound language, articulating how a structure responds harmoniously to dynamic stimuli. This comprehension, akin to deciphering the very lexicon of a structure's motion, is pivotal for grasping its fundamental comportment across an array of vibrational scenarios.

Time-History Analysis: Complementing its structural vocabulary, FNA integrates the core tenets of time-history analysis, orchestrating the superimposition of authentic recorded or meticulously engineered time-varying loads onto the intricate fabric of the structure. This orchestrated choreography grants engineers the privilege to meticulously choreograph lifelike scenarios, notably including seismic events such as the El Centro earthquake—thus offering a panoramic vista into the evolution and interplay of the structure's contours over the unfolding of time.

Nonlinear Behavior: Emerging as pivotal agents within the structural landscape, nonlinearities unfurl as transformative catalysts, emerging from mutable material properties, dynamic geometrical shifts, and evolving boundary conditions. These nonlinear manifestations encompass a rich tapestry of phenomena, spanning plastic deformations, expansive displacements, and fluctuations in stiffness. Diverging from the obedient superposition principle observed in linear systems, nonlinear systems present a compelling conundrum within the landscape of analysis.

Unraveling the Essence of FNA Process:

Modal Decomposition: FNA's inaugural act commences with modal decomposition—a pivotal phase that heralds the delineation of a structure's intrinsic modal properties through the lens of linear modal analysis. These properties set the groundwork, laying out a comprehensive blueprint to unveil the dynamic response of the structure.

Nonlinear Modeling: Guided by modal insights, the FNA narrative artfully introduces nonlinearities into the structural fabric. This is effectuated through the integration of nonlinear elements that encapsulate the intricate nuances of material intricacies and geometric transformations. This integration resonates with phenomena such as material yielding, the emergence of buckling cascades, and the expansive ballet of deflections.

Time-History Loading: A pivotal crescendo within FNA emerges with the orchestration of time-history loading—an act where the symphony of meticulously recorded or synthesized dynamic loading profiles, underscored by seismic phenomena like the El Centro earthquake, takes center stage upon the structural canvas.

Integration of Modes: Departing from the constraints of single-mode approximation, FNA orchestrates a harmonious ensemble of modes. This symphonic interplay gains particular salience in the presence of pervasive nonlinear behavior, where multiple modes collaborate to sculpt a finely nuanced response.

Time-Integration: The equations of motion, enriched by the infusion of nonlinear complexities, embark upon a numerical odyssey through the dimension of time. Employing sophisticated techniques such as Newmark integration, this journey delineates an intricate temporal tapestry that unveils the structure's multifaceted response.

Iteration: Within the narrative of FNA, iterative endeavors often take center stage. These iterative interludes, marked by precision and convergence, ensure the meticulous capture of nonlinear intricacies within the choreography of analysis.

Discerning Structural Realities through FNA:

At its core, the intrinsic merit of Nonlinear Modal Time-History Analysis (FNA) resides in its unparalleled prowess to illuminate the very essence of a structure's response amidst the interplay of multifarious and intricate dynamic loads. This methodological symphony masterfully harmonizes nonlinear complexities with the elegant cadence of vibrational modes, birthing a composite representation that bears witness to the structure's every convolution. This multidimensional understanding stands as a keystone for navigating the realms of structural safety and performance, most notably within the crucibles of seismic challenges, where nonlinear forces hold sway. To provide empirical validation, we operationalized the concept of Fast Nonlinear Analysis (FNA) through a specific case study within SAP2000, elucidated comprehensively in Figure 3.29.

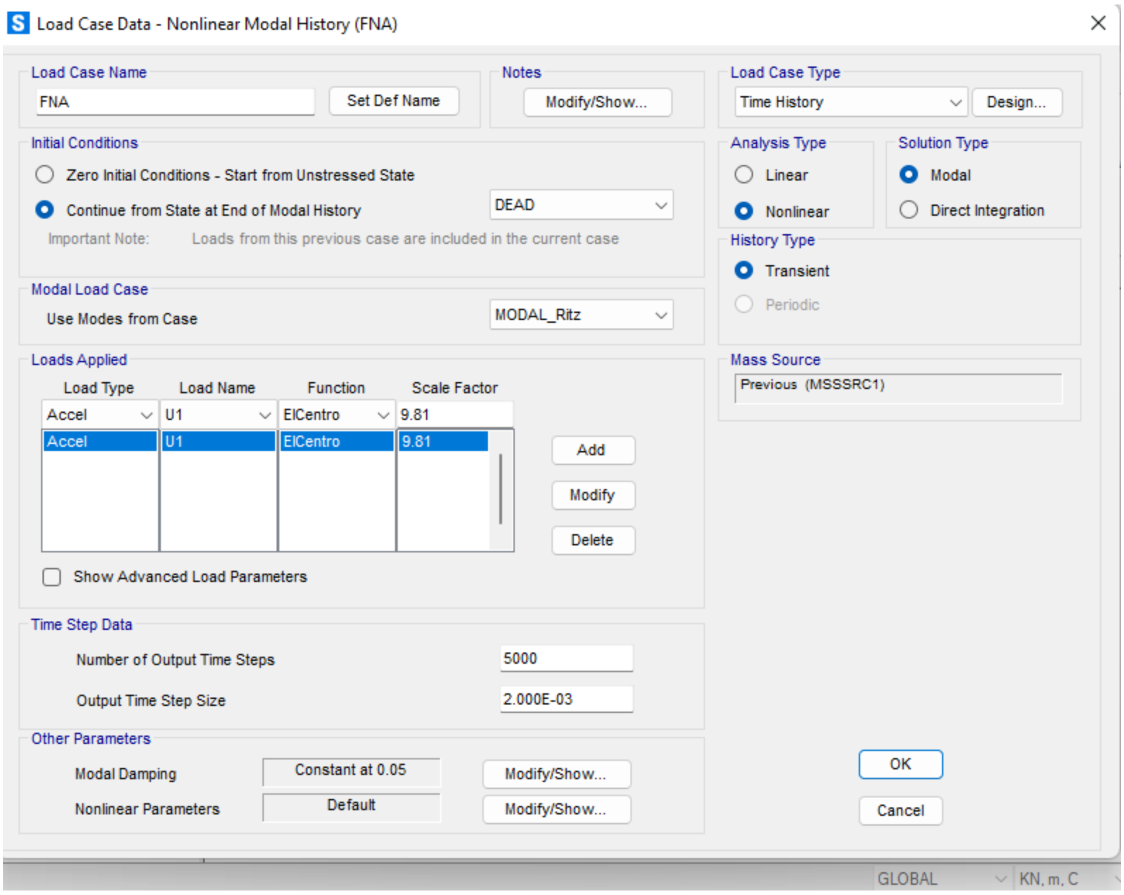

Figure 3.29. Fast Nonlinear Analysis FNA Case Definition.

We will implement a non-linear rubber base isolator system as our seismically base isolation approach, in accordance with the detailed calculations and specifications outlined in section 3.3.2. We are adopting the identical properties of the elastomeric bearings, as elucidated for Effective Stiffness (Keff): 775.82 kN/m, Elastic Stiffness (K1): 1171 kN/m, Post Yield Stiffness (K2): 641 kN/m, Yield Strength (Fy): 82 kN and Post Yield Stiffness Ratio (K2/K1): 0.547 (Unitless), respectively. These specific properties will be seamlessly integrated into the SAP2000 software, as visualized in Figure 3.30. This inclusion will facilitate the accurate simulation of the rubber base isolator system's behavior during our analysis.

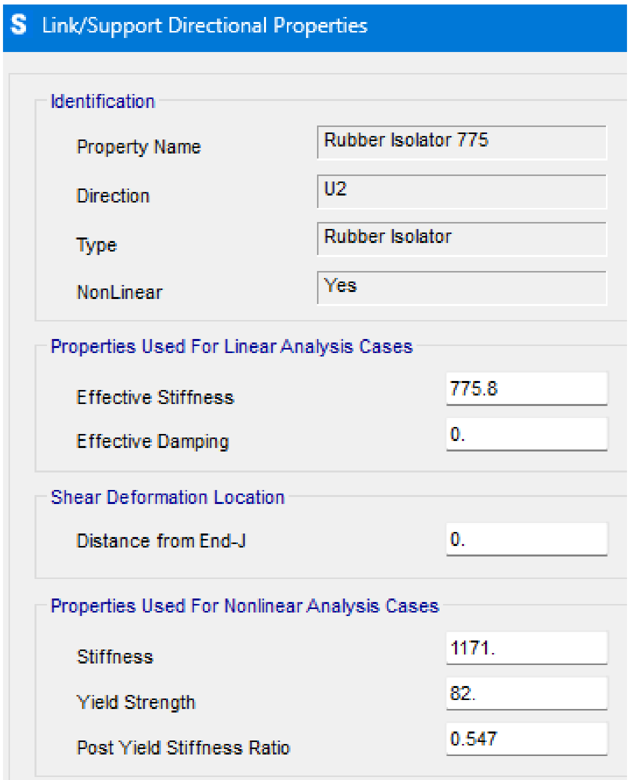

Figure 3.30. Medium Stiffness Rubber Isolator Properties Definition.

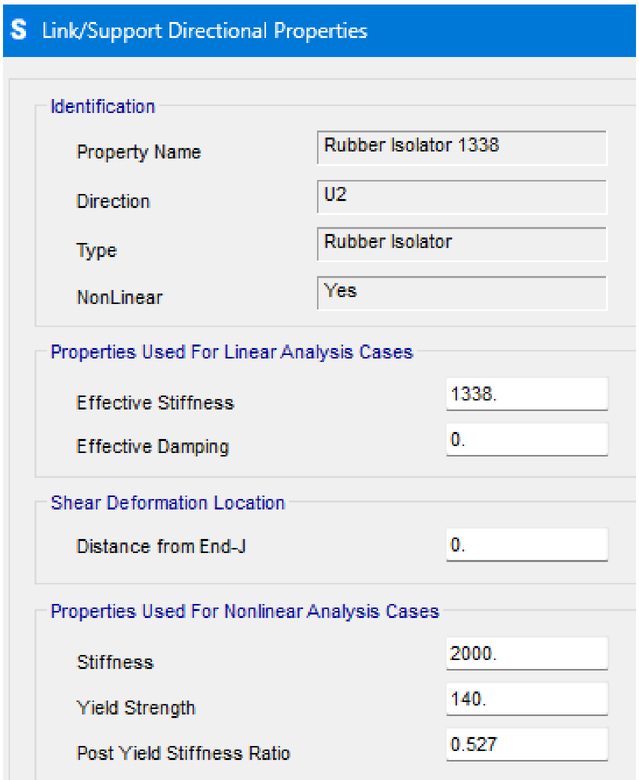

Figure 3.31. High Stiffness Rubber Isolator Properties Definition.

We intend to utilize these calculated properties alongside assumptions derived from the preliminary design for the purpose of conducting a comparative analysis. The assumed properties have been illustrated in Figure 3.32.

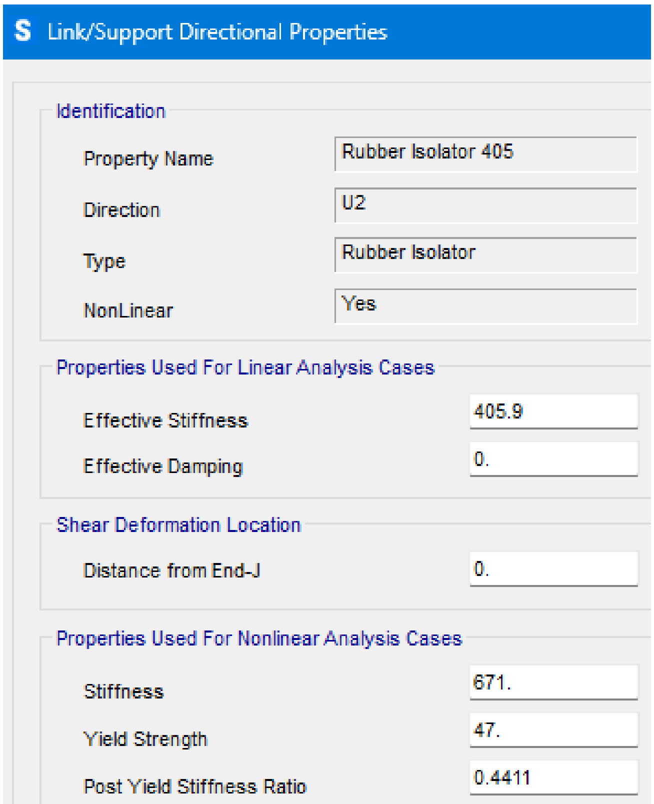

Figure 3.32. Low Stiffness Rubber Isolator Properties Definition.

Certainly, initiating the analysis phase is an essential step to comprehensively evaluate the performance of the proposed non-linear rubber base isolator system. We will diligently conduct the analysis to acquire reliable results that will serve as the foundation for our discussions moving forward.

Once the analysis is complete, we will carefully examine the results to assess how well the system meets the anticipated behavior under various seismic conditions. These results will enable us to make informed decisions and engage in meaningful discussions regarding the system's effectiveness, its response to different loading scenarios, and its ability to mitigate seismic forces.

4. RESULTS and DISCUSSION:

To facilitate informed decision-making and constructive discussions concerning the system's effectiveness, its response under various loading scenarios, and its capacity to mitigate seismic forces, we will conduct a comparative assessment. This assessment will involve comparing the maximum displacement, frame drift, and acceleration for the following six frames:

1- FF = Fixed frame
2- IF_1 = Isolated frame using isolation units with high stiffness (K_{eff}=1338 KN/m)
3- IF_2 = Isolated frame using isolation units with medium stiffness (K_{eff}=1000 KN/m)
4- IF_3 = Isolated frame using isolation units with low stiffness (Keff=775 KN/m)
5- IF_4 = Isolated frame using isolation units with low stiffness (Keff=500 KN/m)
6- IF_5= Isolated frame using isolation units with low stiffness (Keff=406 KN/m)

Hence, it becomes imperative to investigate the cumulative displacement, particularly concentrating on the upper-right point located at the roof level within each individual frame. This thorough examination aims to quantify the combined displacement encountered by this specific point across the diverse frames under examination. The outcomes of this thorough analysis are concisely summarized and encapsulated in Table 4.1. These findings are further substantiated and visually elucidated through the illustrative representations offered in Figures 4.1 and 4.2.

Table 4.1. The total displacement for the top-right point from each frame (including the isolation units' displacements).

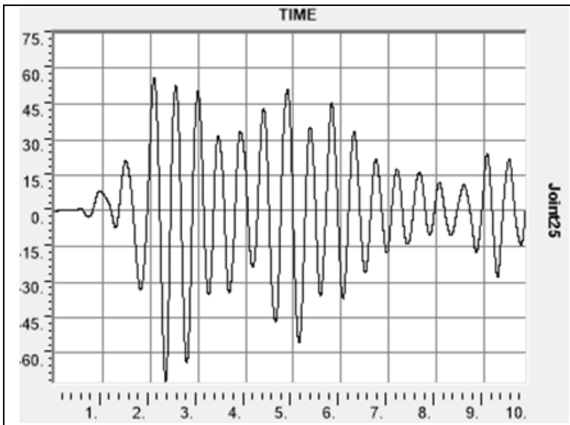	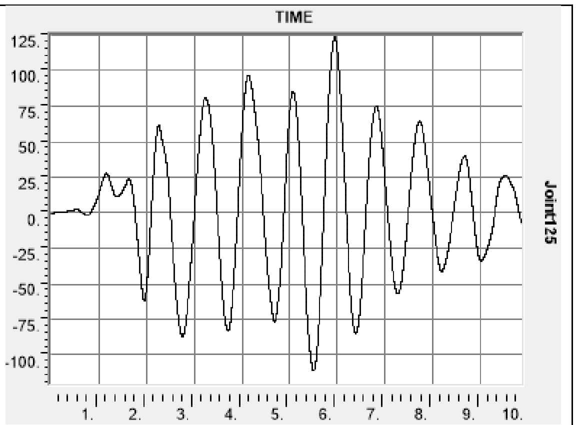
FF: Min = -72 mm, Max = 56 mm	IF1: Min = -111 mm, Max = 124 mm
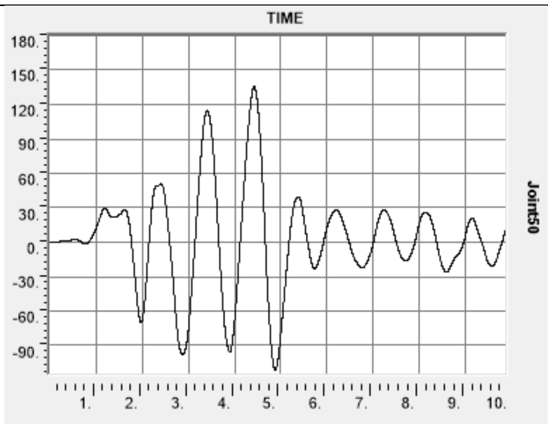	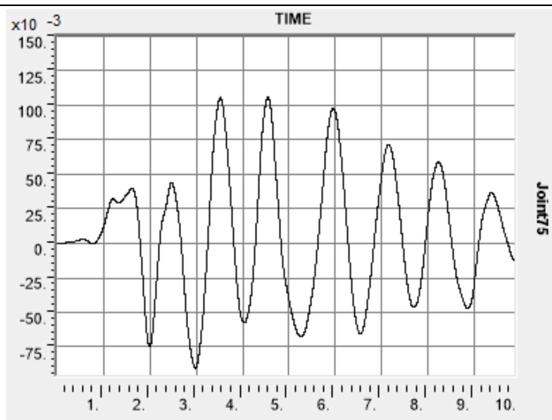
IF2: Min = -111mm, Max = 136 mm	IF3: Min = -90 mm, Max = 106 mm
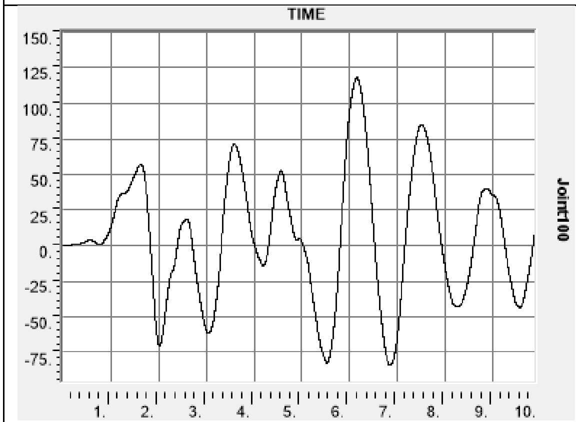	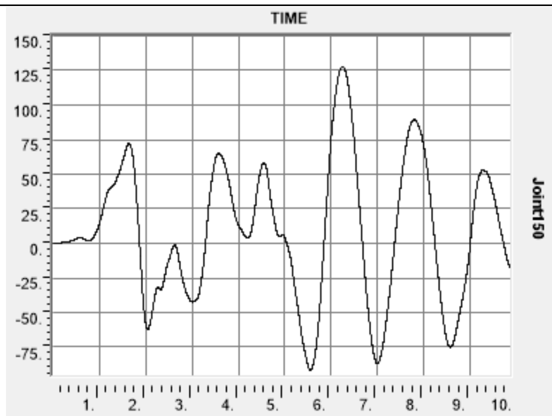
IF4: Min = -84 mm, Max = 118 mm	IF5: Min = -92 mm, Max = 128 mm

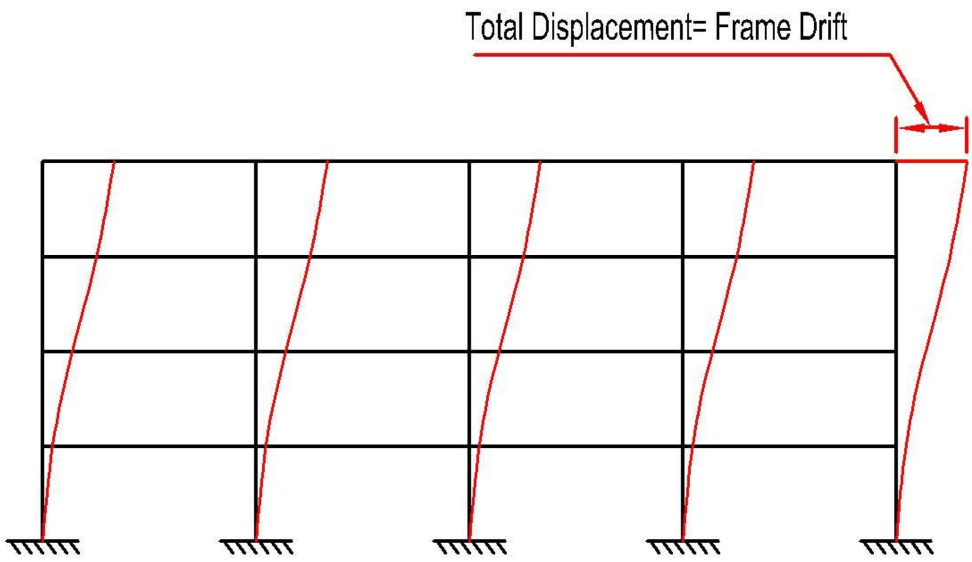

Figure 4.1. The Total Displacement & Frame Drift at The Fixed Frame.

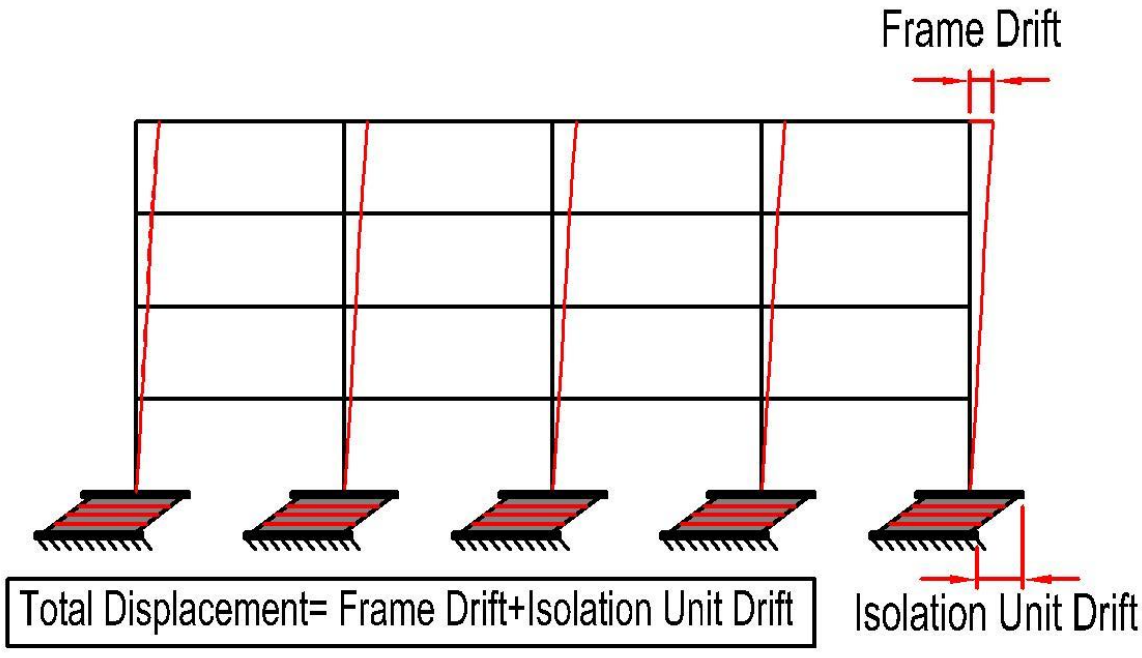

Figure 4.2. The Total Displacement & Frame Drift at The Isolated Frames.

This meticulous investigation provides a thorough understanding of the displacement dynamics showcased by the frames under consideration, with specific emphasis on the specified point positioned at the upper-right corner of each frame. The synergy between tabulated data and graphical depictions offers a comprehensive view of the intricate fluctuations and patterns that underscore the cumulative displacements within the framework of this study.

In the course of our analysis, a significant observation has emerged: the total displacement observed in the fixed frame is notably smaller when compared to the cumulative displacement witnessed in the isolated frames. What is particularly important is that a clear and direct correlation, or its inverse counterpart, between the magnitude of displacement and the stiffness of the isolation system cannot be universally confirmed. This observation becomes particularly evident through the following instances:

Initially, the cumulative displacement measured at Isolated Frame 2 (IF2) was 136 mm. Following a deliberate reduction in stiffness at Isolated Frame 3 (IF3), the cumulative displacement decreased to 106 mm. However, it's important to note that a subsequent decrease in stiffness at Isolated Frame 4 (IF4) unexpectedly resulted in an increase in the cumulative displacement to 118 mm.

This complex pattern of displacement behavior can be attributed to a convergence of various factors. Within these factors, the inherent properties of the structural frame, the specific characteristics of the seismic event, and the level of compatibility between these attributes and the isolation system play pivotal roles. The most comprehensive grasp of this dynamic interplay becomes evident through a synthesis of the displacements observed across all six frames, as illustrated in Figure 4.3.

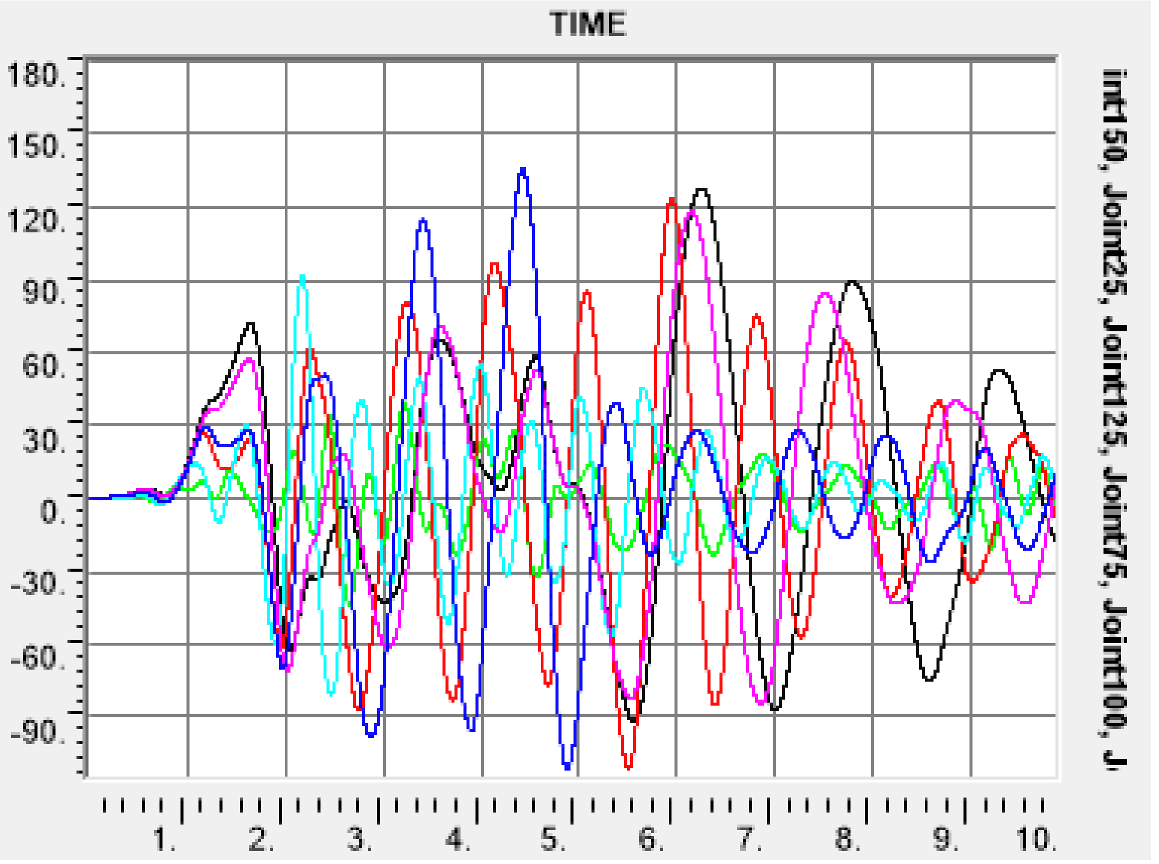

Figure 4.3. The Total Displacement for The Top-right Point from Each Frame. (Including the isolation units' displacements)

This presented result emphasizes the intricate interplay of variables that govern the overall displacement response. It further underscores the complex role that structural properties, seismic attributes, and the effectiveness of the isolation system play in shaping the cumulative displacement outcomes across diverse configurations. This intricate relationship highlights the necessity for a comprehensive perspective that goes beyond simplistic linear associations. It emphasizes the significance of adopting a holistic approach when evaluating displacement behavior within the realm of seismic isolation systems.

Clearly discernible from the data is a significant observation: during the initial five-second interval of the seismic event, the cumulative displacement demonstrated by Isolated Frame 4 (IF4) – represented by the point labeled "Joint100" on the chart – is notably smaller compared to the cumulative displacements exhibited by Isolated Frame 2 and Isolated Frame 3 (IF2 and IF3). The precise points on the chart that correspond to these frames are identified as "Joint 25" and "Joint 50," respectively.

Conversely, there is a reversal in this pattern during the subsequent five-second interval of the earthquake event. Within this time span, the cumulative displacement demonstrated by IF4 surpasses the cumulative displacements exhibited by both IF2 and IF3. It's crucial to recognize that these recorded displacements encompass the drift values associated with the utilized isolation units. Therefore, a more detailed comparative evaluation is imperative to fully understand the dynamics of frame drifts accurately.

To achieve this, we embark on a thorough examination by comparing the displacements recorded at two distinct locations within each frame: one positioned at the upper-right extremity and the other at the lower-right extremity. This analytical methodology leads us to extract the maximum drift values inherent to each frame. A comprehensive overview of these results is succinctly provided in Table 4.2, offering a concise and organized representation of the frames' most notable drift magnitudes.

Table 4.2. The maximum frames drift (excluding the isolation units' displacements)

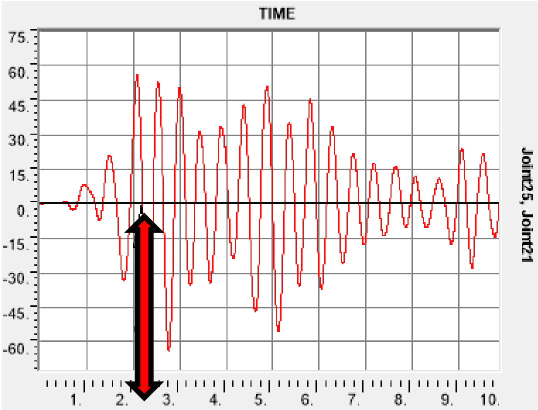	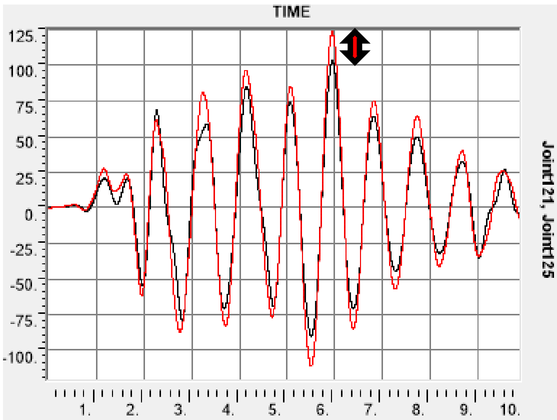
FF: Max Frame Drift = 72 mm	IF1: Max Frame Drift = 20.5 mm
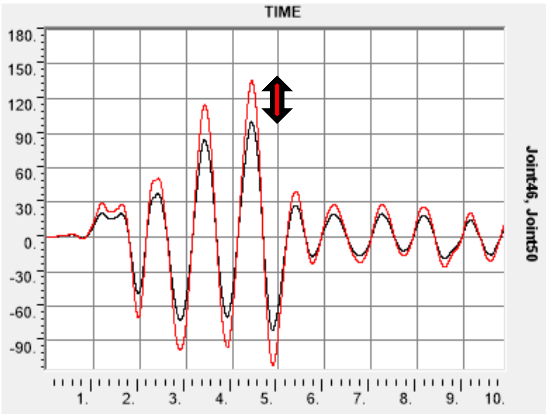	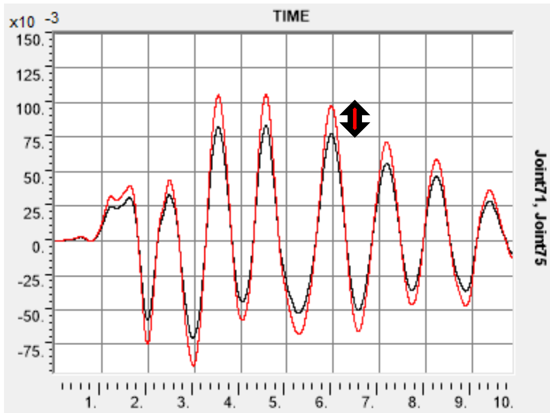
IF$_2$: Max Frame Drift = 36 mm	IF$_3$: Max Frame Drift = 22 mm
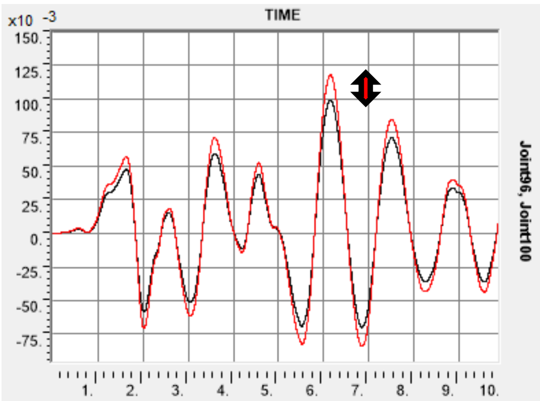	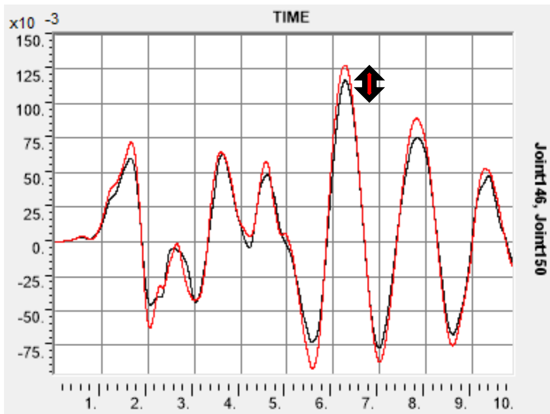
IF$_4$: Max Frame Drift = 19 mm	IF5: Max Frame Drift = 10.4 mm

We observe that the maximum frame drift in the fixed frame exceeds the maximum frame drift observed in the isolated frames. Additionally, it's important to highlight that the maximum frame drift doesn't exhibit a proportional relationship to the stiffness of the isolation system, as illustrated in Figure 4.4.

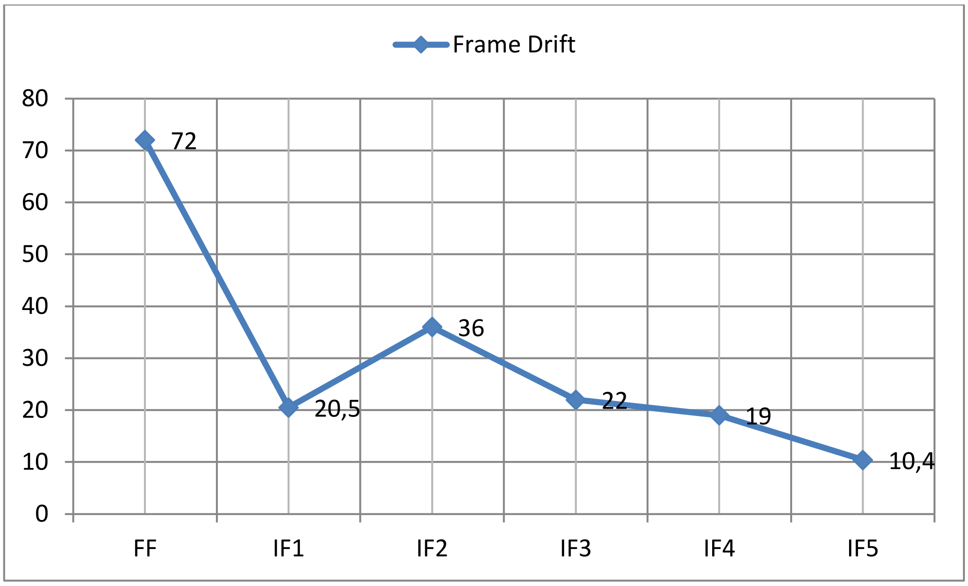

Figure 4.4. The Maximum Frames' Drifts for the Compared Frames.

A comprehensive breakdown of the seismic accelerations relevant to the frames under examination is meticulously presented in Table 4.3. This table serves as a comprehensive compilation of earthquake acceleration values pertinent to the frames being compared. Through the incorporation of this vital data, Table 4.3 provides a holistic overview of the intricate relationship between seismic forces and the structural responses of the frames. As a result, it offers a nuanced comprehension of their performance within the seismic context.

Table 4.3. The acceleration for the top-right point from each frame.

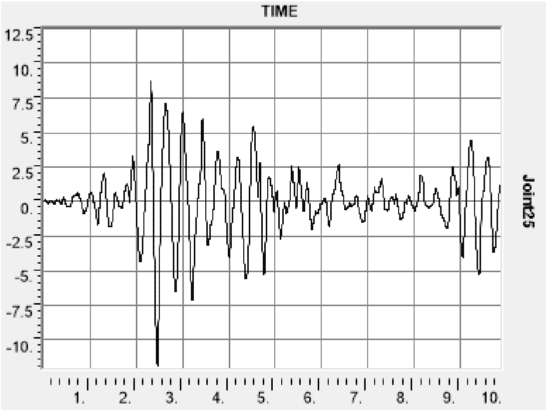	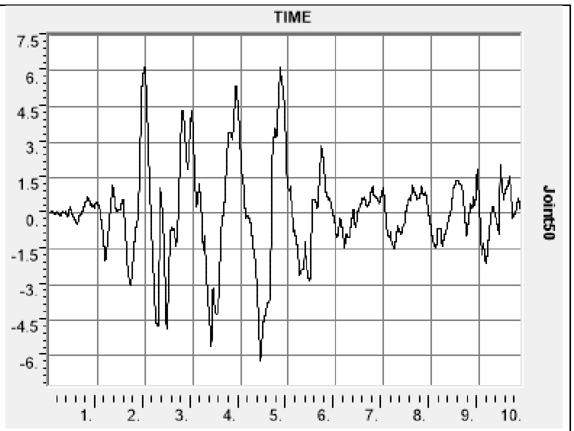
FF: Min = -11.8 m/s^2, Max = 8.7 m/s^2	IF$_2$: Min = -6.22 m/s2, Max = 6.16 m/s2
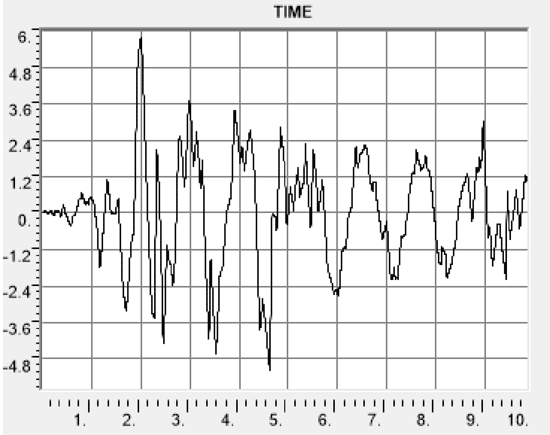	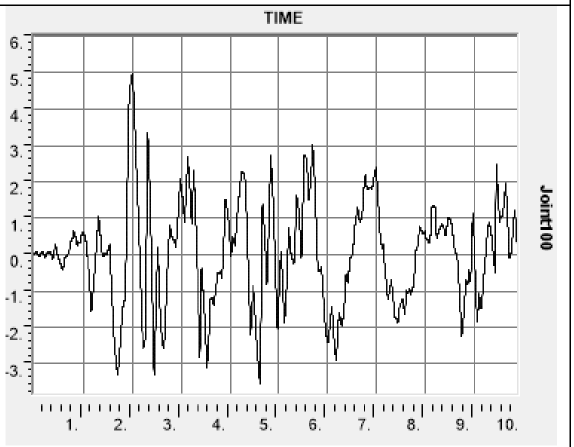
IF$_3$: Min = -5.2 m/s2, Max = 5.7 m/s2	IF$_4$: Min = -3.55 m/s2, Max = 4.98 m/s2
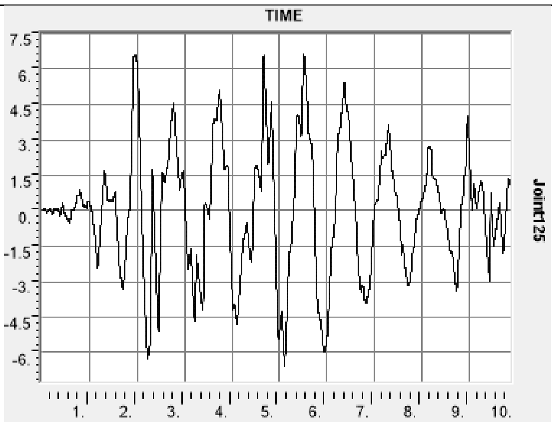	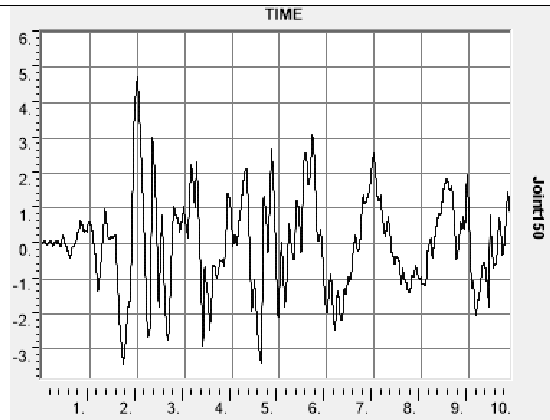
IF1: Min = -6.57 m/s2, Max = 6.66 m/s2	IF5: Min = -3.4 m/s2, Max = 4.7 m/s2

Our analysis unmistakably reveals a clear divergence in acceleration patterns between the fixed base frame and the isolated frames. This divergence becomes particularly evident when observing the response of isolated frames in relation to the decreasing stiffness levels of the isolation system, as gracefully illustrated in Figure 4.5.

The fixed base frame, serving as a point of comparison, demonstrates a significantly higher magnitude in its acceleration pattern. In sharp contrast, the isolated frames exhibit a compelling correlation between the reduction in the stiffness of the isolation system and the corresponding decrease in acceleration magnitudes. This observation highlights the crucial influence that the stiffness of the isolation system wields over the dynamic response of the structural frames to seismic forces. The visual representation in Figure 4.5 offers an intuitive graphical depiction of this intricate relationship, facilitating a more comprehensive understanding of the intricate interplay between isolation mechanisms and seismic accelerations.

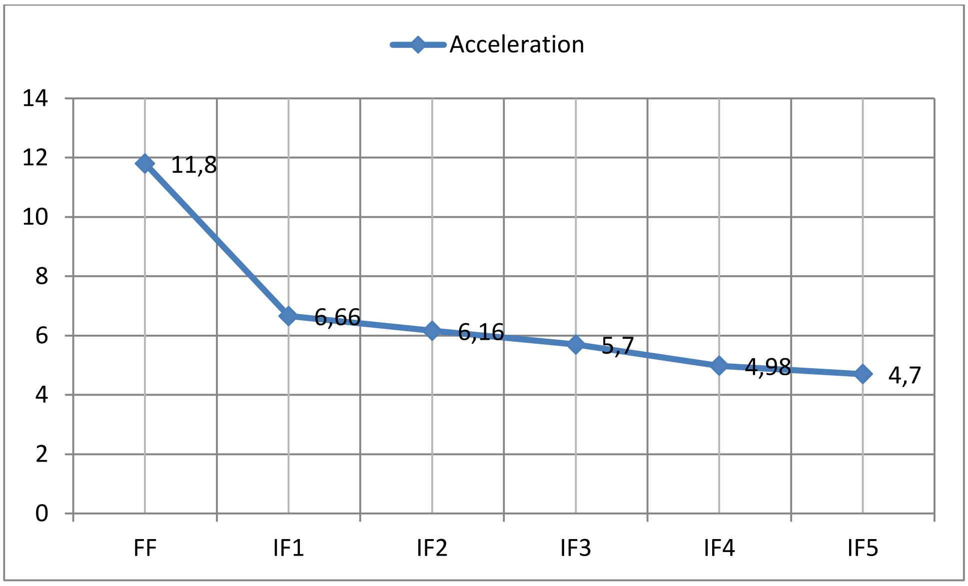

Figure 4.5. The Maximum Accelerations for the Compared Frames.

Investigating the distributions of moment and shear forces across the six frames is a crucial aspect of our investigation. We are set to conduct a comprehensive analysis of these parameters in order to gain a nuanced understanding of their behavior.

A detailed scrutiny of the envelope moments, particularly the maximum or minimum moments arising along the 3-3 axis under the influence of the earthquake load (FNA), yields valuable insights. Significantly, these findings confirm a discernible trend in which the moment experienced within the fixed frame exceeds that observed within the isolated frames. This crucial observation harmoniously aligns with the patterns illustrated in Figure 4.6, thereby reinforcing our earlier evaluations.

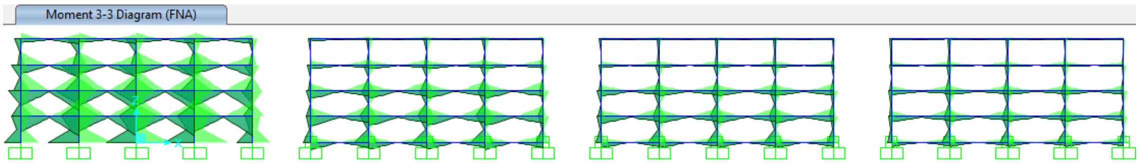

FF IF$_1$ IF$_2$ IF$_3$

Figure 4.6. The Envelope (Max or Min) Moments 3-3, under the earthquake load.

In essence, our investigation highlights the significance of the moment variations between the fixed and isolated frames when subjected to seismic loading. These discrepancies play a pivotal role in unraveling the complex dynamics that dictate the structural response of these configurations. The graphical depiction in Figure 4.6 further clarifies these differences, fostering a comprehensive understanding of the profound interplay between the structural characteristics of these frames and their resultant moment responses.

A glance at Figure 4.7 confirms that the Shear Forces in the fixed frame consistently exceed those in the isolated frames. This graphical representation reaffirms this trend and highlights the differences in Shear Forces across these distinct structural configurations.

Upon close examination of Figure 4.7, it becomes apparent that the fixed frame consistently demonstrates higher Shear Force magnitudes when compared to its isolated counterparts. This visual observation aligns with and strengthens the analytical results, thereby confirming the consistency and significance of the identified Shear Force disparities. This meticulous analysis of Shear Force distributions enhances our grasp of the dynamic interplay between structural composition and seismic loading. Consequently, it enriches our understanding of the inherent characteristics of these frames when subjected to the given conditions.

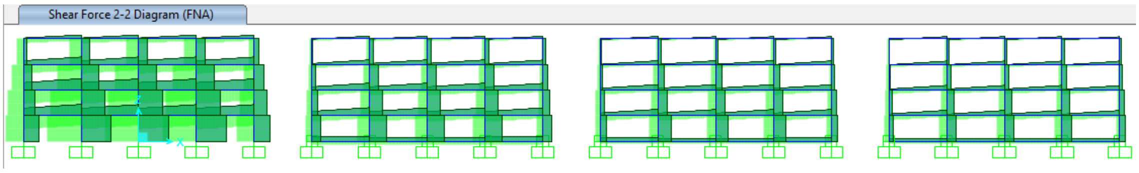

FF IF$_1$ IF$_2$ IF$_3$

Figure 4.7. The Envelope (Max or Min) Shear Forces 2-2, under the earthquake load.

The consistent disparity in Axial Forces between the fixed frame and the isolated frames remains evident, as illustrated in Figure 4.8. This graphical portrayal emphasizes the recurring trend where Axial Forces in the fixed frame consistently surpass those in the isolated frames.

Figure 4.8 stands as concrete evidence of the significance of this disparity, revealing a distinct story of Axial Force distribution. This visual representation aligns with our analytical observations, thus highlighting the consistent trend of higher Axial Forces within the fixed frame in contrast to their isolated counterparts.

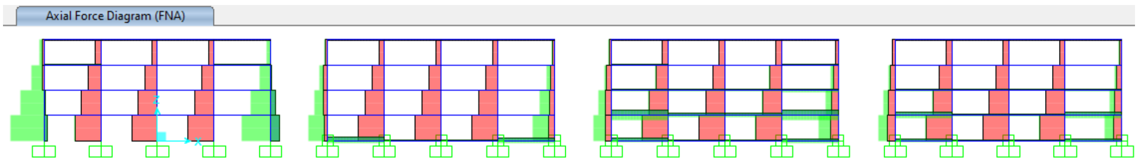

FF IF1 IF2 IF3

Figure 4.8. The Envelope (Max or Min) Axial Forces, under the earthquake load.

This graphical evidence validates the intricate dynamics involved, enhancing our grasp of the intricate interplay between structural characteristics and seismic loading. The thorough examination of Axial Force variations bolsters our understanding of the distinctive responses demonstrated by these frames under varying conditions, further contributing to the comprehensive perspective we aim to foster in our investigation.

5. CONCLUSION:

Within the scope of this research initiative, an extensive investigation was conducted, comprising six distinct scenarios. Each scenario revolved around an identical four-story steel moment frame. Additionally, an Abaqus model was established for the isolation units with the aim of deducing the design properties associated with the rubber bearing. This approach was undertaken to attain a comprehensive understanding of the seismic behavior exhibited by these isolation units.

FF = Fixed frame
IF1 = Isolated frame using isolation units with high stiffness (Keff = 1338 KN/m)
IF2 = Isolated frame using isolation units with medium stiffness (Keff = 1000 KN/m)
IF3 = Isolated frame using isolation units with low stiffness (Keff = 775 KN/m)
IF4 = Isolated frame using isolation units with low stiffness (Keff = 500 KN/m)
IF5 = Isolated frame using isolation units with low stiffness (Keff = 406 KN/m)
These scenarios encompass variations in stiffness characteristics and base configurations, elucidating the diverse behavior of the steel moment frame under distinct conditions.

All six frames underwent analysis using Nonlinear Modal Time-History (FNA) Analyses or Fast Nonlinear Analysis methods. The seismic response, behavior, and performance of the studied five Isolated Frames (IFs) and the Fixed Frame (FF) were then compared. The findings indicated that stresses, inter-story drift, and generated forces were lower in the five Isolated Frames compared to the Fixed Frame. Conversely, the period and total displacement were higher in the five Isolated Frames than in the Fixed Frame.

This comparative assessment demonstrated that among the five Isolated Frames (IFs) and the Fixed Frame (FF), stresses, inter-story drift, and resulting forces were significantly lower in the IFs than in the FF. This indicates an improved structural resilience and decreased susceptibility to seismic forces in the IFs.

Conversely, in terms of period and total displacement, the Isolated Frames showed higher values when compared to the Fixed Frame. This outcome suggests that the Isolated Frames tend to display greater flexibility and experience larger displacements during seismic events.

These collective findings emphasize the benefits of utilizing isolation techniques to mitigate stresses and inter-story drift, while also illuminating the trade-off involving higher periods and displacements in Isolated Frames when compared to Fixed Frames.

The following conclusions have been drawn from this study:

- The largest base shear force was observed in the fixed frame (FF), and this force decreased as stiffness reduced in the five isolated frames (IFs).
- The greatest acceleration was experienced by the fixed frame (FF), with decreasing values as stiffness decreased in the five isolated frames (IFs).
- The shortest fundamental period was exhibited by the fixed frame (FF), with an increasing trend as stiffness decreased in the five isolated frames (IFs).
- The highest stresses were evident in the fixed frame (FF), showing a decline as stiffness reduced in the five isolated frames (IFs).
- The most substantial moments were recorded in the fixed frame (FF), diminishing with decreasing stiffness in the five isolated frames (IFs).
- The most prominent inter-story drifts were detected in the fixed frame (FF), yet there is no direct correlation between inter-story drifts and the isolation system's stiffness in the five isolated frames (IFs).
- The smallest maximum total displacement was observed in the fixed frame (FF), but a straightforward relationship between maximum total displacements and isolation system stiffness is not evident in the five isolated frames (IFs). The maximum total displacement decreased from IF2 to IF3, yet it increased from IF3 to IF4.

In conclusion, it can be stated that an isolation system with lower stiffness proves to be more effective in protecting the steel frame against earthquake loads. Nevertheless, it is advisable to include other lateral loads such as wind loads in future investigations. This broader assessment will enable the determination of the optimal isolation system, accounting for all foreseeable load scenarios.

REFERENCES

ASCE. (2022). Minimum Design Loads for Buildings and Other Structures, ASCE/SEI 7-22. American Society of Civil Engineers, Structural Engineering Institute, Reston, Virginia.

Alhan, S., & Sürmeli, N. (2011). Shear building representations of seismically isolated buildings. Bulletin of Earthquake Engineering, 9(5), 1643-1671. https://www.researchgate.net/publication/225442568_Shear_building_representations_of_seismically_isolated_buildings

FEMA. (2020a). Earthquake Safety at Home, FEMA P-530. Applied Technology Council for the Federal Emergency Management Agency, Washington, D.C.

ANSI/AISC 358-16, Prequalified Connections for Special and Intermediate Steel Moment Frames for Seismic Applications.

ASTM International. (2021). ASTM A992/A992M-21, Standard specification for structural steel shapes. ASTM International.

ASTM International. (2021). ASTM A36/A36M-21, Standard specification for carbon structural steel. ASTM International..

Calvi, G. M. (2010). L'Aquila Earthquake 2009. Reconstruction between Temporary and Definitive. In Proceedings, NZSEE 2010 Annual Conference, Wellington.

Ismail, M., Rodellar, J., & Ikhouane, F. (2010). An innovative isolation device for aseismic design. Engineering Structures, 32(4), 1168-1183. https://doi.org/10.1016/j.engstruct.2009.12.043.

Damptech Company Site, https://www.damptech.com/

CV4 Freyssinet Mechanical Bearings, https://freyssinet.co.uk/wp-content/uploads/2020/02/C-V-4_Freyssinet-Mechanical-Bearings-En_v01.pdf

Nakamura, Y., Hanzawa, T., Hasebe, M., Okada, K., Kaneko, M., & Saruta, M. (2011). Report on The Effects of Seismic Isolation Methods From The 2011 Tohoku–Pacific Earthquake. The Journal of the Anti-Seismic Systems International Society, 2(1).

Jangid, R.S. (2007). "Optimum lead-rubber isolation bearings for near-fault motions", Eng. Struct., 29(10), 2503-2513.

Kelly, T.E. (2001), Base isolation of structures: design guidelines. Holmes Consulting Group Ltd., Wellington, New Zealand.

Kelly, T.E., Robinson W.H. and Skinner, R.I. (2006). Seismic Isolation for Designers and Structural Engineers: Robinson seismic Ltd., Wellington, New Zealand.

Naeim, F. and Kelly, J.M., 1999. Design of Seismic Isolated Structures: From Theory to Practice, John Wiley & Sons, Inc. Design Issues for Base Isolated Bridges: The 1997 Revised.

Kilar, V., & Koren, D. (2009). Seismic behaviour of asymmetric base isolated structures with various distributions of isolators. Engineering Structures, 31(4), 910-921. https://doi.org/10.1016/j.engstruct.2008.12.006.

Barka, A., Akyüz, H. S., et al. (2002). The Surface Rupture and Slip Distribution of the 17 August 1999 Izmit Earthquake (M 7.4), North Anatolian Fault. Bulletin of the Seismological Society of America, 92(1), 43–60.

RESUME

Name Surname	: Mohammad ALFATEH ALSALOUM
Place and Date of Birth	: SYRIA- HAMA 04/01/1986
Foreign Languages	: TURKEY/ENGLISH/ARABIC
Education Status	
High School	: IBN ROSHD SCHOOL
Bachelor's	: UNIVERSITY OF ALEPPO
Master's	: BURSA ULUDAG UNIVERSITY
Work Experience	: Project Management
Contact (e-mail)	: eng.sallom@gmail.com
Publications	: THESIS